

# **DEVELOPMENT OF SPHEROIDAL GRAPHITE CAST IRON FOR NUCLEAR FUEL TRANSPORT CASK**

**RANJAN KUMAR BEHERA**



Department of Metallurgical and Materials Engineering  
**National Institute of Technology Rourkela,**

# **DEVELOPMENT OF SPHEROIDAL GRAPHITE CAST IRON FOR NUCLEAR FUEL TRANSPORT CASK**

*Dissertation submitted in partial fulfilment*

*of the requirements of the degree of*

***Doctor of Philosophy***

*in*

***Metallurgical and Materials Engineering***

*by*

***RANJAN KUMAR BEHERA***

*(Roll Number: 511MM606)*

*Based on research carried out*

*under the supervision of*

***Dr. SUDIPTA SEN***

*and*

***Dr. SUBASH CHANDRA MISHRA***



*August, 2016*

Department of Metallurgical and Materials Engineering  
**National Institute of Technology Rourkela**



Department of Metallurgical and Materials Engineering  
**National Institute of Technology Rourkela**

---

August 20, 2016

## Certificate of Examination

Roll Number: *511MM606*

Name: *Ranjan Kumar Behera*

Title of Dissertation: *Development of Spheroidal Graphite Cast Iron for Nuclear Fuel  
Transport Cask*

We the below signed, after checking the dissertation mentioned above and the official record book (s) of the student, hereby state our approval of the dissertation submitted in partial fulfilment of the requirements of the degree of *Doctor of Philosophy* in *Metallurgical and Materials Engineering* at *National Institute of Technology Rourkela*.

We are satisfied with the volume, quality, correctness, and originality of the work.

---

Subash Chandra Mishra  
Co-Supervisor

---

Sudipta Sen  
Principal Supervisor

---

Santosh Kumar Sahoo  
Member, DSC

---

Mithilesh Kumar  
Member, DSC

---

Saroj Kumar Patel  
Member, DSC

---

Chairperson, DSC

---

Head of the Department

---

External Examiner



Department of Metallurgical and Materials Engineering  
**National Institute of Technology Rourkela**

---

Prof. Sudipta Sen  
Associate Professor

Prof. Subash Chandra Mishra  
Professor

August 20, 2016

## **Supervisors' Certificate**

This is to certify that the work presented in the dissertation entitled *Development of Spheroidal Graphite Cast Iron for Nuclear Fuel Transport Cask* submitted by *Ranjan Kumar Behera*, Roll Number 511MM606, is a record of original research carried out by him under our supervision and guidance in partial fulfilment of the requirements of the degree of *Doctor of Philosophy in Metallurgical and Materials Engineering*. Neither this dissertation nor any part of it has been submitted earlier for any degree or diploma to any institute or university in India or abroad.

---

Sudipta Sen  
Associate Professor

---

Subash Chandra Mishra  
Professor

# Dedication

*I would like to dedicate this dissertation to my parents, elder brother and younger sister, who never left hope on me and kept encouraging and supporting all these years. I am blessed to have them beside me all the time that gave me the moral power to move further and further during the period of course.*

*Signature*

# Declaration of Originality

I, *Ranjan Kumar Behera*, Roll Number *511MM606* hereby declare that this dissertation entitled *Development of Spheroidal Graphite Cast Iron for Nuclear Fuel Transport Cask* presents my original work carried out as a doctoral student of NIT Rourkela and, to the best of my knowledge, contains no material previously published or written by another person, nor any material presented by me for the award of any degree or diploma of NIT Rourkela or any other institution. Any contribution made to this research by others, with whom I have worked at NIT Rourkela or elsewhere, is explicitly acknowledged in the dissertation. Works of other authors cited in this dissertation have been duly acknowledged under the sections “Reference” or “Bibliography”. I have also submitted my original research records to the scrutiny committee for evaluation of my dissertation.

I am fully aware that in case of any non-compliance detected in future, the Senate of NIT Rourkela may withdraw the degree awarded to me on the basis of the present dissertation.

August 20, 2016  
NIT Rourkela

*Ranjan Kumar Behera*

# Acknowledgment

- I would like to thank the faculty members of department of Metallurgical and Materials Engineering, NIT Rourkela, who are directly or indirectly involved in this research work.
- I would like express my gratitude towards the technical staff of the department of Metallurgical and Materials Engineering, who helped me to accomplish the research work.
- I would like to thank my fellow research scholars Mr. Shashanka R, Mr. Ram Kumar Chandran, Mr. Mohan Nuthallapati and friends and family who provide moral support and encouraged me at every stage of this journey.
- I would also like to thank Sri J. S. Dubey (PIED, BARC) and his team, who accepted me as the appropriate candidate for the BRNS funded project and helped me at various stages of the project.
- I would also like to thank Mr. Ashiwini and Dr. S. Das, L&T Kansbahal, Rourkela, India, for providing cast test blocks and M/S Steelage Engineering, Rourkela, India for helping in machining of specimens.
- Lastly I express my gratitude to Dr. Sudipta Sen and Dr. Subash Chandra Mishra, who enlighten me with their knowledge and wisdom at every point and without whom it was impossible to complete this journey.

August 20, 2016  
NIT Rourkela

*Ranjan Kumar Behera*  
Roll Number: 511MM606

# Abstract

In the present work SG iron specimens with carbon equivalent (%CE) ranging from 4.12 - 4.36, has been subjected to annealing, normalizing, quench & tempering, austempering and DMS treatment to obtain different matrix microstructure and microconstituent. Optical microscopy is observed for microstructure, phase volume fraction, nodularity, and nodule count for each of the as-cast and heat treat specimens. XRD analysis is done to validate the phases present in each specimen as well as to determine the amount of carbon dissolution in respective phases. Mechanical properties such as tensile strength, % elongation, Vicker's hardness, and impact strength are measured by conducting necessary test following ASTM standards. Failure mechanisms involved in static and dynamic loading are investigated observing the fracture surfaces after tensile and impact test respectively, under Scanning Electron Microscope. The corrosion behavior of as-cast and heat treated specimens, (in sea water) is also studied. Specimens are immersed completely in sea water at room temperature and pressure, and the weight difference is recorded at regular intervals, for twelve weeks.

The mechanical properties showed a quite good relationship with microconstituents for respective as-cast and heat treated specimens. The as-cast specimens show graphite spheroids within ferritic matrix resulted in increased ductility and impact strength (with increasing ferrite volume fraction) caused by increasing Si content. Annealing treatment led to the presence of completely ferritic matrix for every alloy consequently increasing ductility and impact toughness as compared to as-cast matrices. On the other hand specimens which underwent quenching & tempering treatment show the highest strength and hardness due to the tempered martensitic matrix, among all other heat treatment processes. Strength and ductility values of normalized austempered and DMS-treated specimens are intermediate to those of lowest strength value for annealed specimen and higher elongation value and that of highest strength and lowest elongation value for the quenched & tempered specimens. It is observed that the elongation



increases with increased nodularity can be attributed to increases amount of Mg and Ce, whereas nodule count increases the hardness of respective as-cast and heat treated specimens. The increase of hardness may be due to increase of Ni and Cr content which provides strength to ferrite via solid solution strengthening (for ferritic specimens). Normalizing treatment produced a ferritic/pearlitic matrix and showed increased UTS and hardness with increased pearlite content. Austempered heat treatment resulted in coarse upper bainitic matrix leading to suitable combination of strength and ductility, whereas matrix consists of martensite and ferrite are obtained by DMS treatment. The failure mode for the soft ferritic matrix is observed to be ductile in nature caused by microvoid coalescence, and that of other matrices are mostly brittle signified by the presence of low energy stress paths (River marking) and cleavage facets. Mechanical properties of SG iron alloys studied in current research, found to be well above the recommended properties for fabrication of nuclear fuel cask, (in as-cast as well as heat treated conditions) and hence can successfully be used for the desired purpose.

***Keywords: DUCTILE CAST IRON; ALLOYING; HEAT TREATMENT; MECHANICAL PROPERTIES; MICROCONSTITUENT; CORROSION.***

# Contents

<b>Certificate of Examination</b>	<b>ii</b>
<b>Supervisors' Certificate</b>	<b>iii</b>
<b>Dedication</b>	<b>iv</b>
<b>Declaration of Originality</b>	<b>v</b>
<b>Acknowledgment</b>	<b>vi</b>
<b>Abstract</b>	<b>vii</b>
<b>List of Figures</b>	<b>xi</b>
<b>List of Tables</b>	<b>xv</b>
<b>1. INTRODUCTION</b>	<b>1</b>
1.1. BACKGROUND.....	3
1.2. MOTIVATION AND OBJECTIVE OF PRESENT RESEARCH .....	3
<b>2. RESEARCH SO FAR</b>	<b>4</b>
2.1. NUCLEAR FUEL CASKS .....	8
2.1.1. BACKGROUND AND OBJECTIVE .....	8
2.1.2. TYPES OF SNF CASK .....	11
2.2. SG CAST IRON ... WHY?	13
2.2.1. EMERGENCE & ADVANTAGES OF SG CAST IRON .....	13
2.2.2. TYPES AND GRADES OF SG CAST IRON .....	16
2.2.3. SG CAST IRON AS SNF CASK .....	19
2.3. EFFECT OF ALLOYING ELEMENT ON PHYSICAL & MECHANICAL PROPERTIES OF SGCI .....	21
2.3.1. EFFECT OF BASE COMPOSITION .....	21
2.3.2. EFFECT OF ALLOYING ELEMENTS .....	25
2.4. EFFECT OF HEAT TREATMENT ON PHYSICAL & MECHANICAL PROPERTIES OF SGCI .....	28
2.5. EFFECT OF ALLOYING & HEAT TREATMENT ON CORROSION BEHAVIOR OF SGCI .....	34
<b>3. MATERIALS AND METHODS</b>	<b>36</b>
3.1. PROCESSING OF MATERIALS .....	36
3.2. HEAT TREATMENT PROCESSES .....	47
3.3. OPTICAL MICROSCOPIC ANALYSIS .....	39
3.4. EVALUATION OF MECHANICAL PROPERTIES .....	39
3.5. CORROSION BEHAVIOUR .....	40
3.6. SCANNING ELECTRON MICROSCOPE STUDIES .....	41
3.7. X-Ray DIFFRACTION ANALYSIS .....	41

<b>4. RESULTS AND DISCUSSION</b>	45
4.1    MICROSTRUCTURAL CHARACTERIZATION	
4.1.1    OPTICAL MICROSCOPIC INVESTIGATION	
4.1.1.1    EFFECT OF HEAT TRTREATMENT.....	
4.1.2    X-Ray DIFFRACTION STUDY .....	50
4.1.3    EFFECT OF ALLOYING ON MICROSTRUCTURE.....	52
4.2    MECHANICAL PROPERTIES	55
4.2.1    VICKERS' HARDNESS .....	
4.2.2    TENSILE STRENGTH AND DUCTILITY .....	56
4.2.3    IMPACT ENERGY .....	59
4.2.4    EFFECT OF COMPOSITION .....	61
4.2.5    EFFECT OF PHASE VOLUME FRACTION.....	63
4.2.6    FRACTOGGRAPHIC INVESTIGATION .....	65
4.3    CORROSION STUDIES	67
4.3.1    CORROSION RATE OF ALLOYS .....	
4.3.2    EFFECT OF ALLOYING ELEMENT ON RATE OF CORROSION	70
4.3.3    MORPHOLOGY OF CORRODED SURFACE .....	70
4.3.4    X-Ray DIFFRACTION STUDY OF CORROSION PRODUCT.....	73
<b>5. CONCLUSION</b>	74
<b>6. REFERENCES</b>	77
<b>APPENDIX I</b>	xvi
<b>APPENDIX II</b>	xvii
<b>APPENDIX III</b>	xviii
<b>DISSEMINATION</b>	xix
<b>RESPONSE TO EXAMINER COMMENTS</b>	xx

# List of Figures

Sl. No.	Description	Page no.
Fig. 1.1	Demand forecast of ductile iron till 2015.	2
Fig. 1.2	Relationships between endurance ratio, tensile strength and matrix microstructure for Ductile Iron.	2
Fig. 2.1	Nuclear power plant status worldwide as on 1st June 2015 (IAEA 2015)	7
Fig. 2.2	Schematic diagram for working principle of nuclear power plant	8
Fig. 2.3	(a) Generic Truck Cask for Spent Fuel (cutaway view) (b) Generic Rail Cask for Spent Fuel (cutaway view)	10
Fig. 2.4	(a) Steel-concrete cask design. (b) Cermet type cask design. (c) Basket type design.	10-11
Fig. 2.5	(a) Micrograph of Gray Iron showing the crack-like behavior of graphite flakes (b) Micrograph of Ductile Iron showing how graphite spheroids can act as "crack-arresters"	15
Fig. 2.6	Comparison of the engineering characteristics of SG cast iron versus competitive ferrous cast materials.	16
Fig. 2.7	Microstructure and tensile strength of various types of SG cast iron.	17
Fig. 2.8	Variation of carbide percentage (a) and nodule count (b) in ductile cast iron with Silicon content	22
Fig. 2.9	Influence of silicon content on the v-notched Charpy energy of ferritic Ductile Iron	23

Fig. 2.10	The relationship between tensile strength, elongation, average hardness and pearlite content versus Mn content (0.05% Cu)	24
Fig. 2.11	Comparison of nodular graphite of the Co & Ni alloyed SG cast irons: (a) nodularity and (b) nodule count	26
Fig. 2.12	Comparison of constituent content in the microstructure of the Co & Ni alloyed SG cast irons: (a) graphite, (b) ferrite and (c) pearlite	26
Fig. 2.13	Relationship between the mechanical properties and the Copper content for different Mn level	27
Fig. 2.14	Dependence of: a) volume fraction $X_{\gamma}$ of retained austenite; b) austenite carbon content $C_{\gamma}$ ; c) total carbon austenite content $C_{\gamma, tot.}$ , and d) untransformed austenite $X_{\gamma.\alpha}$ on austempering time $t_a$ and austenitizing temperature $T_{\gamma}$ .	32
Fig. 2.15	The effect of austempering time on: (a) 0.2% proof stress; (b) UTS and (c) impact energy at different austempering temperatures	32
Fig. 2.16	Influence of heat treatment on the V-notched Charpy Behavior of Ductile Iron	33
Fig. 2.17	(a) A comparison of weight loss of various irons after salt-spray (b) Weight loss of uncoated and coated ADIs in 10 Vol.% $H_2SO_4$ aqueous solution	35
Fig 2.18	Graph of corrosion rate vs. time for castings produced by varying chill thickness	35
Fig. 3.1	SGCI test block after sand mold casting.	36
Fig. 3.2	Heat treatment processes employed in present study	38
Fig. 3.3	(a): ASTM E8, flat subsize tensile specimen, (b): ASTM E23-12c, Izod impact specimen.	40
Fig. 4.1	Microstructure of Unetched as-cast and heat treated specimens.	46-47
Fig. 4.2	Microstructure of As-cast and heat treated specimens after etching	49-50

(Nital 2%).

Fig. 4.3	X-ray Diffraction patterns of as-cast and heat treated specimens of individual alloys.	51-52
Fig. 4.4	(a) Wt. % of Silicon vs. Ferrite and Graphite volume fraction, (b) Wt. % of Manganese vs. Pearlite volume fraction, (c) Wt. % of Silicon vs. Ferrite volume fraction for normalized specimens, (d) Combined effect of Manganese and Nickel on tempered martensite volume fraction, (e) Wt. % of Nickel vs. Bainite volume fraction.	54
Fig. 4.5	Vickers hardness of as-cast and heat treated specimens of respective alloys.	56
Fig. 4.6	UTS of as-cast and heat treated specimens of respective alloys.	58
Fig. 4.7	% Elongation of as-cast and heat treated specimens of respective alloys.	59
Fig. 4.8	Izod impact energies of as-cast and heat treated specimens of respective alloys.	60
Fig. 4.9	(a) wt.% Si vs. Elongation and Impact energy of as-cast and annealed specimens, (b) wt.% Ni vs. UTS of as-cast and annealed specimens, (c) wt.% of Mn vs. UTS and Hardness of normalized specimens, (d) wt.% Si vs. Elongation and Impact energy of normalized specimens, (e) wt.% of Ni vs. UTS of quench & tempered specimens, (f) wt.% of Ni vs. UTS and hardness of austempered specimens, (g) combined effect of Ni and Mn on UTS of DMS-treated specimens, (h) wt.% Si vs. Elongation and Impact energy of DMS-treated specimens.	62-63
Fig. 4.10	Relationship between different phase volume fractions with corresponding mechanical properties. (a) Ferrite volume fraction vs. ductility and impact energy of as-cast specimen, (b) Ferrite volume fraction vs. ductility and impact energy of annealed specimen, (c) Pearlite volume fraction vs. UTS and Hardness, (d) Pearlite volume fraction vs. % elongation and impact energy.	64-65
Fig. 4.11	Fracture surfaces of as-cast and heat treated specimens after tensile failure.	66
Fig. 4.12	Fracture surfaces of as-cast and heat treated specimens after Impact failure.	67
Fig. 4.13	Corrosion rate vs. time interval plot for as-cast and heat treated condition for individual alloys.	69-70
Fig. 4.14	Surface morphology of corroded surfaces and the porous product after 1 <sup>st</sup> week of immersion.	72

Fig. 4.15	Surface morphology of corroded surfaces and the porous product after 12 <sup>th</sup> week of immersion.	73
Fig. 4.16	XRD pattern for corroded surfaces after 1 <sup>st</sup> and 12 <sup>th</sup> week of exposure.	74-75

# List of Tables

<b>Sl. No.</b>	<b>Description</b>	<b>Page no.</b>
Table 2.1	Nuclear power plants worldwide, in operation and under construction, IAEA as of 1 <sup>st</sup> June 2015.	6-7
Table 2.2	Various standards for SG iron design engineers	18-19
Table 3.1	Chemical composition of alloys studied in present research (in wt. %).	37
Table 3.2	Dimension for tensile specimen according to ASTM E8, FLAT SUBSIZE SPECIMEN	40
Table 4.1	Nodularity and Nodule Count of As-Cast and Heat Treated Specimens of Respective Alloys.	46
Table 4.2	Volume fraction of austenite and ferrite and carbon content in austenite of respective austempered specimens.	51
Table 4.3	Tensile strength of respective alloys in as-cast and heat treated conditions.	58
Table 4.4	% Elongation of respective alloys in as-cast and heat treated conditions.	59
Table 4.5	Impact energy of as-cast and heat treated specimens of respective alloys.	60



# 1. INTRODUCTION

## 1.1. Background

Spheroidal graphite cast iron (SGCI)/ Ductile Iron (DI) as the name suggests, has graphite in a spherical form embedded in the matrix. The spherical shape is achieved by the addition of Magnesium (Mg) and/or Cerium (Ce) as inoculants, to the grey cast iron melt during the casting process. The graphite spheroids do not interfere with matrix continuity and eliminate the stress concentration effect that generates due to the presence of flaky graphite in case of grey cast iron, leading to improved ductility and impact toughness without affecting the strength and hardness. In addition, to these advantages, it possesses ease of castability, machinability and less cost of production. Because of these enhanced properties over the other cast irons, during the last five decades, the production and commercialization of SGCI have grown immensely. According to number of sources production of SGCI is increased and will keep growing compared to other cast iron [1]–[5]. The reason behind this growth of production is quite clear. SGCI offers a broad range of properties which is achieved and controlled by addition of alloying elements and/or heat treatment processes. Alloying of SGCI or application of heat treatment processes leads to a change in microconstituents of the material resulting in desired properties of the component. This is why SGCI is itself regarded as a family consisting ferritic, pearlitic, martensitic, ausferritic, ferritic + martensitic and austenitic spheroidal graphite cast iron rather than a single material [6]–[10]. Ferrite matrix induces a high ductility around 25–30% with low strength value of 250–400 MPa, whereas the pearlitic matrix show strength in the range of 500–700 MPa with maximum elongation about 18% and that of the martensitic matrix provides maximum strength around 1100 MPa with 10–12% elongation. A strength value of 1600 MPa and elongation about 6–8% can be achieved in thin walled ductile iron with an ausferritic matrix with a uniform distribution of nodules and higher nodule count. The austempering treatment produces a matrix of lower acicular bainite or coarse upper bainite depending on the transformation temperature and time. Austempering involves isothermal transformation of primary austenite ( $\gamma_0$ ) into acicular ferrite ( $\alpha$ ) and carbon enriched stable austenite ( $\gamma_c$ ), resulting in an ausferritic matrix structure [11]–[17]. Fig. 1.2 illustrates relationships between endurance ratio, tensile strength and matrix microstructure for ductile iron. This allows design engineers to choose appropriate kind of material for the desired application.

Nuclear power generation contributes about 11% of the world electricity. Though the production of nuclear power is safe and pollution free, the post-processing of used nuclear fuels is a challenging task. After half-life period, the nuclear fuels are cooled in the near reactor pool at least for a year and then transported to a safe disposal site, contained in a robust structure called spent nuclear fuel cask. In the early stages of spent nuclear fuel cask production in 1980, Steel and Lead were used as the preferred material. Lead act as a neutron absorber and was placed in between two steel sheets which provide toughness to the structure. In some cases, depleted Uranium was also used as shielding material instead of Lead. But this sandwich structure didn't prove to be the ultimate solution. During severe accidental conditions, it has been observed that there is a possibility of leakage of Lead from the structure, which no more prevents the radiation leakage. Hence, SGCI has been opted due to its versatile mechanical properties. The benefit of using DI is that it can be cast to near final cask dimensions that reduce machining efforts/costs. The cask can be cast monolithically which eliminate welds in the containment boundary & serves both as the structural containment boundary & the gamma shield. It also eliminates the needs for the "sandwich" type designs that includes welds & are harder to fabricate. Finally, the cheap material & fabrication costs compare favorably with the traditional sandwich stainless steel cask cost. In the year 2005, SGCI is included in the structural standards for fabrication of spent nuclear fuel cask by American Society of Mechanical Engineers (ASME). During the last two decades, SGCI has been tested and used for fabrication of spent nuclear fuel cask.

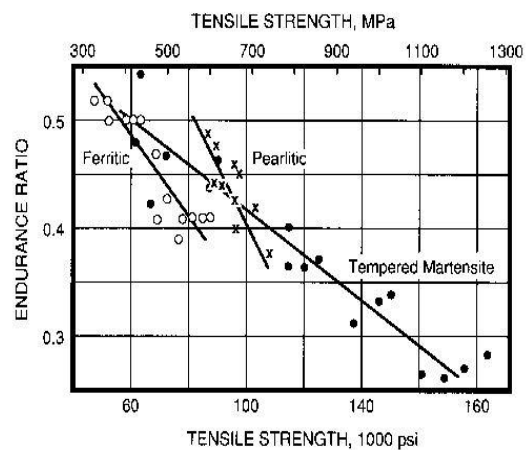
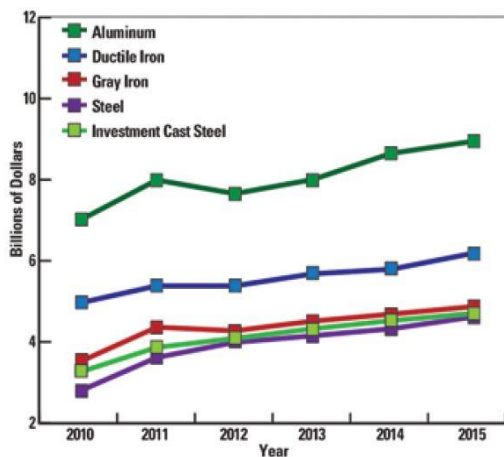


Fig. 1.1: Demand forecast of ductile iron till 2015 [18]. Fig. 1.2: Relationships between endurance ratio, tensile strength and matrix microstructure for Ductile Iron [19].

## **1.2. MOTIVATION AND OBJECTIVE OF PRESENT RESEARCH**

Our world is on the edge of transformation towards a new era where life without electricity will be impossible and hence the requirement for power generation is increasing day by day all over the world and especially in developing countries like India, where scarcity of energy is a serious problem. On the other hand, it is necessary to save the environment from pollution and foreign elements that are generated from the conventional power plants and many more sources. Hence, the whole world is moving towards safe and green energy production such as nuclear, wind and renewable energy sources. However, nuclear power plant also has environmental issues that need to be taken care of. Disposal and storage of nuclear waste are a significant factor in the generation of nuclear energy as the radiation affect not only human bodies but is also very dangerous for our environment. Hence, a small step is taken towards finding a solution to this issue in this present work. However, researchers all over the world are still hunting for suitable properties for SGCI casting, and many works have already been reported. Most of the works are concentrated on developing the properties of austempered SG cast iron and very less investigation on the properties of SG cast iron subjected to full annealing, normalizing and tempering and intercritical austenitizing followed by quenching treatment.

Present work is focused on solving the above important matters, and the objectives are;

1. To develop properties of different types of spheroidal graphite cast iron material subjecting them to different heat treatment processes like annealing, normalizing, tempering, austempering and intercritical austenitizing followed by quenching heat treatment processes and also by alloying, for transport application of nuclear fuel bundles.
2. To investigate the structure-property correlation and material response in as-cast and heat treated conditions, towards the corrosive environment.
3. Investigation of optimum chemical composition and heat treatment condition for mechanical properties and corrosion resistance of the material for fabrication of nuclear fuel transport cask.

## 2. RESEARCH SO FAR

### 2.1. Nuclear Fuel Casks

#### 2.1.1. Background And Objective

According to International Atomic Energy Association (IAEA) (as on 1<sup>st</sup> June 2015), there are 438 nuclear reactors operational, and 67 are under construction worldwide, among which in India 21 reactors are operational in 7 nuclear power plants (NPP) and 6 are being built. The total capacity of installed reactors is 5780MW producing 30,292.91GWh of electricity while the six under construction reactors are designed to generate additional 4,300 MW [20]–[25]. The reactor plays an important role and treated as the heart of NPP. NPP uses isotopes of Uranium (U-235 & U-238) as fuels to generate heat through a fission reaction and produces steam that is used to run the turbine and hence converts the atomic energy into electricity. A protective shield surrounds the nuclear fission results in radioactivity and hence the reactor core. This containment absorbs radiation and prevents radioactive material from being released into the environment. Also, many reactors are equipped with a dome of concrete to protect the reactor against both internal casualties and external impacts such as flight collision or terrorist attack. The nuclear fuel cycle consists of three main stages viz. (i) *front end*, deals with mining, milling, uranium conversion, enrichment and fabrication of fuels, (ii) *service period*, when fuels are put into reactor in operation and (iii) *back end*, where it is necessary to safely manage the spent nuclear fuel (SNF), they are either re-processed or disposed of.

During the early stage of operation, the nuclear fuels, after reaching their service life (referred as half-life period) were drawn out of the reactor core and put into the water pool (termed as Spent Fuel Pool) built near the reactor. Water acts as a coolant as well as prevents the radiation from the SNF into the atmosphere. The SNF after spending 10 to 12 months inside the pool were again brought out and sent for reprocessing and made ready to go into the reactor again. This process was continued for many decades, till the end of the 70's and early 80's of the twentieth century when the fuel pools near reactor site were overwhelmed their capacity, and the reprocessing of fuels was prohibited all over the world. A new problem was raised in the context of the SNF. The question was; How and where to store the SNF?

The only answer available to the question is the dry storage of SNF. In this process, the SNF after cooling down in the fuel pool were taken out and kept inside a container, suitable enough to absorb the residual heat and to contain the gamma radiation from the fuel cells, followed by transportation to desired geological sites for disposal and storage. These containers were called as Spent Nuclear Fuel Casks. The geological sites for disposal of SNF were carefully chosen so that if accidentally the casks fail to perform its objective and radiation leakage happens, it should not affect the living being and the environment. Hence, these sites were selected such that it should be far away from the residential areas. Till now not a single country has the desired disposal site according to the Nuclear Regulatory Commission (NRC). Radiation from nuclear waste may cause death of human body cell, genetic mutation, cancer, leukemia, birth defects, and disorders of the reproductive, immune and endocrine systems. Also after the 9/11 attack on World Trade Centre (WTC) in the USA, the world came to know the capacity of terrorism and focus was also shifted towards the protection of disposal sites as well as SNF casks. These casks are transported through public route to the disposal sites and hence care must be taken that it should have enough radiation leakage resistance. During transportation by road or rail line accidents may happen and catch fire leading to failure of casks depending on the crash severity and temperature generation. Considering all these aspects of transportation and safe disposal issues in hand, the major requirements for cask fabrication are:

1. The cask should have sufficient dynamic toughness so that it can withstand severe accidental condition as well as terrorist attacks, without failure and radiation leakage.
2. The cask material should possess high thermal conductivity to sustain severe fire accidents and heat generated from the spent fuel.
3. The dynamic fracture toughness cannot be neglected as it determines the rate of crack propagation, initiated due to various loading conditions; hence the cask material should possess adequate fracture toughness.

Since the late 1970's; research has been going on to obtain a suitable material for the fabrication of SNF cask. Efforts were made all around the world and especially states with high capacity and usage of nuclear power, in the direction of development of not only material properties but also policies for the nuclear waste disposal and storage.

Table 2.1: Nuclear power plants worldwide, in operation and under construction, IAEA as of 1<sup>st</sup> June 2015 [21].

Country	In Operation		Under Construction	
	Number	Electricity Net Output (MW)	Number	Electricity Net Output (MW)
Belarus	-	-	2	2,218
United Arab Emirates	-	-	3	4,035
Armenia	1	375	-	-
Iran	1	915	-	-
Netherlands	1	482	-	-
Slovenia	1	688	-	-
Brazil	2	1,884	1	1,245
Bulgaria	2	1,926	-	-
Mexico	2	1,330	-	-
Romania	2	1,300	-	-
South Africa	2	1,860	-	-
Argentina	3	1,627	1	25
Pakistan	3	690	2	630
Finland	4	2,752	1	1,600
Hungary	4	1,889	-	-
Slovakian Republic	4	1,814	2	880
Switzerland	5	3,333	-	-
Czech Republic	6	3,904	-	-
Taiwan, China	6	5,032	2	2,600
Belgium	7	5,921	-	-
Spain	7	7,121	-	-
Germany	9	12,074	-	-
Sweden	10	9,651	-	-
Ukraine	15	13,107	2	1,900
United Kingdom	16	9,373	-	-
Canada	19	13,500	-	-
India	21	5,308	6	3,907
Korea, Republic	24	21,667	4	5,420

China	27	23,025	24	23,738
Russian Federation	34	24,654	9	7,371
Japan	43	40,290	2	2,650
France	58	63,130	1	1,630
USA	99	98,639	5	5,633
Total	438	379,261	67	65,482

**Nuclear Power Plant Status Till 1st June 2015**

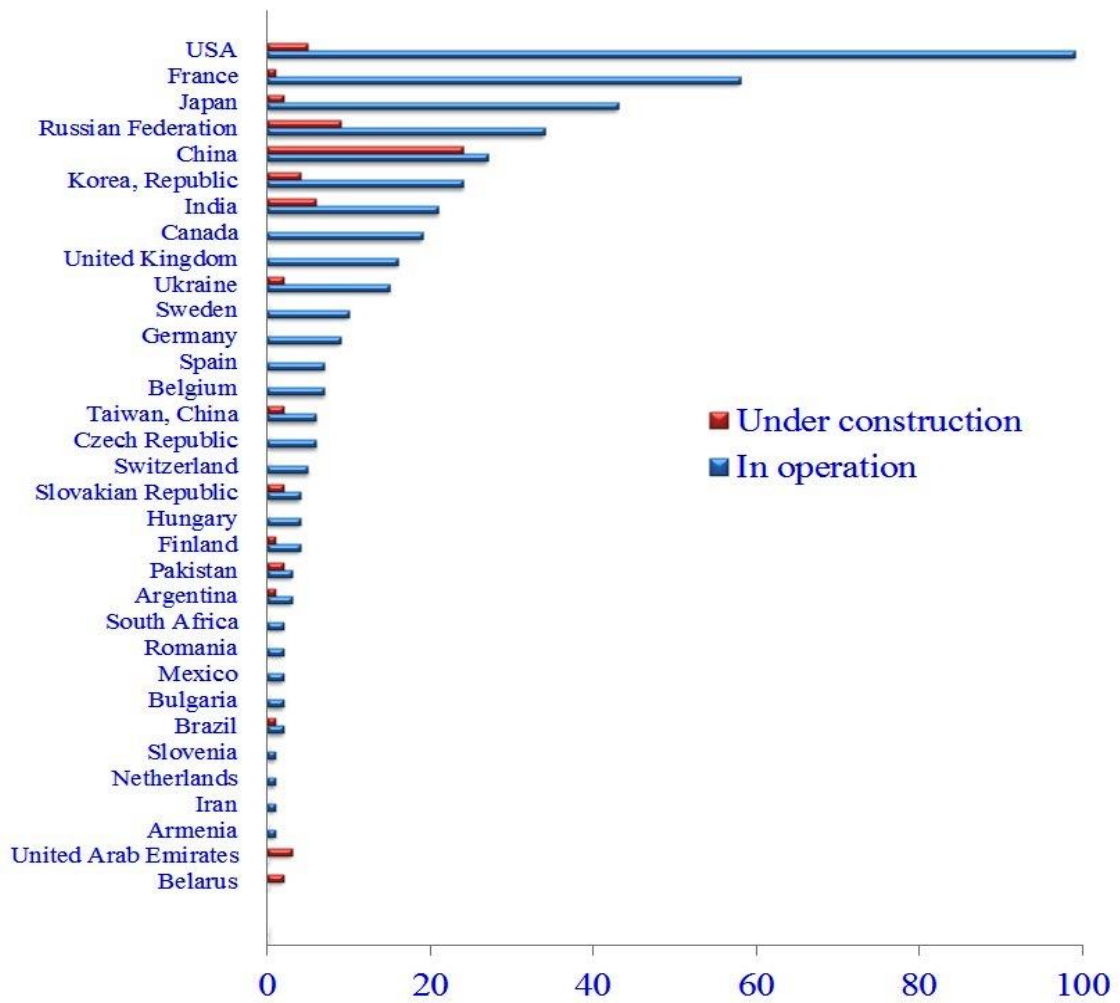


Fig. 2.1: Nuclear power plant status worldwide as on 1st June 2015 (IAEA 2015) [21].

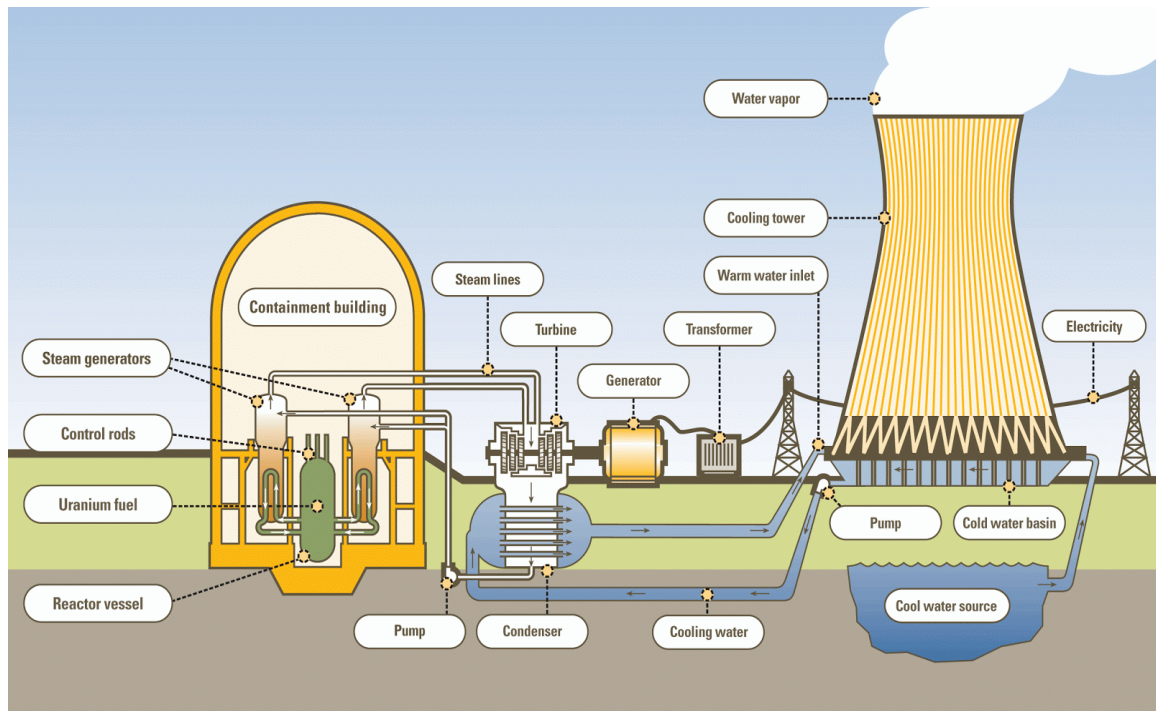


Fig. 2.2: Schematic diagram for working principle of nuclear power plant [25].

### 2.1.1. Types Of SNF Cask

Spent fuel transportation casks are sturdy containers that provide protection, containment, shielding, heat management, and nuclear criticality safety for the spent fuel contained within. Spent fuel transport casks are designed in a variety of sizes and configurations depending on the characteristics of the spent fuel to be carried. The very first cask was made following a sandwich structure consisting of thick-walled stainless steel cylinder as inner and outer shell and Lead or depleted Uranium that act as a gamma shield, in between the shells. This was the most common type structural configuration for a spent nuclear fuel cask. The outer cylinder contains hydrogenous materials like polyethylene and protects the containment from leakage of gamma radiation. The spent fuel casks are employed with detachable external protective structures called impact limiters that reduce the mechanical forces act on the package under accident conditions. The interior spaces of the cask are filled with Helium to enhance the heat transfer and to build a non-oxidizing environment for the spent fuels. However, some designs use a monolithic thick-walled steel cylinder that provides both gamma shielding and structure integrity.



The other type of design uses brittle ceramic materials like ( $\text{DUO}_2$ ,  $\text{Al}_2\text{O}_3$ ,  $\text{Gd}_2\text{O}_3$ , etc.) embedded in a strong, ductile steel metal matrix with a high thermal conductivity, thus combining the best properties of both materials. These cermet type casks offer greater capacity for same gross weight of cask, greater capacity for the same external dimension, improved resistance to assault and superior repository performance. The addition of depleted uranium dioxide to the cermet increases shielding density and effectiveness and capacity of the cask for a given weight and size. The low-density aluminum oxide is added to the upper and lower section of the cask to reduce the cask weight and increases the assault resistance when used in appropriate locations. Repository performance may be improved by compositional control of the cask body to (1) create a local geochemical environment that slows the long-term degradation of the SNF and (2) enables the use of  $\text{DUO}_2$  for long-term criticality control. The benefits of cermet cask are achieved by controlling the composition, volume fraction and particle size of the ceramics [26]–[28]. The SKODA JS offers a double barrier type SNF cask consisting cast manganese steel body (260mm thickness) and CrNi austenitic steel canister containing spent fuels welded to the body. From the point of view of achieving advantageous brittle-fracture and plastic properties compared to other materials the casting material of the cask body is tested first [28]. Similar to these cermet type casks, Germany and Russia are employing composite structures consisting steel-concrete and austenitic stainless steel type design [often called multi-canister overpack (MCO)], with welded joints [29], [30]. On the other hand, the Korean NPP uses basket type design to incorporate a large amount of SNF and reduce the transportation and fabrication cost as well as less space utilization [31]. Despite all these benefits provided by composite structures, the primary challenge is to develop low-cost fabrication methods for cermet composition.

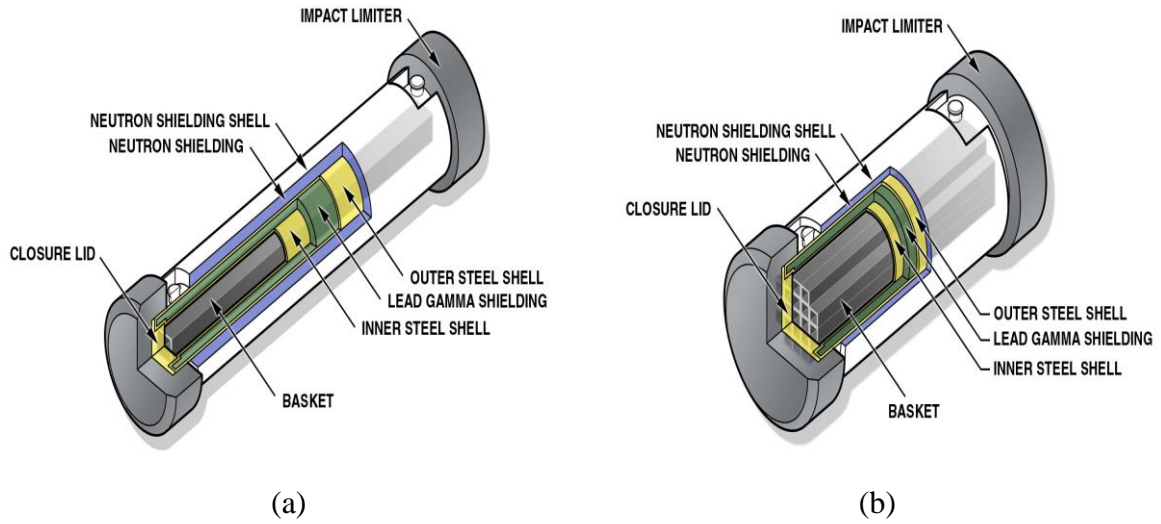
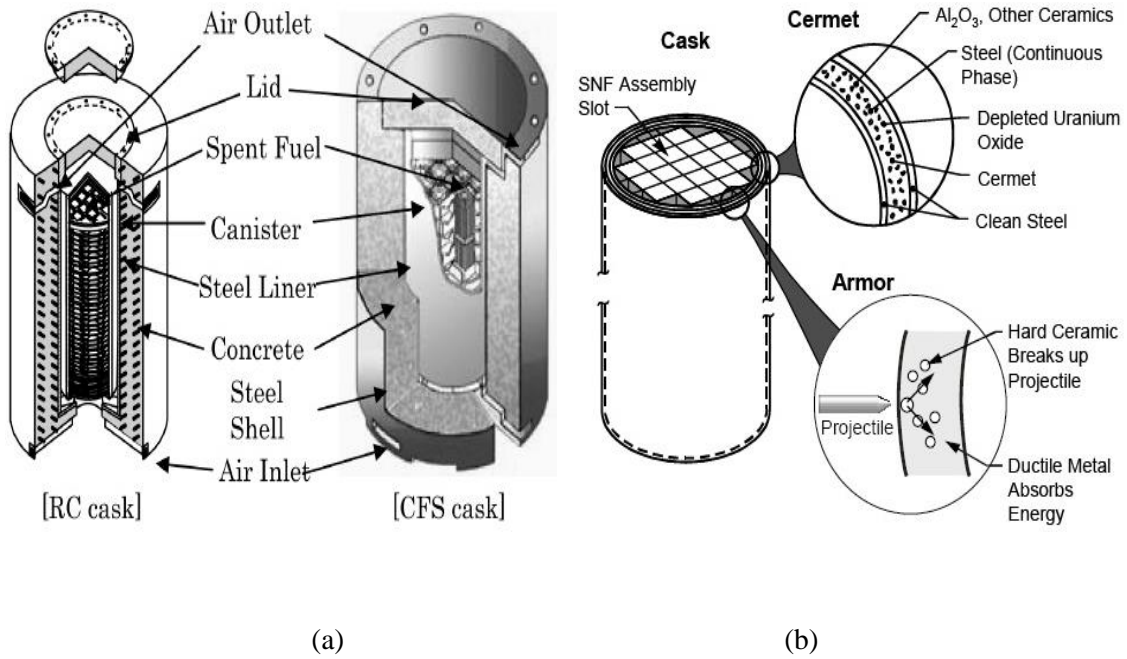


Fig. 2.3: (a) Generic Truck Cask for Spent Fuel (cutaway view), (b) Generic Rail Cask for Spent Fuel (cutaway view) [32]



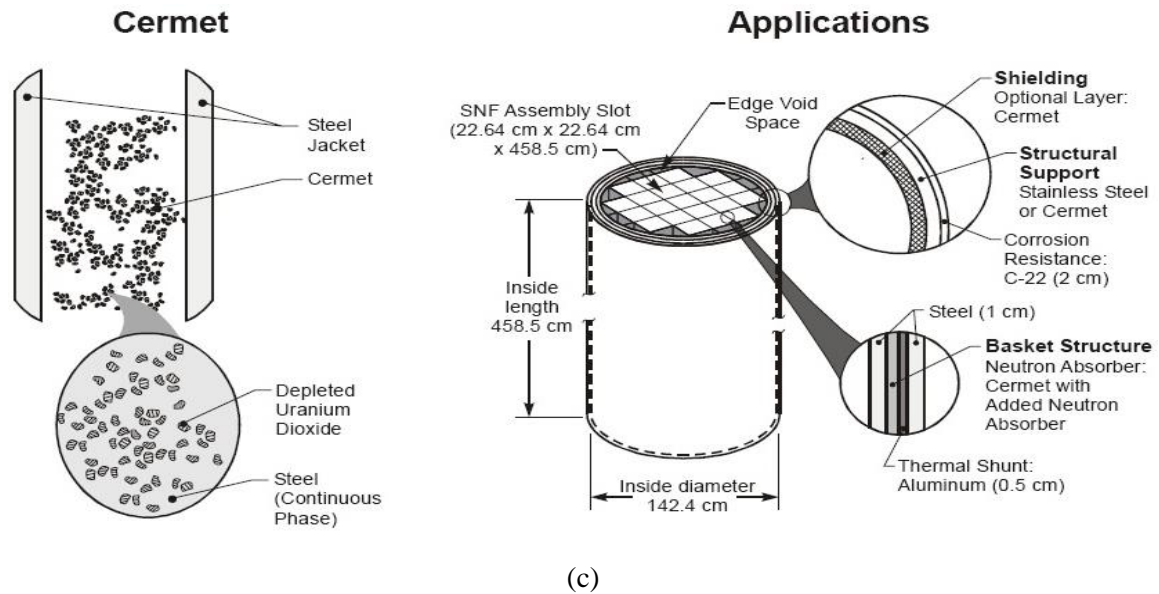


Fig. 2.4: Different types of cask design. (a) Steel-concrete cask, (b) Cermet type cask, (c) Basket type design [28], [31]

### 2.1.2. Property Requirements For SNF Cask

The material selection for fabrication of transport cask for radioactive materials involves careful selection that depends on the type of radioactive material to be transported. These container designs need to meet certain standards regardless of the fabrication process, and agreed by various national and international bodies, to protect the person involved, and those who may come across, till the whole process of transportation is accomplished. The transportation of used nuclear fuel requires primarily good shielding against radiation and thermal conductivity, sufficient dynamic fracture toughness and excellent impact resistance. The IAEA Safety Regulations for the Safe Transport of Radioactive Material (2009 Edition) [33], articulates various provisions regarding the type of radioactive material and its transport container mentioning the acceptable level of radiation under different transport and environment conditions.

The transport containers should be designed in such a way that as far as practicable, its surface should prevent collection and retention of water, free from projecting features and can be decontaminated easily. Furthermore, the attachments on the surface should only be necessary for supporting the mass of the container, and the package can easily and safely be transported. The container materials shall be chosen so that, those are physically and chemically compatible with each other and the radioactive content. The behavior

under irradiation condition and ambient pressure and temperature, need to be taken into account because they can deteriorate the efficiency of the container. The container should withstand the effects of acceleration, vibration which may arise under different transport condition without affecting the performance of closing devices or the integrity of the package as a whole. Additionally, if the containments are to be sent by air transport, then care must be taken so that the surface temperature should not exceed 50°C at an ambient temperature of 38°C. The container shall have the capacity to withstand, without leakage, an internal pressure difference of not less than the maximum normal operating pressure plus 95KPa. However if the containment, in any case, is exposed to an ambient temperature ranging from -40°C to +55°C, the integrity of it should not be damaged. Portable tanks may also be used for transport of radioactive materials, which has to meet the above requirements and additionally capable of withstanding a working pressure of 265KPa and should be designed to prevent more than 20% increase in radiation level that may be generated from static and dynamic stresses during general transport condition.

In addition to above criteria, the containers traveled by rail/road transport, certain mechanical properties such as strength, toughness, and heat resistance capacity of container material play an important role. The design should meet the requirements those may arise from accidental conditions. If the container meets these accidental conditions, in any case, it should not fail to fulfill its objective of preventing damage to the nuclear fuels and/or leak radiation to the environment. In view of this, specific testing methods were established by the IAEA, which should be followed before putting the container into actual service. The mechanical test consists of three different drop tests so as to cause maximum damage to the container. In drop I, the specimen is dropped from a height of 9m., measured from the lowest point of the specimen to the upper surface of the target. The target should be flat, horizontal and the surface character should be such that any increase in its resistance to displacement or deformation upon impact by the specimen would not significantly increase damage to the specimen. The second drop test comprises of dropping the specimen onto a bar rigidly mounted and perpendicular to the target. A height of 1m., from the point of impact to the upper surface of the bar shall be maintained. The bar should be cylindrical and shall of mild steel of diameter of  $15.0 \pm 0.5$  cm and 20 cm long. The upper end of the bar onto which the specimen will be dropped shall be flat and edges rounded off to a radius below 6mm. In the 3<sup>rd</sup> drop, a dynamic crushing test should be carried out by dropping a mass of 500kg from 9m., onto the specimen so that

the specimen suffers maximum damage. The mass should be of solid, mild steel plate of 1m×1m and fall in a horizontal attitude. This is followed by mechanical testing thermal and water immersion test is carried out to assess the integrity of the container.

The container should be in thermal equilibrium conditions of an ambient temperature of 38°C and subjected to the design, maximum rate of internal heat generation within the package from the radioactive material. The thermal test comprises of two methods. In first method specimen is exposed to a thermal environment that provides a minimum average flame emissivity coefficient of 0.9 and temperature of at least 800°C, for 30 minutes. The test involves fully engulfing of the specimen with a surface absorptivity coefficient of 0.8 or the value that of the packaging material. The second method comprises of subjecting the specimen to an ambient temperature of 38°C and subjected to the design, maximum rate of internal heat generation within the package from the radioactive material for sufficient period to ensure that the specimen temperature is decreasing or approaching initial steady state condition from everywhere. The specimen should not be cooled artificially, and the combustion should proceed naturally. The water immersion test consists of immersion of specimen under a head of 15m least, for not less than 8 hours. An external pressure of at least 150KPa shall be maintained.

## **2.2. Spheroidal Graphite Cast Iron ... Why?**

### **2.2.1. Emergence & Advantages of SG Cast Iron**

Iron castings have been there in our society and produced for weapons of war, art and culture, somewhere symbolizing strength & toughness of human being and many more functional forms, for more than 2000 years and still have an influence on our day to day life. The iron industry in a sense produces many usual and key products, and most of them are additionally processed, assembled, and then incorporated as an integrant of various machines, equipment and consumer items. The Fe-C binary system is broadly divided into two parts, i.e., steel and cast iron, on the basis of % of C. The first part is steel containing up to 2.1% of Carbon diffused into pure iron, whereas the other one has 2.1% - 6.67% of Carbon, and known as cast iron. Cast iron is not a single alloy; rather it is set of different alloys consisting white cast iron, gray cast iron, and malleable cast iron, which are differentiated on the basis of graphite orientation in the matrix. White iron and gray

cast irons are brittle due to the presence of different carbides and flake-like shaped graphite respectively. The flaky graphite acts as stress raiser [Fig.2.6 (a)] and helps in premature localized plastic flow leading to the brittleness of gray cast iron. Unlike these, the malleable cast iron is carbidic and has to undergo a “malleablizing” or “annealing” heat treatment that converts the carbides into roughly spherical graphite form referred as “temper carbon.” Due to this spherical form of graphite, the malleable iron becomes more ductile compared to white or gray cast iron, but the carbide formation at the time of solidification causes shrinkage resulting the need for more feeder material; consequentially increasing the production cost.

Despite the fact, there was much progress achieved in the manufacture of cast iron, at the American Foundrymen’s Society (AFS) in 1943 J.W. Bolton made a statement, "Your indulgence is requested to permit the posing of one question. Will real control of graphite shape be realized in gray iron? Visualize a material, possessing (as-cast) graphite flakes or groupings resembling those of malleable iron instead of elongated flakes" [34]. In response to this statement in 1948 at AFS convention Henton Morrogh of the British cast iron research association publicize their successful production of spherical nodules in gray cast iron via the addition of small amount of cerium. After Morrogh’s declaration, the International Nickel Company disclosed their development, starting with Millis' discovery in 1943, of magnesium as a graphite spheroidizer. The International Nickel Company received US patent 2,486,760 On October 25, 1949, assigned to Keith D. Millis, Albert P. Gegnebin, and Norman B. Pilling.

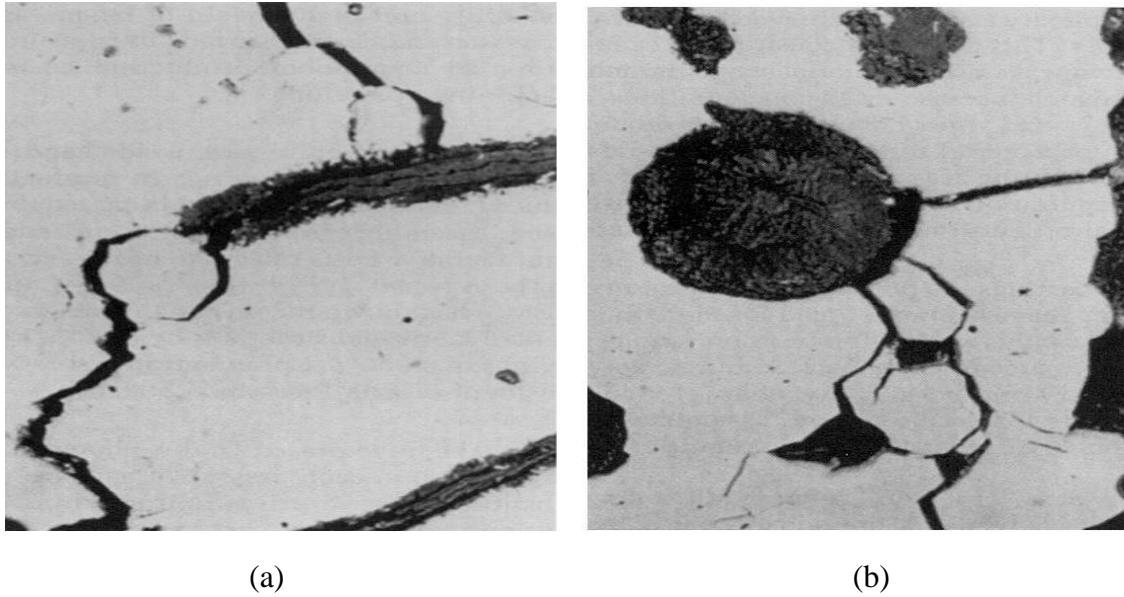


Fig. 2.5: (a) Micrograph of Gray Iron showing the crack-like behavior of graphite flakes [35], (b) Micrograph of Ductile Iron showing how graphite spheroids can act as "crack-arresters" [36].

Over the years from the emergence of SG cast iron, it has shown great improvement in terms of properties through alloying addition and heat treatment processes resulting evolution of desired microstructure for numerous applications. The major applications include agricultural equipment, earth moving machinery, pipes, automotive components, aerospace applications, energy sectors and power production, special engineering castings, decorative castings, hydro applications and many more. Because of the spherical graphite particles SG cast iron possess good ductility without compromising strength and as it is easily castable, it is widely preferred over other ferrous cast materials. A comparisomal data of properties of SG cast iron with other cast ferrous materials is presented in Fig. 2.7. Although every material has some individual properties which make them preferable in respective applications, the versatility of SG cast iron regarding mechanical properties and higher performance at a lower cost often attracts manufacturers. SG cast iron offers the designers to choose the highly ductile material, with grades having more than 20% ductility and tensile strength exceeding 900 MPa. Austempered Ductile Iron (ADI) even offers the strength of about 1600MPa for thin wall casting. Furthermore, most industrial casting like steel and malleable iron requires additional attached reservoirs to compensate the shrinkage during solidification. On the other hand, the formation of spherical graphite causes an internal expansion of SG cast iron, and as a result, it can be cast without any significant shrinkage defects leading to the reduced requirement for additional material and increases the productivity of SG cast iron.

Characteristics	Ductile Iron	Malleable Iron	Gray Iron	0.3% C Cast Steel	White Iron
Castability	Dark Blue	Medium Blue	Light Blue	Very Light Blue	White
Ease of Machining	Dark Blue	Medium Blue	Light Blue	Very Light Blue	White
Vibration Damping	Dark Blue	Medium Blue	Light Blue	Very Light Blue	White
Surface Hardenability	Dark Blue	Medium Blue	Light Blue	Very Light Blue	White
Modulus of Elasticity	Dark Blue	Medium Blue	Light Blue	Very Light Blue	White
Impact Resistance	Dark Blue	Medium Blue	Light Blue	Very Light Blue	White
Corrosion Resistance	Dark Blue	Medium Blue	Light Blue	Very Light Blue	White
Strength/Weight	Dark Blue	Medium Blue	Light Blue	Very Light Blue	White
Wear Resistance	Dark Blue	Medium Blue	Light Blue	Very Light Blue	White
Cost of Manufacturing	Dark Blue	Medium Blue	Light Blue	Very Light Blue	White

BEST  WORST

Fig. 2.6: Comparison of the engineering characteristics of SG cast iron versus competitive ferrous cast materials. [37]

### 2.2.2. Types and Grades of SG Cast Iron

SG cast iron can be of different types and they are generally named according to their microstructure. Each member has unique typical strength, ductility, and surface characteristics, but they all share the nearby spherical graphite embedded in the matrix. Ferritic SG cast iron consists of graphite spheroids lodged into ferrite matrix, resulting in high ductility, low-temperature toughness, and low strength. It can be produced directly at the time of casting, but additional annealing treatment is also provided to achieve more ductility and uniform distribution of matrix without residual stress. The pearlitic grade of



ductile iron has spheroids of graphite in the matrix resulting higher strength and wear resistance than that of the ferritic grade. One of the most common grades, which can be produced by casting is the ferritic-pearlitic SG cast iron that has properties intermediate between ferritic and pearlitic grades with excellent machinability and lower production cost. These are the grades that can be directly produced by casting methods and controlling the rate of cooling during solidification. However, the addition of alloying elements such as Cu, Ni, Mo, etc. and application of heat treatment can change the as-cast microstructure into martensitic, bainitic (upper and lower) and austenitic matrices. The tensile strength values for different matrices have been presented in Fig. 2.8.

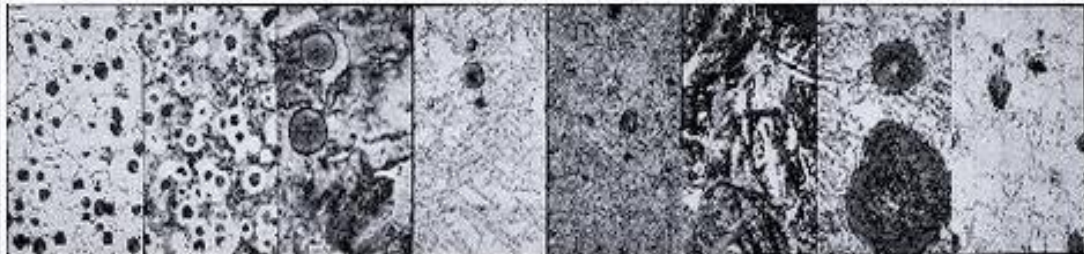
Matrix							
Ferritic Grade 5	Ferritic-pearlitic Grade 3	Pearlitic Grade 1	Martensitic (With retained austenite)	Tempered Martensitic	ADI Grade 150	ADI Grade 230	Austenitic
80,000 p.s.i. (414 mPa)	80,000 p.s.i. (552 mPa)	100,000 p.s.i. (690 mPa)	N.A.*	115,000 p.s.i. (793 mPa)	150,000 p.s.i. (1050 mPa)	230,000 p.s.i. (1600 mPa)	45,000 p.s.i. (310 mPa)
							
*Approximate ultimate tensile strength 87,000 p.s.i. (600 mPa) Hard, Brittle. (Note that the magnifications are different.)							

Fig. 2.7: Microstructure and tensile strength of various types of SG cast iron. [38]

Concerning the need and requirements of design engineers and foundries, a set of standards is created specifying the properties of SG cast iron, that simplifies the selection and purchasing appropriate grades of material for desired application. Once the bid is made according to the specified standard, the foundry is responsible for the casting to meet or exceed the properties regardless of the casting method, unless until specifically mentioned by the designer. The SG cast iron standards are defined by American, European, Japanese and national/international bodies like ASTM, SAE for promoting and ease of availability of design engineers. There are five different standards set by ASTM, out of which ASTM A536 is the most preferable and widely used grade. With the formation of European Community, the EN (EuroNorm) standards becoming increasingly

demand specification as compared to other standards of national and international specifications. All the standards are specified based on respective mechanical properties except austenitic and austempered SG cast iron.

Table 2.2: Various standards for SG iron design engineers [39].

Country	Standard	Grade	Tensile Strength (MPa)	Yield Strength (MPa)	% Elongation	Impact Energy (J)	Matrix Structure
North America	ASTM A536	60/40/18	414	276	18		
		65/45/12	448	310	12		
		80/55/06	552	379	6		
		100/70/03	689	483	3		
		120/90/02	827	621	2		
	SAE J434	D400	400	275	18	120	F
		D450	450	310	12	80	P+F
		D500	500	345	6	54	P+F
		D550	550	380	4	40	P+F
		D700	700	450	3	27	P
	ASTM A897	D800	800	480	2		P or TM
		850/550/10	850	550	10	100	
1050/700/7		1050	700	7	80		
Japan	JIS G5502	1200/850/4	1200	850	4	60	
		FCD 350-22	350	220	22	17	
		FCD 400-18	400	250	18	14	
		FCD 400-15	400	250	15		
		FCD 450-10	450	280	10		
Europe	EN 1563	FCD 500-7	500	320	7		
		EN-GJS-350-22	350	220	22		
		EN-GJS-400-18	400	240	18		
		EN-GJS-450-15	450	250	15		
		EN-GJS-450-10	450	310	10		
	EN 1564	EN-GJS-500-7	500	320	7		
		EN-GJS-800-8	800	500	8		
		EN-GJS-1000-5	1000	700	5		
		EN-GJS-1200-2	1200	850	2		
		EN-GJS-1400-1	1400	1100	1		

South Africa	SABS 936/937	SG 38	375	245	17		F
		SG 42	410	275	12		F
		SG 50	490	345	7		F & P
		SG 60	590	390	4		P
		SG 70	685	440	3		P
		SG 80	785	490	2		P/TM
	SABS 1656	ADI 850	850	550	10	100	
		ADI 1050	1050	700	7	80	
		ADI 1200	1200	850	4	60	
		ADI 1400	1400	110	1	35	
		ADI 1600	1600	1300			

F - Ferrite, P - Pearlite, TM – Tempered Martensite

ASTM A897, EN 1564, SABS 1656: Austempered grade

### 2.2.3. SG Cast Iron as SNF Cask

Since the late 70's and early 80's of the twentieth century, when transportation and dry storage of spent nuclear fuel came into the picture, SGCI was considered the appropriate candidate. Use of SGCI offers near net final shape monolithic casting without shrinkage in product dimension, wide range of property variation, elimination of welds in the containment boundary and above all its cost of fabrication over other types of designs and materials. These benefits draw quite an interest to study the behavior of SGCI under the specified conditions, for fabrication and to be used for nuclear material transport and storage casks.

In 1983, Lawrence Livermore National Laboratories prepared a report which was reviewed by Transnuclear, Incorporation addressing the design criteria for ductile failure and developing criteria for preventing brittle failure in SG cast iron shipping containers in accordance with U. S. Nuclear Regulatory Commission (NRC) guide [40]. In the report, it was recommended that a safety factor of 4 for stress intensity factor on minimum ultimate tensile strength and a ductility value high enough should be considered for SGCI material to be used as a nuclear fuel transport cask fabrication. Also, the fracture toughness of 37 Ksi $\sqrt{\text{in}}$  (40.65 MPa $\sqrt{\text{m}}$ ) is the most appropriate value to be considered for designing the ductile cast iron spent fuel cask. Schwartz [41], in the preceding year, proposed similar conditions for SG cast iron to be used as nuclear fuel cask. Mochizuki & Matsushita [42] conducted experiments to evaluate the structural integrity of spent nuclear fuel cask fabricated with an unalloyed ductile iron equivalent to FCD 37 in the JIS Standard. The fracture toughness value of ferritic ductile iron was found to be very low, but analytically

it was confirmed that nodular cast iron containers are strong enough to withstand an impact load during drop tests if the applied stresses are less than the yield stress. Also, the critical flaw sizes associated with the yield stress were within the non-destructive inspection capabilities. Compared to steel, cast irons have shown brittle behavior under similar loading conditions. However, SGCI has more ductility compared to other cast irons due to the spherical shape of graphite, which prevents the stress concentration effect and restricts the path of crack propagation. Over the years SG cast iron with full scale or 1:2.5/1:3 scales of cask dimension, the safety against brittle failure under severe accidental conditions was being studied, following the test parameters recommended in the IAEA regulation [43]–[45]. It was reported that to get satisfied as a candidate material for nuclear fuel transportation and storage cask SGCI need to be ferritic grade which provides better elongation property along with strength. In addition to that, the tensile strength should be maintained 50% of the proof stress and a fracture toughness value of  $55\text{MPa}\sqrt{\text{m}}$ . In order to avoid testing of prototype casting which involves an enormous amount of money, finite element methods can be approached for the study. Brynda et al. [28] reported the major criterion for fabricating SNF transportation and storage casks. They addressed three major considerations: the structural integrity of the cask, damage due to radiation, and resistance to corrosion during loading of the SNF and under the climatic conditions at the storage sites. Ductile iron and austenitic corrosion-resistant 1% boronated Cr-Ni steel were used for cask fabrication (1:2.5 scale) and were tested using a 9m drop impact test on the edge of the casks dropped onto a flat base and a 1m flat-drop impact onto a spine protruding from a flat base. They concluded that both ductile iron and the austenitic corrosion-resistant 1% boronated Cr-Ni steel are suitable for the fabrication of SNF casks and satisfy the specified requirements. Teng et al. [46] and Jaksic and Nilsson [47] used an MSC (MacNeal-Schwendler Corporation)/Dytran three-dimensional program and continuum mechanics approach to solving this problem via analytical methods. Their test procedure consisted of a 1m drop impact test onto a flat undeformed concrete base and onto a steel bar to investigate the dynamic, nonlinear behavior of SGCI full-scale casks. The obtained results were in good agreement with the physically investigated results.

In the year 2005, SG cast iron was included in the ASME standard for material properties for spent nuclear fuel cask. The primary reason behind is that SGCI offers

homogeneous matrix structure and less production cost with better mechanical properties over other type of materials designed to be used for the SNF cask fabrication. The required properties of ferritic ductile iron to be used under low temperature conditions are specified in ASTM A874/874M standard. It is recommended that to be used as nuclear fuel transport cask or for applications concerning service in  $-40^{\circ}\text{C}$ , the microstructure of SGCI should be ferritic with no massive carbides. In addition to that the graphite must belong to type I and type II i.e., the nodularity value should be higher than 90% and the maximum percentage of carbon equivalent be 4.5. Tensile strength, proof strength and elongation should have minimum value of 300MPa, 200MPa and 12% respectively. During the last two decades number of works had been carried out and reported following different experimental as well as analytical techniques of investigation, to understand and enlighten the behavior of SGCI under various static and dynamic loading paradigms [48]–[53].

### **2.3. Effect of Alloying Element on Morphological & Mechanical Properties of SGCI**

To achieve desired properties for a particular application, control over matrix structure and morphological aspects is necessary, and that can be achieved by controlling processing parameters and the addition of alloying elements. The addition of alloying elements influences the mechanical properties by changing the cast matrix microstructure from ferritic to pearlitic, ferritic/pearlitic and/or austenitic depending upon the alloy composition. If the processing parameters such as tapping temperature and cooling rate are kept constant, the final matrix tends towards the matrix influencing element. Incorporation of Ni from 12-38% (max.), a highly ductile material of austenitic SGCI is obtained. On the other hand, a higher Si amount results in ferritic matrix and that of Cu and Mn lead to the formation of harder pearlitic matrix. A proper control of ferrite and pearlite influencing elements results in a mixed ferritic/pearlitic structure having properties intermediate between ferritic and pearlitic grades of SGCI.

#### **2.3.1. Effect of Base Composition**

**Silicon** is the most vital element in the production of SGCI and influences the solidification process in conjunction with Carbon. An increase of 1% Si content shifts the

eutectic composition towards the left (approximately 0.30% of Carbon), resulting in low solidification temperature. With increasing Si content the eutectoid Carbon content is lowered, and hence transformation occurs over a broadening range. Silicon is a graphitizer and ferrite promoter, hence reduces the strength properties of ferritic ductile iron, which if needed, further can be improved by the addition of desired amount of Nickel. Increased Silicon content increases the carbon equivalent (%CE), hence prevents the precipitation of carbides and allows the formation of more free form of carbon leading to increased nodule count and decreased hardness and UTS [54]–[57]. On the other hand, for austenitic grades increase in Si content increases the tensile strength & 0.2% yield strength [54]. The substantial influence of silicon on the ductile-brittle transition temperature of ferritic Ductile Iron is shown in Fig. 2.8 [58]. From the figure, it is clearly understood that to achieve optimum low-temperature toughness, the amount of Si should be maintained as low as possible. Fully ferritic carbide free ductile iron production needs high purity charge materials, proper holding and casting practice and highly effective inoculation for maximum nodule count. Higher amount of Silicon leads to a reduction in low impact toughness, increased DBTT and decreased thermal conductivity. Si is held below 2.2% when producing the ferritic grades and between 2.5% and 2.8% when producing pearlitic grades [59], [60].

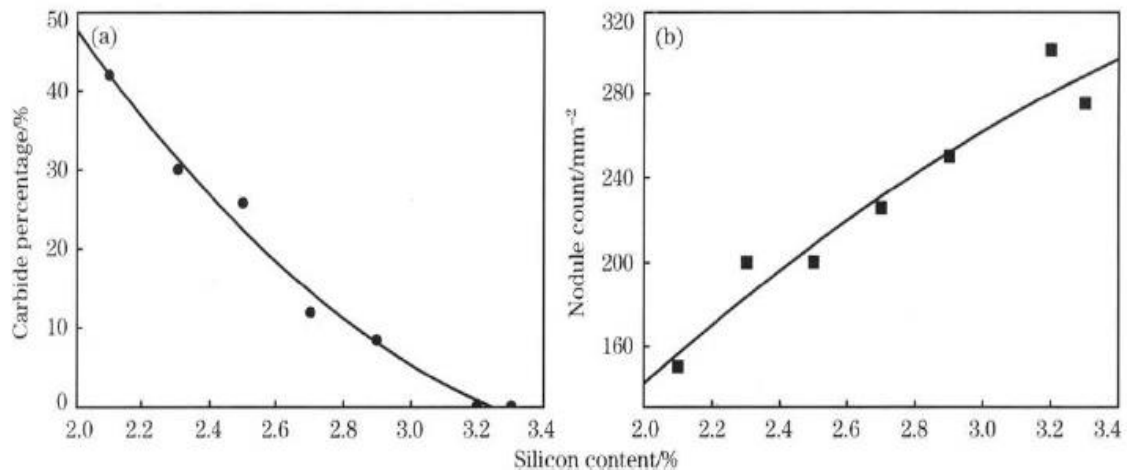


Fig. 2.8: Variation of carbide percentage (a) and nodule count (b) in ductile cast iron with Silicon content [55]

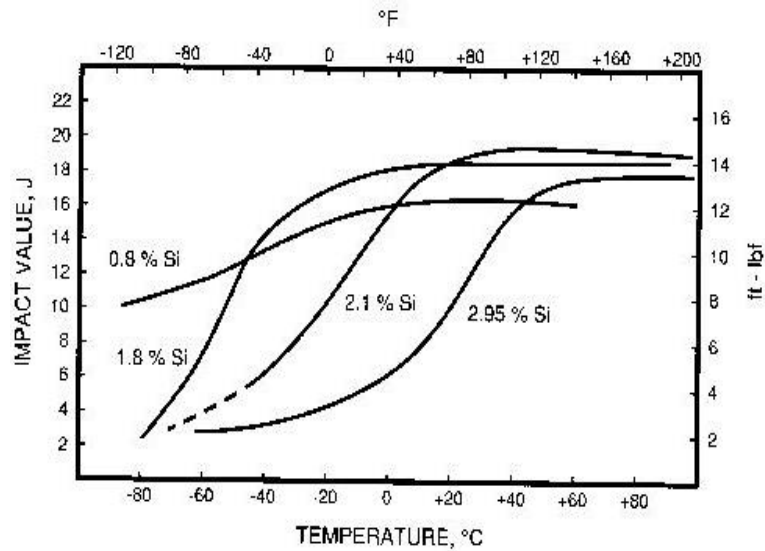


Fig. 2.9: Influence of silicon content on the v-notched Charpy energy of ferritic Ductile Iron [58].

**Manganese** stabilizes carbide very strongly at eutectoid graphitization and increases the amount of combined carbon. Excess Mn has little effect on solidification and only weakly retards primary graphitization. The presence of a correct amount of Mn forms manganese sulfide and reduces the proportion of combined carbon by removing the effect of sulfur [36]. Being a mild pearlite promoter, it influences only a few properties like proof stress, hardness to a small extent. Mn retards the onset of the eutectoid transformation, decreases the rate of diffusion of Carbon in ferrite and stabilizes cementite ( $\text{Fe}_3\text{C}$ ). However, the problem here is the embrittlement caused by it so that the limiting range would be (0.3-1.01) [59]–[62]. Mn is held between 0.4% and 0.6% when making pearlitic grades and below 0.3% when making ferritic grades and can be achieved by dilution with high purity pig iron to avoid pearlite and carbide formation [60], [61]. Higher Mn content leads to increased pearlite content resulting in increased strength and hardness and decreased elongation. However for a ferritic grade of SGCI Mn dissolved into the ferrite matrix and improves strength [63]. Use of higher Mn level is not preferred as it causes segregation at the grain boundaries that causes grain boundary carburet and creation of secondary phase along the boundaries leading to degradation in plasticity in SG cast iron. In combination with Ni, higher manganese content can stabilize austenite and increases carbide by depressing the solidification cooling curve encouraging graphite to segregate at a lower temperature consequentially resulting lower generation of free graphite and reduced ductility and impact toughness [64]–[67].

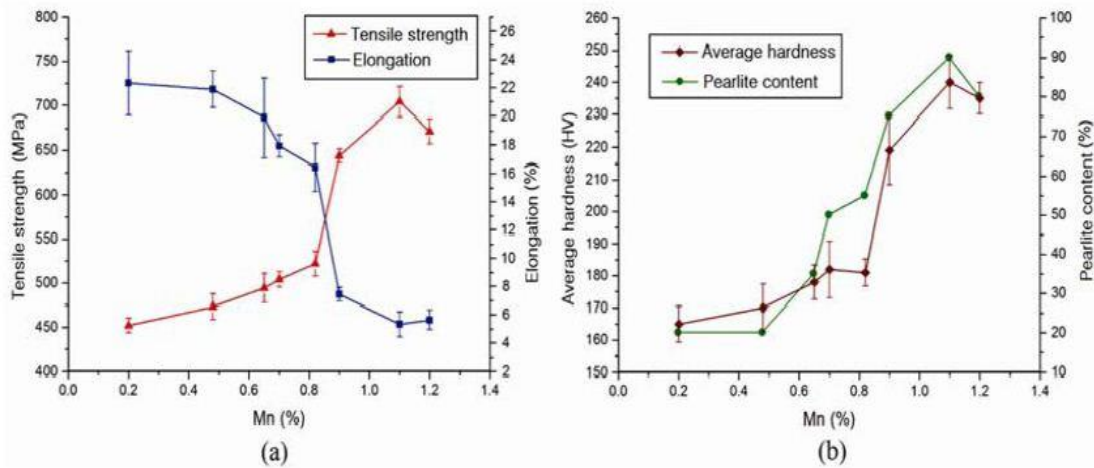


Fig. 2.10: The relationship between tensile strength, elongation, average hardness and pearlite content versus Mn content (0.05% Cu) [63]

**Sulfur** affects the form of carbon in a manner which is opposite to that of Si. The higher the S content, the higher will be the amount of combined carbon, thus tends to form a hard and brittle matrix. An excessive amount of S will increase the tendency of gross defects more than 0.015% promote the formation of quasi-flaky graphite [35, 43]. The addition of S is done for better machinability, but it is kept around 0.009%, and maximum 0.015% as the larger additions of Sulfur may cause the hot (red) shortness[59]. Sulfur is an active interfacial element and has less solid solubility in austenite, therefore, gets enriched in liquid melt and at the freezing point. The presence of S encourages the eutectic graphite to branch frequently resulting in formation of chunky graphite [68].

**Phosphorus** combines with iron to form iron phosphide and produces a ternary eutectic with cementite and austenite. The ternary eutectic is known as steadite, which is relatively brittle and tends to form a continuous network outlining the primary austenite dendrites resulting lower toughness. It increases fluidity and extends the range of eutectic freezing, thus increasing primary graphitization when Si content is high. Incorporation of P above 0.05% can produce internal defects. It also causes embrittlement of iron, increases the ductile-brittle transition temperature, promotes galvanizing and temper-embrittlement. P often segregates to grain boundaries and produces carbide/phosphide complexes, hence needs to be maintained as low as possible. P is kept intentionally low as it causes cold shortness and so the properties of ductile iron will be degraded [59].



**Magnesium** is used as nodularizer and responsible for spherical form of graphite, but at lower level chunky graphites are formed. Like Sulphur, it is also an interfacial element and has less solid solubility in austenite. Magnesium makes the eutectic graphite grow with screw dislocations along the crystal orientation, giving the eutectic graphite growth characteristic into a spherical form. The lower level of Mg counteracts the surface activity of Sulphur and Oxygen promoting the formation and growth of chunky graphite particles. Due to the segregation effect when Magnesium content becomes high enough the graphite shape converts to spherical form [68].

If these elements are controlled at proper levels, then the only remaining variable is the shape, size, and distribution of graphite nodules that influence the mechanical properties of as-cast SGCI. However besides the base composition the properties of SGCI of any type and grade can be developed by incorporating different alloying elements separately or in combination.

### 2.3.2. Effect of Alloying Element

**Chromium** prevents the corrosion by forming the layer of chromium oxide on the surface and prevents the further exposition of the surface to the atmosphere. However, as it is a strong carbide former, it is not required in carbide free structure. In general it is kept around 0.05%. It must be kept <1% in GGG-50 grade [59].

**Nickel** is used for strengthening ferrite in addition to Si leading to increased UTS without compensating ductility and impact values. It is usually added in traces due to high cost and also to avoid the embrittlement of matrix (if it exceeds 2%) [59]. Increased Ni content decreases the ductility for austenitic grade SGCI [54]. Nickel is known to shift the transformation temperature range, i.e. the effect produced at higher temperatures for nickel-free iron is attained at lower temperature ranges when it is alloyed with nickel. Nickel has the ability to stop the precipitation of secondary carbides in the upper bainitic range. Uma et.al [69] studied the effect of toughened austempered SG cast iron with increasing Ni content up to 2.5%. It is reported in their work that, with increasing Ni content pearlite content is increased in the as-cast matrix. Also, the retained austenite gets stabilized in the final microstructure. It is increased due to the fact that Ni concentrates in the austenite phase in the ( $\alpha+\gamma$ ) region, resulting in increased impact toughness and wear resistance. When subjected to austempering treatment, SG cast iron with Ni content higher than 0.5% slows down the bainitic reaction and causes the formation of martensite at the

austenite cell boundaries on cooling [70]. Although the addition of Ni promotes the stabilization of austenitic matrix in SG cast iron, it accelerates the formation of pearlite by shifting the knee of transformation diagram to higher time intervals. Thus, the eutectoid transformation of ductile cast iron in cooling austenite has resulted in a significant amount of pearlite structure and decreasing nodule count and increased yield and tensile strength and hardness and decreased ductility and impact toughness [71].

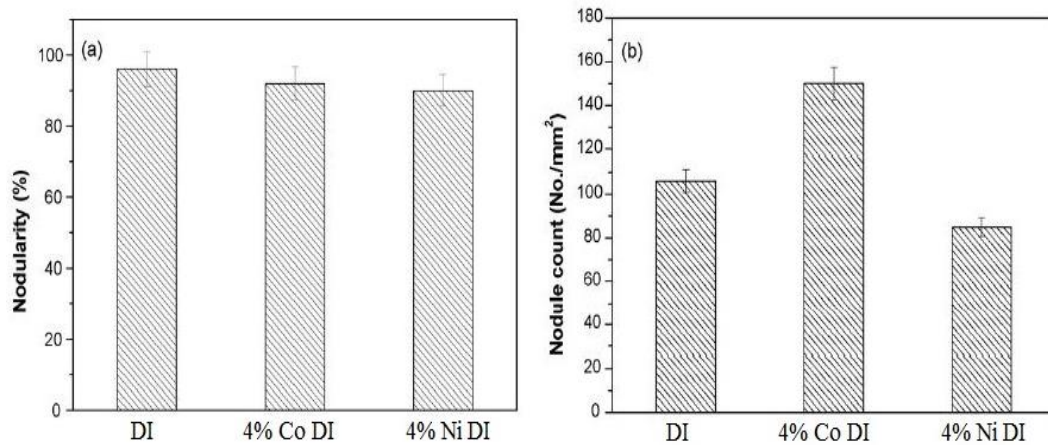


Fig. 2.11: Comparison of nodular graphite of the Co & Ni alloyed SG cast irons: (a) nodularity and (b) nodule count [71].

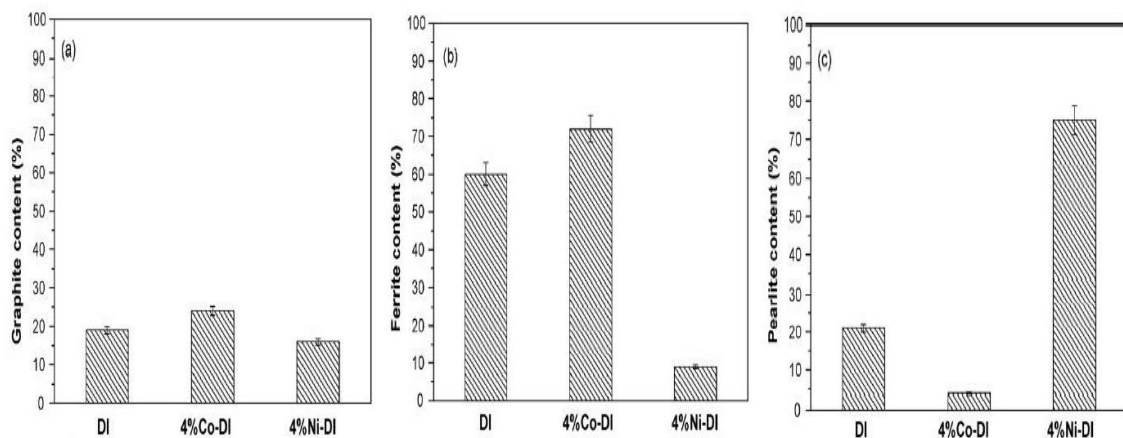


Fig. 2.12: Comparison of constituent content in the microstructure of the Co & Ni alloyed SG cast irons: (a) graphite, (b) ferrite and (c) pearlite [71].

**Copper** is a strong pearlite promoter and is undesirable in ferritic grade. It increases the UTS, 0.2% yield strength and hardness without an embrittlement in the matrix. In total Cu is kept between 0.4-0.8% [57], [59], [60]. Along with promoting, it also refines the slice distance of pearlite in the eutectoid transformation period and is beneficial in stabilizing super-cooled austenite and increases the closing rate of the

austenite shell that enables graphite to achieve perfectly spherical shape [63], [70]. Copper strengthens the matrix when Mn levels are low. Unlike Mn, copper has an adverse effect on segregation and usually gathers at the interface between graphite and matrix. As a result, the diffusion of C is restricted due to a higher concentration of Cu, which leads to the formation of perfectly spherical nodules and increased nodule count. The combined effect of Cu & Ni, when subjected to austempering treatment, balances the hardenability, segregation tendency of Mn and inhibits the transformation of untransformed austenite into pearlite during quenching to austempering temperature. An excess amount of Cu results in the evolution of copper or copper-rich phase that affects the mechanical properties [72], [73].

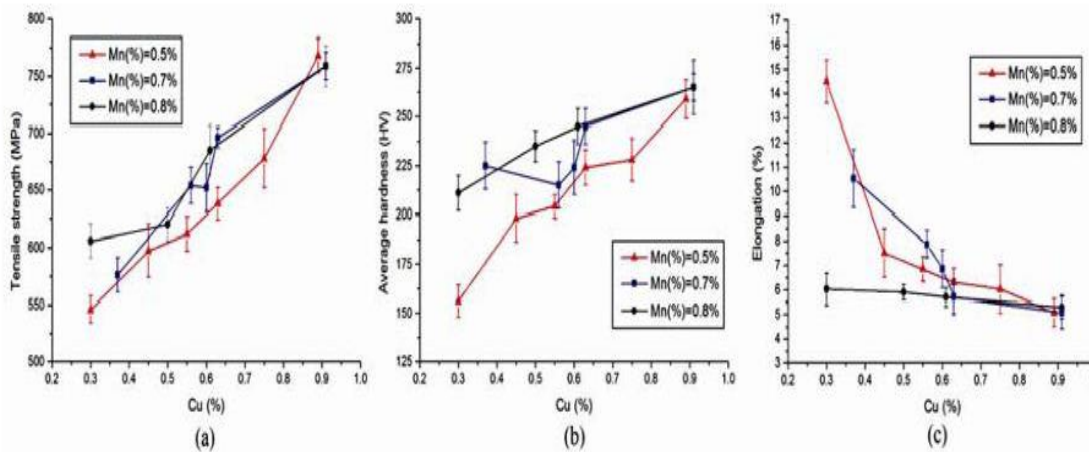


Fig. 2.13: Relationship between the mechanical properties and the Copper content for different Mn level [63].

**Molybdenum** is a mild pearlite promoter and forms intercellular carbides especially in heavy sections leading to increased proof stress and hardness and also improves properties at elevated temperature [59]. Also, Mo segregates at the grain boundaries causing decrease in impact toughness. When subjected to austempering or ausforming process, increased amount of Molybdenum stabilizes and increases austenite and bainite content. At zero Mo content the matrix is mainly bainitic, but with the increased amount it also increases the amount of carbide [74]. Mo, with an extreme tendency of segregating to the last solidification area, retards the bainite reaction and causes the micro shrinkage porosity in the intercellular region. Consequently, the Mo alloyed iron offers the lowest impact strength [75].

**Rare earth (RE) materials** in the nodularizer can eliminate the bad effect of the interferential elements like Titanium, Bismuth, Arsenic, Antimony, etc. and reduce the content of Si and Mg, which is helpful to avoid graphite degeneration [57]. Ferro et al [76] in their work reported that the graphite structure and nodule count can be improved by a well-dosed amount of RE elements in the inoculant composition. This is caused by a large decrement in surface free energy at liquid/graphite interface due to adsorption on graphite. RE elements also favor the graphite shape due to their neutralization effect of excesses of contaminants which cause nodule degeneration. However excess RE metals may cause graphite deterioration, especially in heavy castings where they form micro-segregation at grain boundaries, which can be neutralized by proper addition of Bismuth. In another work by Choi et al [77] it was reported that addition of rare earth elements influences the formation of ferrite at the vicinity of graphite nodules. The addition of RE increases the ferrite thickness with increased casting thickness due to slower cooling rate than that of castings without RE. However, in the case of thicker casting (40mm), it does not play any significant role on ferrite formation. Also increasing RE up to 0.02% there was a reduction in nodule size and the nodule size increases with increasing RE from 0.02% to 0.03%. However, the graphite nodule size is further decreased when the RE content is again increased to 0.04%. Furthermore, the presence of RE changes nucleation and growth rate by changing the liquidus temperature. The addition of RE appears to increase undercooling, as a result of which its nucleation rate is increased, but the growth rate is decreased. Rare earth elements like Lanthanum increases nodule count with increasing content when La to S ratio is as low as 1, hence increases the strength and ductility. However, it does not show any significant development in the nodularity value, which remains almost constant with increasing La amount [78].

## **2.4. Effect of Heat Treatment on Morphological & Mechanical Properties of SGCI**

Heat treatments are applied to obtain desired properties for any particular application to minimize the production cost by avoiding the addition of alloying elements. The heat treatments carried out by heating the component up to or above critical temperature (referred as austenitizing temperature) followed by different rate of cooling or quenching in furnace, air, certain oil or water bath and sometimes even in salt baths, leading to transformation of as-cast matrix into various fine or coarse matrix structures. The final microstructure obtained depends on the chemical composition, austenitizing

temperature and time, cooling or quenching medium and in some cases further reheating to certain temperature (referred as second stage transformation temperature) and soaking period at that particular temperature. This transformation results in variation of microstructure and micro constituents leading to enhanced properties. The application of heat treatment is chosen based on the desired property and application of the end product. In general, for ferritic or pearlitic grade of SGCI following heat treatments are applied.

**1. Stress Relieving:** Castings with complicated shapes requires stress relieving treatment to remove stresses generated during the solidification process. This operation does not affect the microstructure of as-cast specimen, rather helps grain refinement and results in slight increase in toughness and reduction in hardness. It is carried out at 510-675°C and holding there for 1 hour plus 1 hour per 25mm section thickness, followed by furnace cooling to 290°C followed by cooling in air to room temperature.

**2. Annealing:** To achieve maximum ductility and good machinability of SGCI, annealing treatment is carried out resulting in fully ferritic matrix with graphite nodules embedded within. Annealing can be performed in three different ways. (i) Austenitizing the casting to 900-950°C and holding there for 1 hour plus 1 hour per 25mm section thickness followed by furnace cooling to 690°C and keeping there for 5 hours plus 1 hour per 25mm thickness. After this, the casting is furnace cooled to room temperature. The holding time at austenitizing temperature may be up to 8 hours for heavy castings. (ii) In the second method after austenitizing the casting is furnace cooled to 650°C by maintaining the cooling rate below 20°C/hour, followed by furnace cooling to room temperature. In both of these cases, the final matrix obtained is necessarily fully ferritic. However, when impact strength is not of great significance and carbides can be tolerated in the matrix the 3<sup>rd</sup> method of annealing is opted. In this case, austenitization is carried out at 700°C and hold there for 5 hours plus 1 hour per 25mm section thickness followed by cooling to 590°C in a furnace. For superior machinability Mn, P and alloying elements such as Cr, Ni and Mo should be kept as low as possible, because these are carbide promoters and among them chromium carbides take the longest time to decompose at 925°C. Annealing usually produces partial decomposition of the pearlite structure and improves machinability [60]. Annealing of SG cast iron comprises of a slow process of diffusion process, and hence does not have a significant effect on nodule count, but can improve the nodularity in the ferritic matrix compared to that of as-cast matrix [79], [80].

This facilitates the removal of thermal stresses involved during the casting process and improves microstructure refinement, consequently increases the ductility and toughness but reduces the strength and hardness of the component. In the work carried by El-Banna[80], it was reported that with increasing the austenitizing temperature above 900°C the ferrite volume fraction increases, whereas at temperatures below 900°C the ferrite matrix also contain some sub boundary structure.

**3. Normalizing:** This process is opted when tensile strength and hardness is required to enhance. Casting is austenitized at the temperature range of 870-940°C and soaked for 1 hour followed by air cooling to room temperature. The temperature and time of soaking vary with composition, especially with Si and Cr contents. It is generally followed by tempering at 510-650°C and soaking for 1 hour, to achieve required hardness and relieve stresses during air cooling. Tempering is also adopted to improve toughness and impact resistance in addition to tensile strength. The microstructure after normalizing generally contains globular graphite logged in fine pearlite matrix. The martensitic structure can be obtained after normalizing treatment in case of alloyed light weight casting. Normalizing process involves a faster cooling rate as compared to annealing resulting in increased pearlite content and decreased lamellar spacing of pearlite structure. As a result of this, the material hardness and strength is increased with increasing pearlite content [81].

**4. Hardening & Tempering:** After austenitizing the casting is oil quenched followed by immediate tempering in the range of 300-600°C for 1 hour plus 1 hour per 25mm section thickness. To reduce the stress development during quenching, oil is preferred as quenchant; however, water and brine solution can also be used. For castings with complex shapes, oil is maintained at 80-100°C to avoid quench cracks. The microstructure of quenched SGCI appears to be martensitic, with tensile strength ranging from 700-1300 MPa, yield strength from 540-880 MPa and elongation of 10-12%. Shaker [82] in his work showed that hardening and tempering increases the workability limits with increasing tempering temperature. Also it was observed in the work that with increasing tempering temperature to 400°C, the martensite broke and formed tempered martensitic structure leading to reduced ductility as the embrittlement had already been progressed to detrimental degree. Depending on the chemical composition and nodule count, tempering treatment in the temperature range from 350-450°C lead to decreased hardness and provide ductility coupled with high strength.

**5. Surface hardening:** Pearlitic type SG cast iron are preferred for flame or induction hardening as time required for austenitizing is comparatively less. Prior to the hardening process, the casting are tempered at 595-650°C for 1 hour plus 1 hour per 25mm section thickness to remove virtually all the internal stresses. In this case the hardness increases to 600-750 BHN.

**6. Austempering:** It is the most preferred and commonly applied heat treatment for SGCI, to achieve the full potential of the material. It offers two different matrix microstructures depending upon the processing parameters such as austempering temperature and time. A tensile strength value of 1600 MPa with 1% elongation can be achieved in thin wall SGCI, whereas lowest strength value of 800 MPa with 16% ductility is achieved for heavy castings. However if the as-cast material is defective, then austempering lead to the inferior end product and the very advantage of adopting austempering will be lost. The casting is austenitized at 850-950°C and then quickly transferred to a liquid bath (salt solution) maintained in the temperature range of 235-425°C, and soaked there for a period of up to 4 hours followed by air cooling to room temperature. The final microstructure obtained in this case is bainitic matrix with spherical graphite particles embedded within. Due to the bainitic matrix austempered SGCI possess good machinability and wear resistance compared to other grades of SGCI. However, if high hardness is aimed the material needs to be machined prior to the treatment. The bainitic matrix of unalloyed SG cast iron is available either as lower bainitic or upper bainitic depending on the austempering temperature and time. The austempering process involves isothermal transformation of primary austenite ( $\gamma_0$ ) into acicular ferrite ( $\alpha$ ) and carbon enriched stable austenite ( $\gamma_c$ ), resulting in an ausferritic matrix structure. This ausferritic matrix may contain supplemental martensite, carbide, pearlite, and retained austenite when the austempering temperature ranges from 250 to 350°C, resulting in high strength with lower toughness. However, when the austempering time is increased to more than 2hr, the retained austenite disappears from the matrix, resulting in increased static as well as dynamic toughness [12]–[15], [17], [83], [84]. Furthermore, increasing the austempering temperature to greater than 350°C and the austempering time to more than 2 h results in only ferrite ( $\alpha$ ) and carbon enriched stable austenite ( $\gamma_c$ ) being present [85]–[88]. However, for austempering temperatures greater than 350°C and time shorter than 2 h, respectively, traces of retained austenite may be

present. The resulting matrix at higher austempering temperatures comprises coarser ferrite and austenite, leading to a coarse upper bainitic matrix that causes a considerable increase in strength along with increased toughness.

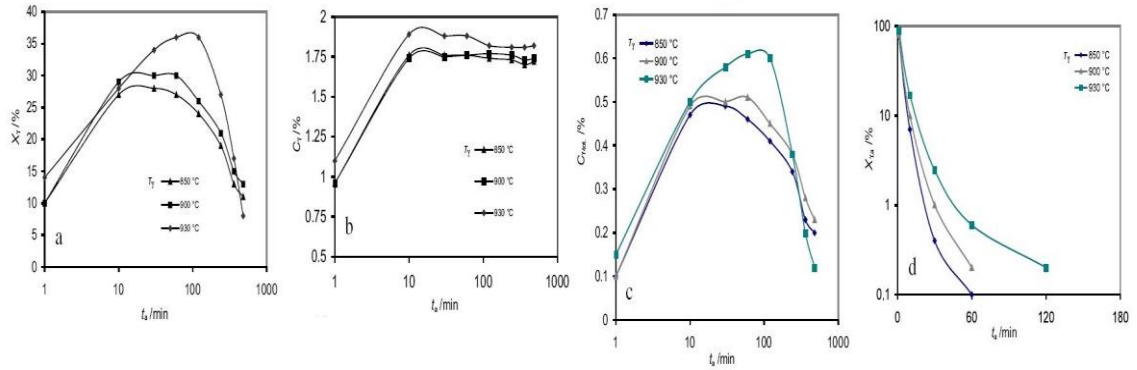


Fig. 2.14: Dependence of: a) volume fraction  $X_\gamma$  of retained austenite; b) austenite carbon content  $C_\gamma$ ; c) total carbon austenite content  $C_{\gamma,tot}$ , and d) untransformed austenite  $X_{\gamma,\alpha}$  on austempering time  $t_a$  and austenitizing temperature  $T_\gamma$ . [89]

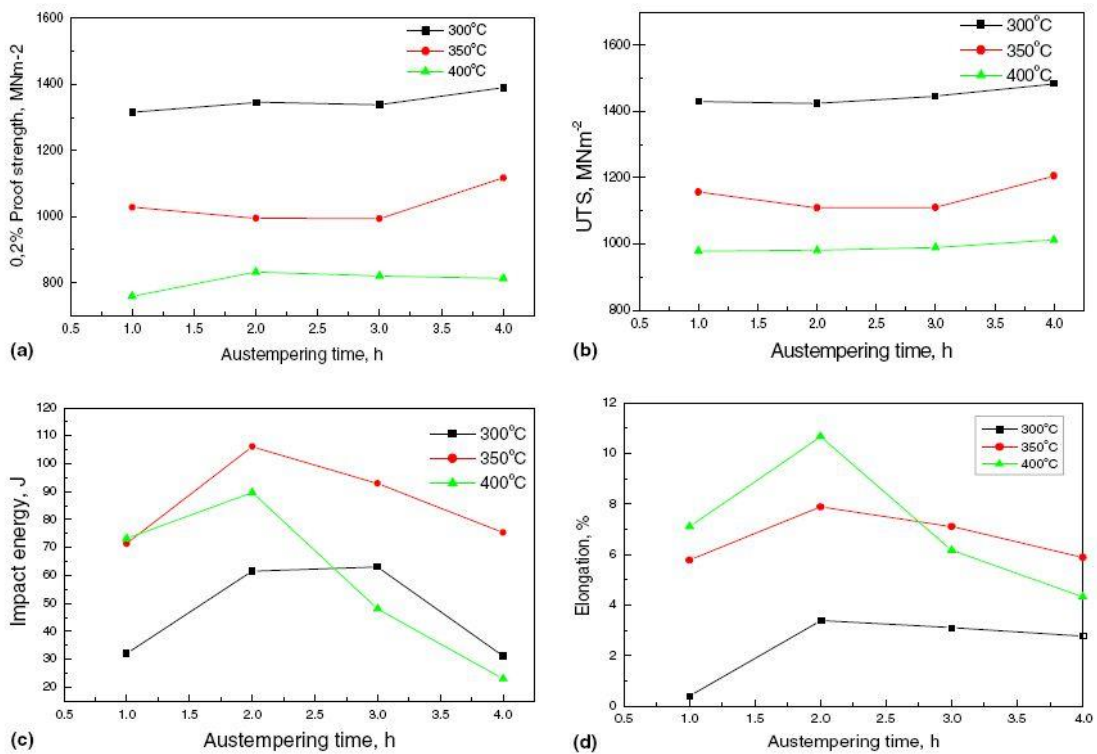


Fig. 2.15: The effect of austempering time on: (a) 0.2% proof stress; (b) UTS and (c) impact energy at different austempering temperatures[11].



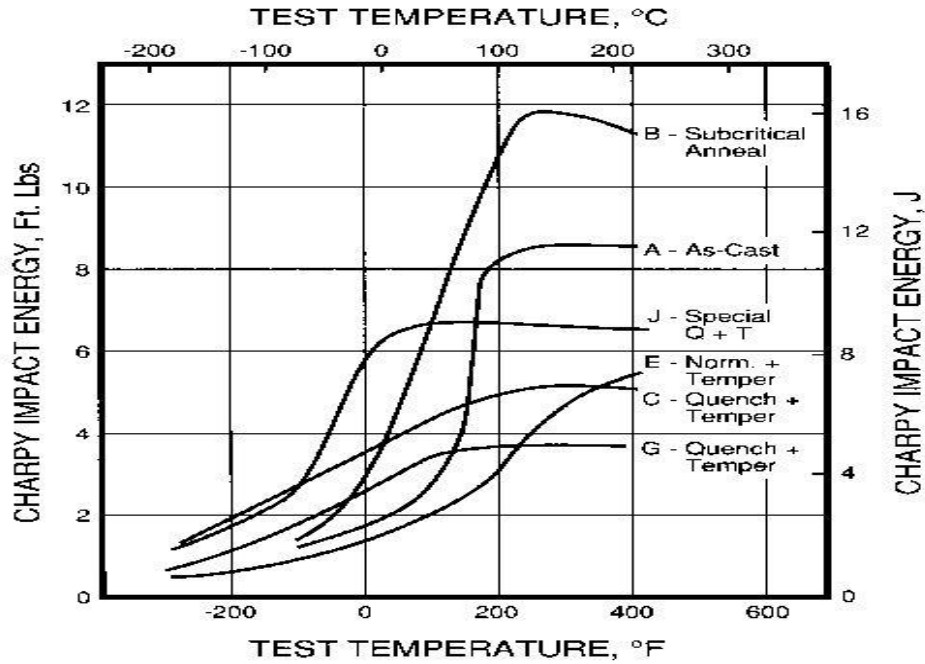


Fig. 2.16: Influence of heat treatment on the V-notched Charpy Behavior of Ductile Iron [90].

For the austenitic grade (obtained by adding Ni in the range of 12-30%) the heat treatments applied are:

- 1. Stress Relieving:** Large and complex SG Ni-Resist iron castings should be mold-cooled to 315°C before shakeout to relieve stresses. When required, stress-relief should be performed at 620-675°C.

- 2. Annealing:** Annealing, which softens and improves ductility primarily by the decomposition and spheroidization of carbides, should be conducted at 960-1035°C for 1 to 5 hours, depending on section size and the degree of decomposition and spheroidization required. Annealing should be followed by air cooling or furnace cooling if minimum hardness and maximum elongation are required. When SG Ni-Resist iron is to be used at temperatures of 480°C and above, the casting can be stabilized to minimize growth and warpage by holding at 870°C for two hours, followed by furnace cooling to 540°C, followed by air cooling to room temperature. To assure dimensional stability for all Types of SG Ni-Resist iron, the following heat treatment should be performed: holding at 870°C for 2 hours plus 1 hour per 25mm of section size; furnace cool to 540°C; holding for 1 hour per 25mm of section size, and slowly cool to room temperature. After rough

machining, reheating to 450-460°C and holding for 1 hour per 25mm of section size to relieve machining stresses followed by furnace cool to below 260°C.

## **2.5. Effect of Alloying & Heat Treatment on Corrosion Behaviour of SGCI**

Corrosion is an electrochemical process involving the oxidation of metal (the anodic reactions) and the corresponding reduction of another material (the cathodic reactions). Corrosion may be defined as “the undesirable reaction of a metal or alloy with its environment” and it follows that the control of the process may be affected by modifying either of the reactants (the metal or the environment). Corrosion is the gradual degradation of a material. SGCI components like pipes, windmill casing, nuclear and hazardous waste material container, etc., could be affected by environmental corrosion and hence reduced mechanical and physical properties leading to a shorter service life. Cast iron corrosion products are generally large in volume formed by reaction of the environment with ferrous ions that migrate from the underlying metal to the surface. Studies performed by Krawiec et.al [91] and Mohammadi et.al [92] confirmed the development of Si-rich layer on the surface that decreases the rate of corrosion and recommended that Cast irons with higher silicon content or nickel corrosion resistant cast irons should opt for components that fail due to corrosion. Ukoba et.al [93] investigated the response of SG cast iron to different corrosive environments and suggested that the components need to be stored in an air-conditioned environment for protection against corrosion failure. Corrosion in SG cast iron initiates at the ferrite-graphite interface and localizes near the nodules due to galvanic coupling where graphite nodules act as a cathode and accelerates anodic dissolution of the nearby ferrite [94]–[97]. Hence, the lesser nodule count means better corrosion resistance [92], [97]. Nickel addition decreases the rate of corrosion because it dissolves in the ferrite matrix and improves the electrode potential of the matrix that reduces the potential difference between graphite and ferrite which results in slowing down the reaction rate. Nickel and Copper addition reduces the nodule count and additionally form a compact  $\text{Cu}_2\text{O}$  passive oxide film over the alloy surface in chloride solution which is mainly responsible for better corrosion resistance. On austempering condition alloying elements like Cu, Ni, and Mo improves corrosion resistance significantly by reducing nodule count and increasing retained austenite in the bainitic matrix [97]–[99].

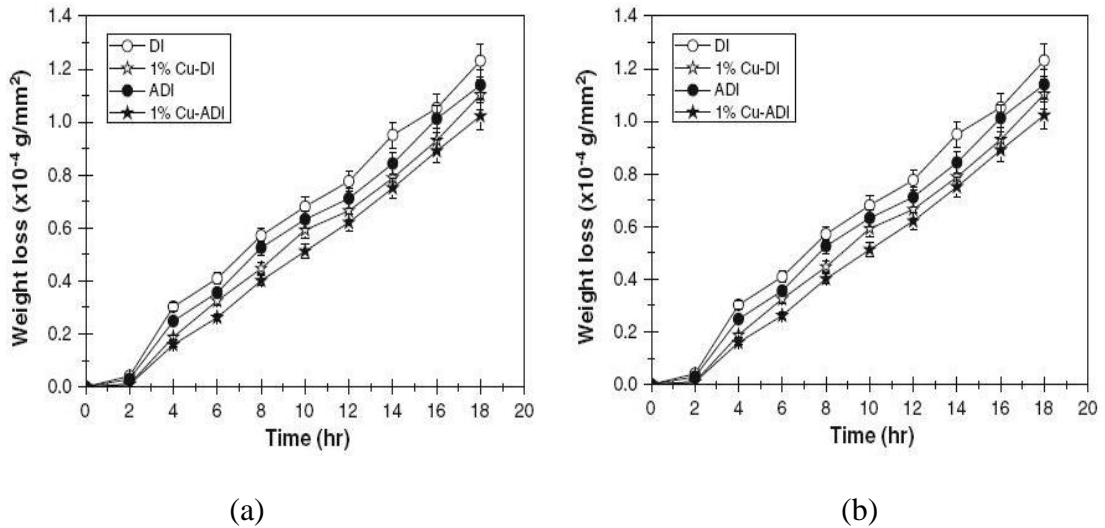


Fig. 2.17: (a) A comparison of weight loss of various irons after salt-spray [100],  
 (b) Weight loss of uncoated and coated ADIs in 10 Vol.% H<sub>2</sub>SO<sub>4</sub> aqueous solution [100].

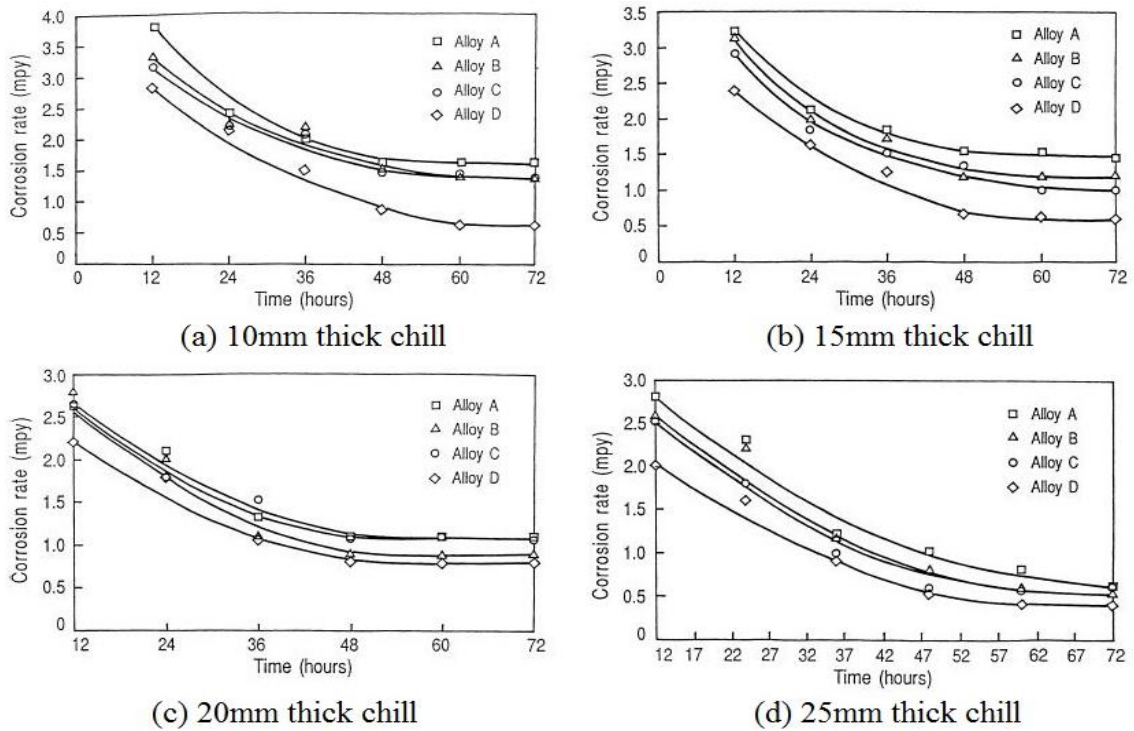


Fig. 2.18: Graph of corrosion rate vs. time for castings produced by varying chill thickness [101].

### 3. MATERIALS AND METHODS

#### 3.1. Processing of Materials

Spheroidal graphite cast iron material was melted and cast into (210×65×75) mm<sup>3</sup> ingots using open ladle treatment method at a commercial foundry(L&T Kansbahal, India). SG iron was produced by melting Pig iron, steel scrap; coconut charcoal and SG iron returns (scraps) in a coreless medium frequency induction furnace. Spheroidization was carried using Ferro-Silicon-Magnesium (45.5% Si and 6% Mg) and Ferro-Silicon (75% Si) inoculant was used for inoculation process. The molten metal was poured into the ladle at 1450°C (tapping temperature) and covered with tundis. After tapping commercial Argon gas was punched into the ladle for proper mixing and initiation of spheroidization process followed by addition of Fe-Si inoculant. Pre-inoculation, post-inoculation, and late-inoculation techniques were followed to produce quality ductile iron. After inoculation, liquid metal was poured at 1370°C into a sand mold for casting process. A similar process was followed to obtain SG iron with eight different compositions. Final chemical compositions of the alloys studied are presented in Table 3.1. Carbon equivalent was calculated according to the formula as in equation 3.1. The cast test blocks are shown in Fig. 3.1.

$$\%CE = \%C + 0.33(\%Si) + 0.33(\%P) + 0.4(\%S) - 0.027 (\%Mn) \quad \text{-----} \quad (3.1)$$



Fig. 3.1: SGCI test block after sand mold casting.

Table 3.1: Chemical composition of alloys studied in present research (in wt. %).

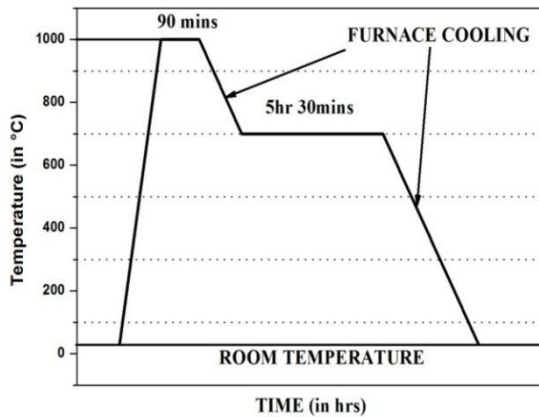
Alloy		SG-1	SG-2	SG-3	SG-4	SG-5	SG-6	SG-7	SG-8
<b>Elements (in wt. %)</b>	<b>C</b>	3.45	3.61	3.59	3.52	3.48	3.48	3.63	3.50
	<b>Si</b>	2.07	2.10	2.01	2.04	2.14	1.93	2.19	2.07
	<b>Mn</b>	0.15	0.20	0.17	0.17	0.14	0.19	0.25	0.17
	<b>S</b>	0.008	0.007	0.009	0.009	0.008	0.008	0.008	0.009
	<b>P</b>	0.024	0.022	0.023	0.022	0.021	0.019	0.033	0.018
	<b>Cr</b>	0.02	0.03	0.01	0.02	0.03	0.03	0.03	0.03
	<b>Ni</b>	0.15	0.47	0.45	0.11	0.46	0.49	0.09	0.44
	<b>Mo</b>	0.001	0.001	0.001	0.001	0.001	0.001	0.001	0.001
	<b>Cu</b>	0.007	0.009	0.007	0.020	0.010	0.010	0.014	0.009
	<b>Mg</b>	0.043	0.043	0.026	0.042	0.034	0.044	0.042	0.038
<b>Ce</b>	0.004	0.004	0.006	0.007	0.007	0.009	0.007	0.003	
<b>Carbon Equivalent (% CE)</b>		4.14	4.30	4.25	4.20	4.19	4.12	4.36	4.18

### 3.2. Heat Treatment Processes

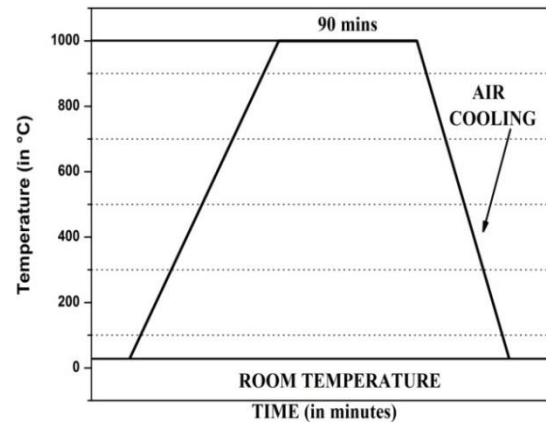
The physical and mechanical properties of ductile iron have a direct relationship with morphological characteristics such as phase volume fraction, nodularity, and nodule count that can be controlled according to desired property requirement and application. In general, it is done by either addition of alloying elements like Cu, Cr, Ni, Mo, etc. or application of suitable heat treatment processes. The effect of both the methods on properties of ductile iron is elaborately discussed in chapter 2.

In present work five different heat treatment processes viz. annealing, normalizing, quenching & tempering, austempering and intercritical austenitizing followed by quenching were employed to obtain different microstructures. The heat treatments were carried out with the help of OKAY raising hearth furnace (Max. Temp. – 1700°C) for austenitizing. And a pit furnace (Make - Process Instrumentation & Engineering CO.,

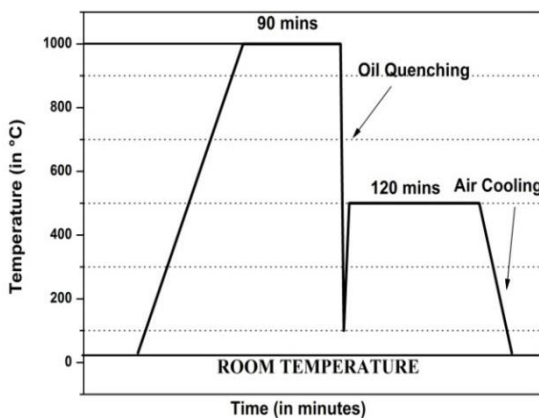
Max. Temp. – 2000°C) for reheating after quenching in the case of austempering and quench & tempering heat treatment. For austempering, specimens were quenched in  $\text{KNO}_3 + \text{NaNO}_3$  (1:1 ratio) and in the event of quench & tempering as well as intercritical austenitizing process specimens were quenched in mineral oil maintained at 100°C. The processes are presented in Fig. 3.2. For every heat treatment process except intercritical austenitization followed by quenching treatment (DMS-treatment), the austenitizing temperature was kept 1000°C and austenitization time is 90 minutes. The purpose of selecting such parameter was to achieve complete austenitization, consequentially homogenous matrix at room temperature after subsequent cooling or quenching process. Whereas, for DMS-treatment the austenitization temperature was kept at 800°C and 2 minutes of austenitization time, to avoid complete transformation of parent matrix into austenite.



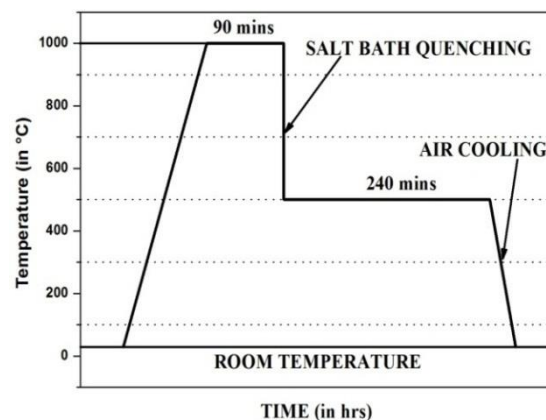
(a) Annealing



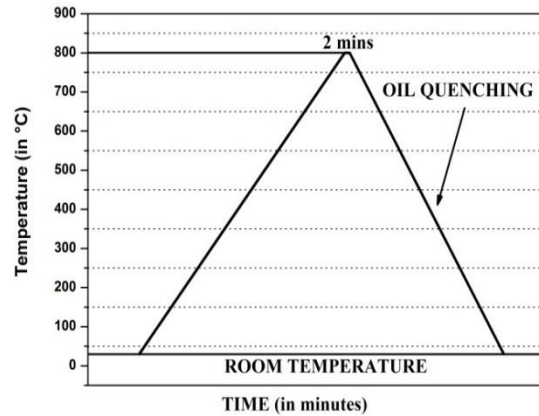
(b) Normalizing



(c) Quench &amp; tempering



(d) Austempering



(e) DMS treatment

Fig. 3.2: Heat treatment processes employed in present study.

### 3.3. Optical Microscopic Analysis

To understand the correlation between microstructure and mechanical property of SG cast iron in as-cast as well as heat treated condition the optical microscopic investigation was employed. Standard metallographic sample preparation technique was followed prior to conducting the microstructural analysis. Microscopic images of as-cast and heat treated specimens of individual alloys were taken, before as well as after etching with 2% Nital solution. The polished surfaces of individual alloy in as-cast and heat treated specimens were observed under the optical microscope incorporated with computer interface with ‘Metal Power’ Image Analyser tool. All the unetched specimens were observed at 10X magnification and undergone for quantitative metallographic analysis for measuring graphite characteristics such as nodularity and nodule count following ASTM E2567-13a Standard. The specimens after etching were viewed at 10X magnification except the austempered specimens which were observed at 20X magnification. The quantitative metallographic technique was also applied to the etched specimens to determine the phase volume fractions in respective as-cast and heat treated specimens of each alloy. The magnification was set to 10X for each and every specimen, before taking the image. A set of 10 clean and appropriate frame was captured for each and every specimen. Once the frames were captured, post processing was carried out with the image analyser tool. The graphite particles and the respective phases were differentiated by Yellow and Blue colour code. The minimum diameter of the nodule was measured by “Linear Measurement” option, which was found to be 8  $\mu\text{m}$ , and in the analyser tab the minimum nodule area was set to 50  $\mu\text{m}^2$ . all the frames were put for Nodularity and Nodule count analysis. Based on the colour code and area of the nodule a

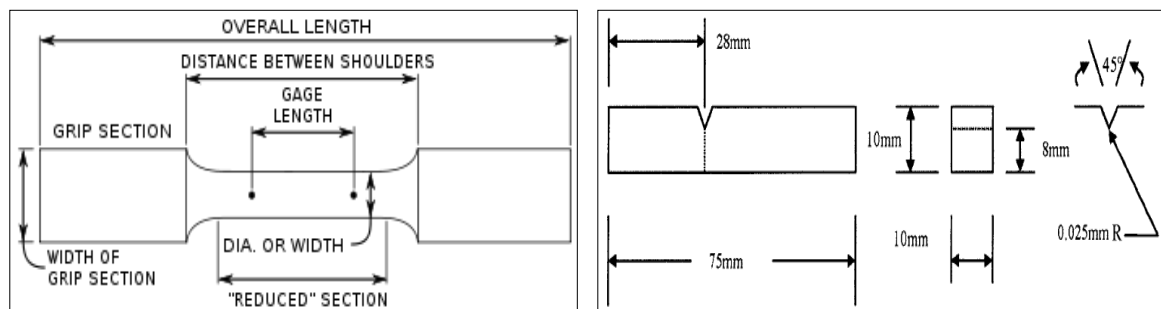
computer generated report was obtained for each specimen, mentioning nodularity and nodule count for each frame and average value as well

### 3.4. Determination of Mechanical Properties

After demoulding the ingots were machined into tensile and Izod impact specimens according to ASTM E8 and E23 – 12c standards respectively (at M/S Steelage Engineering Works, Rourkela, India). The tensile and impact specimens are shown in Fig. 3.2 (a) & (b) and the dimension of tensile specimen is presented in Table 3.2. Tensile strength, 0.2% yield strength and % elongation were determined by conducting tension test on INSTRON 1195 universal testing machine incorporated with a computer, at a crosshead speed of 1mm/min. Vickers hardness (HV) was measured using Vickers hardness tester applying 20 kg load. VEEKAY - TL VS4 Izod impact tester was used for obtaining the impact energy, applying 50 J hammer blow at a striking angle of 150°.

Table 3.2: Dimension for tensile specimen according to ASTM E8, FLAT SUBSIZE SPECIMEN

Grip section	1.25 inch
Width of grip section	3/8 inch
Gauge length	1±0.003 inch
Width	0.25±0.005 inch
Reduced section	1.25 inch
Overall length	4 inch
Thickness	0.005≤t≤0.25 inch



(a)

(b)

Fig. 3.3 (a): ASTM E8, flat subsize tensile specimen, (b): ASTM E23-12c, Izod impact specimen.



### 3.5. Corrosion Behaviour

Corrosion study was carried out by subjecting each specimen to sea water immersion under room temperature and pressure for ten weeks following ASTM G52 – 00 (Reapproved 2011) standard. Weight loss of each specimen is noted down after a regular span of time, i.e., 173 hours with the help of Contecmicrobalance (0.001 gm. accuracy). The corrosion rate is calculated by equation 3.2, as stated in the Standard ASTM G1 – 03 (Reapproved 2011).

$$\text{Corrosion rate} = \frac{K \times W}{A \times T \times D} \quad \text{----- (3.2)}$$

Where:

K =  $8.76 \times 10^4$ , A constant (decided on the basis of final unit i.e., mm/year in this case),

T = 173 hours, Time of exposure in hours,

A = 0.66 cm<sup>2</sup>, Area in cm<sup>2</sup>,

W = Mass loss in grams, and

D = Density in gm/cm<sup>3</sup>

### 3.6. SCANNING ELECTRON MICROSCOPE STUDIES

To investigate the mode of failure under monotonic tensile and dynamic impact loading condition, fractured surfaces for each as-cast and heat treated specimens after tensile and impact test is investigated under JEOL - JSM 6480LV, Scanning Electron Microscope.

To investigate the corrosion mechanism as well as role of chemical composition, corrosion products were investigated under SEM/EDAX elemental mapping. Two different type of products were analysed i.e., the corrosion scale over the surface of specimens and the porous product collected after 1<sup>st</sup> and 12<sup>th</sup> week of immersion.

### 3.7. X-Ray Diffraction Analysis

X-ray diffraction technique was employed to analyse the crystal structure and determination of phases of as-cast as well as heat treated specimens for every alloy studied. Rigaku Ultima – IV X-ray diffractometer with filtered Cu-K $\alpha$  target ( $\lambda = 0.1542$

nm) was used for getting the diffraction patterns by scanning specimens between  $40^{\circ}$ - $90^{\circ}$  at a rate of  $10^{\circ}$  per minute. Further, the patterns were analysed by Xpert Highscore and JCPDS software to get the crystallographic planes. The volume fraction of austenite and ferrite in individual austempered specimens were calculated using the Direct Comparison Method, assuming only two phases, i.e., austenite & ferrite were present in the matrix. The carbon content in austenite was also calculated using empirical formula stated in equation 3.4.

The corrosion products were also subjected to X-ray diffraction analysis to investigate the role of alloying elements in corrosion process during subsequent weeks of immersion. The scanning was carried out from  $20^{\circ}$ - $90^{\circ}$  at a scanning rate of  $10^{\circ}$ /minute.

## 4. RESULTS AND DISCUSSION

### 4.1 Microstructural Characterization

#### 4.1.1 Optical Microscopic Investigation

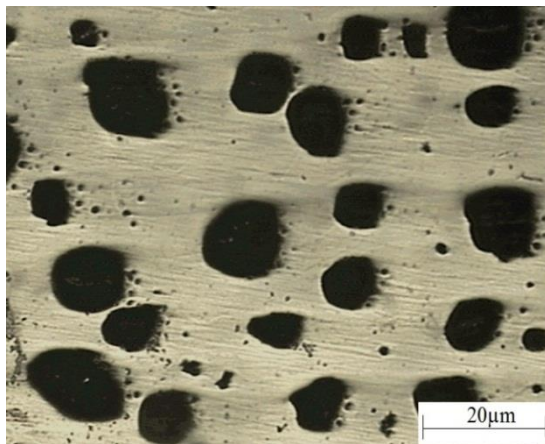
##### 4.1.1.1 EFFECT OF HEAT TREATMENT

The microstructure of as-cast and heat treated specimens without etching is presented in Fig. 4.1. It can be seen that graphite nodules are lodged into the respective as-cast and heat treated matrices. Quantitative metallographic analysis was carried out on these images to determine the nodularity, and nodule count for individual as-cast and heat treated specimens of respective alloys. Even though all the microstructure looks alike but the difference in nodularity and nodule count is clearly noticeable. Apart from the graphite nodules and the concerned phase, secondary graphite particles (which are not considered as nodules and ignored while determining nodularity and nodule count) can also be observed in as-cast as well as heat treated specimens. The nodularity and nodule count values of as-cast and heat treated specimens of respective alloys are presented in Table 4.1. The normalized, quench & tempered and austempered specimens are observed to have higher no. of nodules per unit area than those of as-cast and annealed specimens. The increased nodule count in specimens heat treated with faster rate of cooling was attributed to the increased cooling rate that suppressed the diffusion of carbon atom into the large graphite nodules during transformation resulting generation of more no. of graphite nucleation sites [7], [102]–[104]. Furthermore, due to the high rate of cooling the diffusion of carbon atoms from austenite into the parent nodules was restricted resulting increased nodule count as well as precipitation of secondary graphite particles. On the other hand, the annealed specimens have higher nodularity as compared to the as-cast samples. Annealing involves very slow transformation process, and consequentially no significant difference in nodule count was observed. The intercritically austenitized specimens did not show any marginal change in nodule count because it barely undergone a process of carbon movement due to minuscule austenitization time. However, the heat treated specimens observed to have increased nodularity as compared to the as-cast condition. The annealing heat treatment provided sufficient time for carbon accumulation into the neighboring graphite nodules resulting increased nodularity and decrease in no. of nodules per unit area. Whereas the normalizing, quench and tempering, austempering and

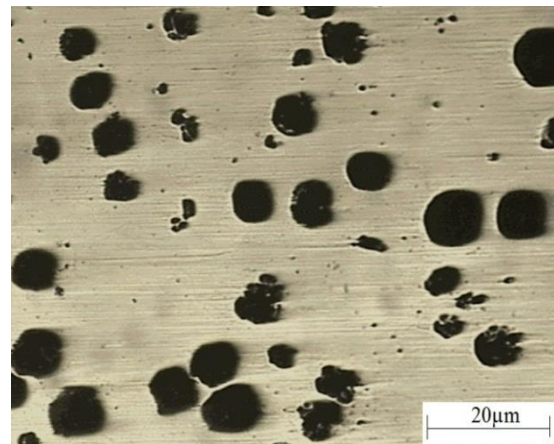
DMS treatment involves a higher rate of cooling that restricts the gathering of carbon into near graphite nodules and hence, led to smaller nodule diameter and increasing nodule count.

Table 4.1: Nodularity and Nodule Count of As-Cast and Heat Treated Specimens of Respective Alloys.

Alloy	Nodularity (%)						Nodule Count (mm <sup>-2</sup> )					
	As-cast	Ann ealed	Nor mali zed	Quenc h & Temp ered	Aust emp ered	D M S	As-cast	Ann ealed	Nor mali zed	Quenc h & Temp ered	Aust emp ered	D M S
SG-1	92	95	95	98	91	91	33	35	48	52	50	30
SG-2	95	100	97	99	93	100	28	30	46	49	43	25
SG-3	100	100	97	97	96	94	40	43	59	63	51	28
SG-4	94	96	96	96	93	92	29	33	39	43	33	35
SG-5	92	94	97	95.5	97	93	34	36	42	49	39	26
SG-6	100	100	100	97.5	94	96	40	42	47	51	42	33
SG-7	98	98	90	100	92	95	30	34	37	43	33	36
SG-8	92	94	95	96	90	98	33	36	39	47	36	39



(a) As-cast



(b) Annealed

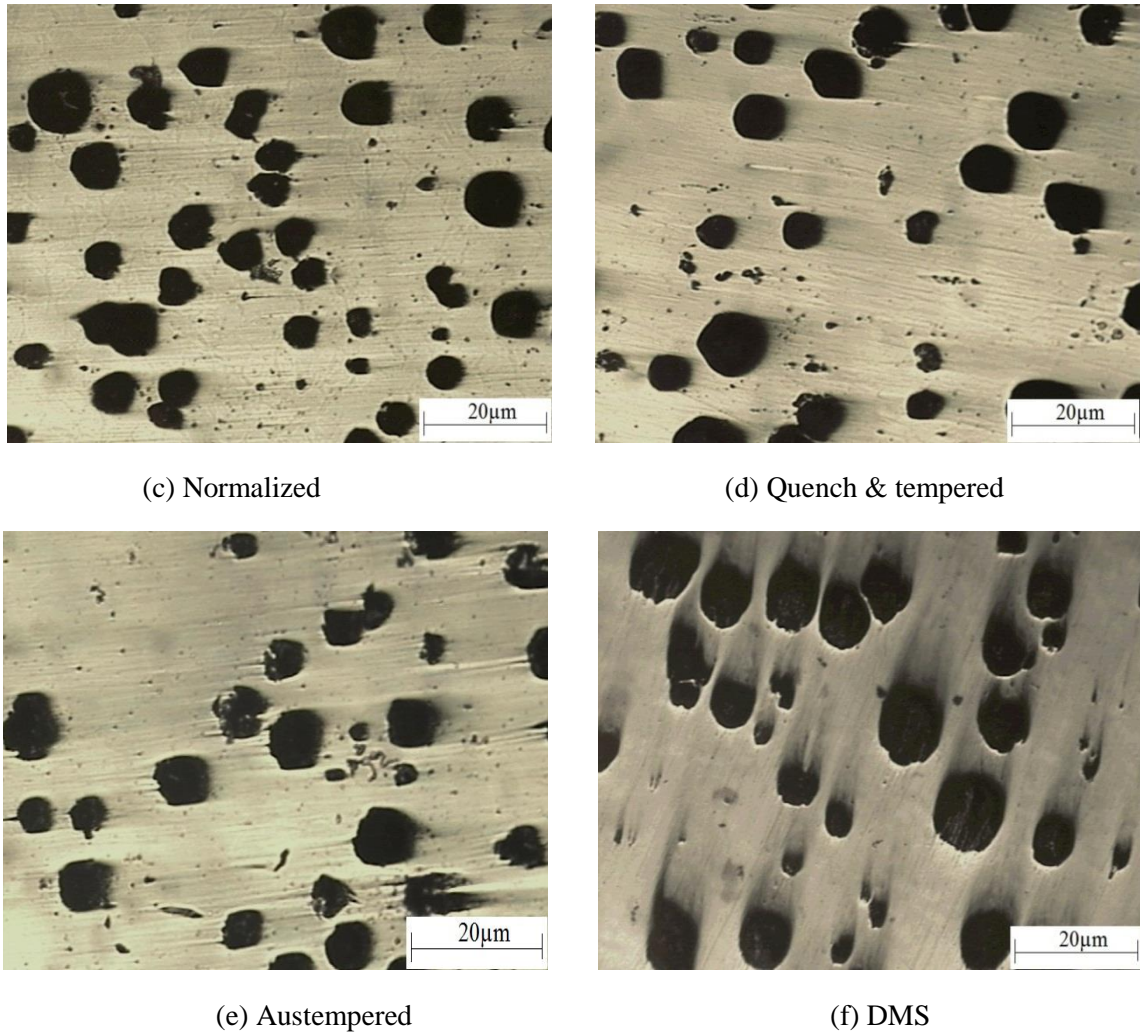
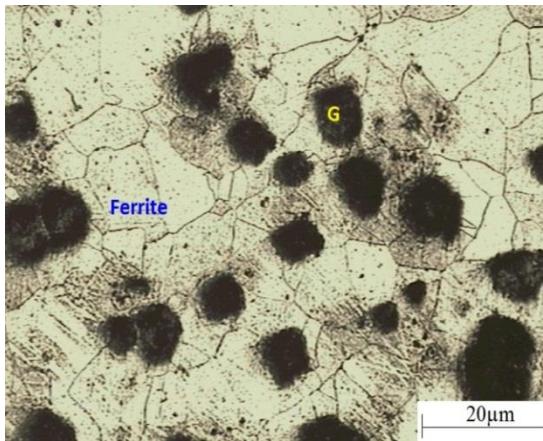


Fig. 4.1: Microstructure of Unetched as-cast and heat treated specimens.

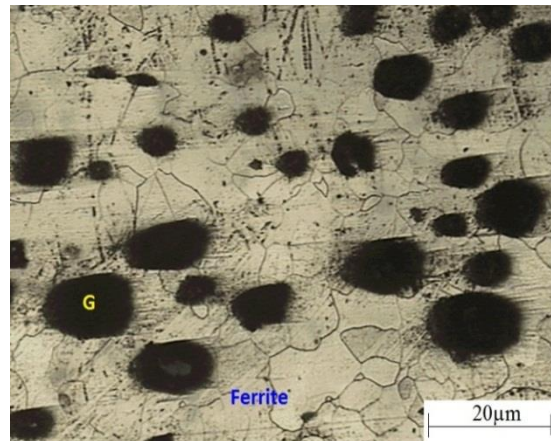
The microstructures after etching for respective alloys in as-cast and heat treated conditions are illustrated in Fig. 4.2. It was observed that the as-cast (Fig. 4.2 (a)) and annealed (Fig. 4.2 (b)) specimens have a fully ferritic matrix. The chemical compositions and the wt.% of alloying elements were so maintained; as required to obtain ferritic matrix in the as-cast microstructure. On the other hand, the annealing from high austenitizing temperature ( $1000^{\circ}\text{C}$ ) followed by longer holding time (330 minutes) at subsequent transformation temperature ( $700^{\circ}\text{C}$ ); provided large transformation window to achieve the fully ferritic matrix. The full annealing treatment resulted in a significant reduction in cooling rate (close to equilibrium eutectoid transformation temperature), which significantly increased the ferrite fraction in the matrix [105]. Specimens treated with normalizing heat treatment have transformed from as-cast ferritic to the pearlitic/ferritic structure (Fig. 4.2 (c)). Pearlite growth is a consequence of diffusion that depends on the transformation temperature. A higher transformation temperature leads to the lower

driving force resulting less growth rate about the diffusion speed giving rise to large pearlite spacing, whereas lower temperature results in finer spacing [106]. The quench & tempering heat treatment resulted in the transformation of the as-cast ferritic matrix into the tempered martensitic structure (Fig. 4.2 (d)). The tempering of oil quenched specimens at 500°C resulted in breaking of large martensite into tempered martensite [107]. The austempering treatment lead to the transformation of the as-cast matrix into the coarse upper bainitic matrix (Fig. 4.2 (e)) that can be accredited to two facts. One is the high austenitizing temperature and longer austenitizing time, leading to increased stable austenite and less ferrite formation [108] and secondly high austempering temperature and time that results in coarsening the ferrite [109]. Austempering involves a two-step reaction process consisting transformation of primary austenite into acicular ferrite and carbon enriched austenite in 1<sup>st</sup> stage reaction, and the 2<sup>nd</sup> stage reaction comprises a decomposition of carbon enriched austenite in ferrite-carbide aggregate depending on the temperature and time. The austempered specimens were observed to free from carbide and martensite due to the higher austenitizing temperature that resulted in complete austenitization and higher austempering temperature and time, i.e., 500°C and 240 minutes respectively that suppresses the carbide precipitation and martensite formation [88], [110]–[112]. Sohi et.al [113] in their work reported that, increase in austempering temperature resulted in higher amount of carbon in austenite leading to difficulty in martensite transformation on subsequent cooling. They have observed that the ductility and impact energy was increased and strength decreased when specimens were austempered at 350°C as compared to 315°C. Higher austenite volume fraction was expected in final microstructure in this study due to such higher austempering time, was found to be quite in agreement with the explanation provided by Sohi, and hence resulted in lower strength and higher ductility and impact energy. The bainitic ferrite is formed by the rejection of carbon from the graphite nodules or retained austenite. With the increase of bainitic ferrite size and amount, the austempering progresses by the further rejection of carbon into neighboring austenite. The increased austenitization time resulted in coarse austempered microstructure that can be credited to the grain growth of austenite resulting lower heterogeneous nucleation of ferrite . Specimens treated with intercritical austenitizing followed by quenching in mineral oil at 100°C observed to have graphite spheroids embedded with ferrite + martensite matrix (Fig. 4.2 (f)). Intercritical heat treatment commences with partial austenitization that depends on the alloy composition and temperature. The partial austenite transforms to martensite upon quenching in oil

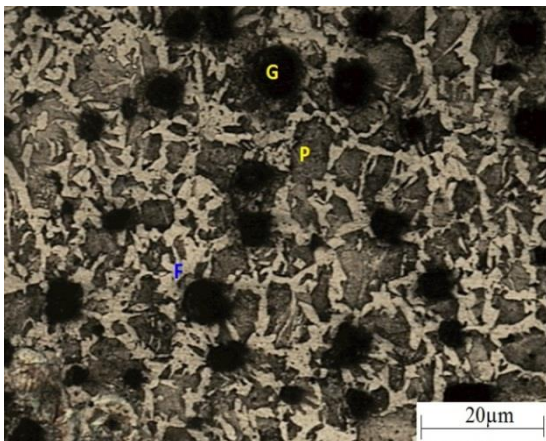
resulting in a final matrix of graphite nodules embedded in ferrite + martensite [114]. It was observed that most of the alloys have the large graphite spheroids surrounded by ferrite phase, which is further localized by martensite. Such arrangement of phases can be explained by the nucleation and growth of martensite at the intercellular boundaries [115]. It was noticed that the martensite was continuous and distributed uniformly in every alloy. All of the specimens was observed to undergone a complete transformation without any precipitation of carbides or retained austenite after respective heat treatment processes, which is good enough for obtaining higher ductility in respective materials. However, in every case presence of secondary graphite particles was observed that is associated with individual alloying elements and the presence of concerned matrix that restricts the diffusion of carbon from the neighboring austenite as the transformation progresses.



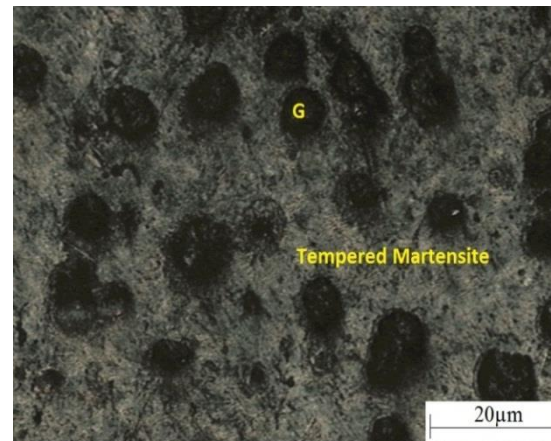
(a) As-cast (Ferritic)



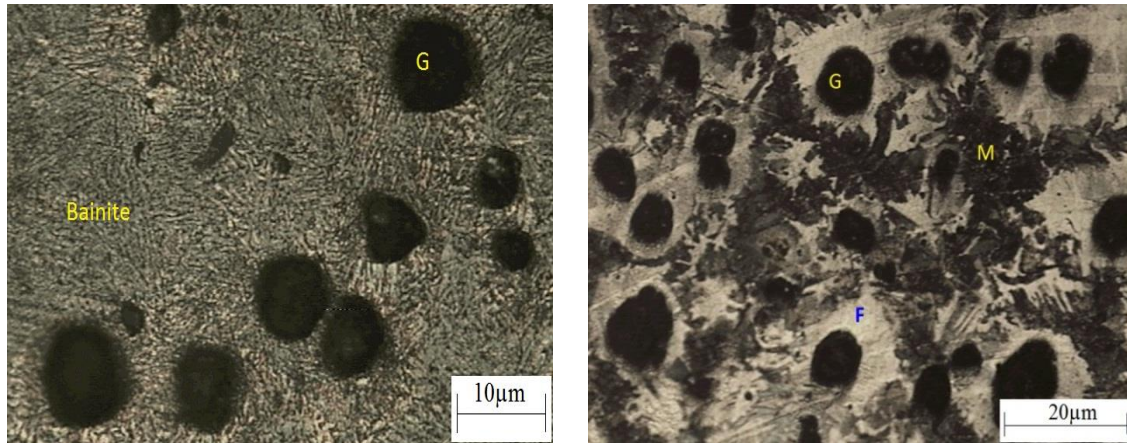
(b) Annealed (Ferritic)



(c) Normalized (Pearlitic/Ferritic)



(d) Quench &amp; tempered



(e) Austempered (Coarse Upper Bainitic)

(f) DMS (Ferrite + Martensite)

Fig. 4.2: Microstructure of As-cast and heat treated specimens after etching (Nital 2%).

F – Ferrite, G – Graphite, P – Pearlite, M – Martensite

#### 4.1.2 X-Ray Diffraction Studies

To investigate the structural changes in microstructure due to chemical composition and heat treatment processes small piece from all the specimens belong to each composition in as-cast as well as heat treated condition, was put to X-ray diffraction study. The respective XRD plots of every alloy in as-cast and heat treated conditions are shown in Fig. 4.3. It can be noticed that there was only three major crystallographic planes were found for every state i.e., plane (1 1 0) at  $43^\circ$ ,  $2\theta$  position with d-spacing of 2.02, plane (2 0 0) at  $65^\circ$  with d-spacing of 1.43 and plane (2 1 1) at  $82^\circ$  with d-spacing of 1.17. All of these planes belong to BCC crystal structure which confirms the ferritic, pearlitic-ferritic, tempered martensitic, and ferritic + martensitic matrix for as-cast, annealed, normalized, quench & tempered, and DMS treated specimens, as obtained from metallographic investigation. However for specimens underwent austempering heat treatment a plane of (3 1 1) was obtained at  $65^\circ$  with d-spacing of 1.43. The plane (3 1 1) belongs to the FCC crystal structure and thus confirms the presence of retained austenite in the matrix microstructure of austempered specimens. Quantitative XRD analysis was carried out for austempered specimens to determine the volume fraction of ferrite and austenite in individual alloys, following the Direct Comparison Method and assuming only ferrite and austenite was present in the matrix. The austenite and ferrite volume fraction and carbon content in the retained austenite was calculated from the equation stated in equation 4.1 and 4.2 respectively. It was observed that the carbon content in the retained austenite was increased with increase in the carbon content of the alloy. The



phase volume fractions in respective alloys are presented in Table 4.2. The volume fraction of retained austenite was observed to increase with the increase in Ni content as was observed from the quantitative metallographic investigation.

$$X_{\gamma} = \frac{I_{\gamma}/R_{\gamma}}{(I_{\gamma}/R_{\gamma}) + (I_{\alpha}/R_{\alpha})} \quad \text{----- (4.1)}$$

$$a_{\gamma} = 0.3548 + 0.0044C_{\gamma} \quad \text{----- (4.2)}$$

Where  $I_{\gamma}$  and  $I_{\alpha}$  are the integrated intensities and  $R_{\gamma}$  and  $R_{\alpha}$  are the theoretical relative intensity for the austenite and the ferrite, respectively. And  $a_{\gamma}$  is the lattice parameter of austenite in nanometre and  $C_{\gamma}$  is the carbon content of austenite in wt.%.

Table 4.2: Volume fraction of austenite and ferrite and carbon content in austenite of respective austempered specimens.

Alloy	Carbon content in austenite ( $C_{\gamma}$ )	Austenite volume fraction	Ferrite volume fraction
SG-1	2.5387	88.51%	11.49%
SG-2	2.5941	70.00%	30.00%
SG-3	2.6393	87.95%	12.05%
SG-4	2.5873	85.07%	14.93%
SG-5	2.5549	88.63%	11.37%
SG-6	2.5528	89.53%	10.47%
SG-7	2.6673	88.04%	11.96%
SG-8	2.5655	87.71%	12.29%

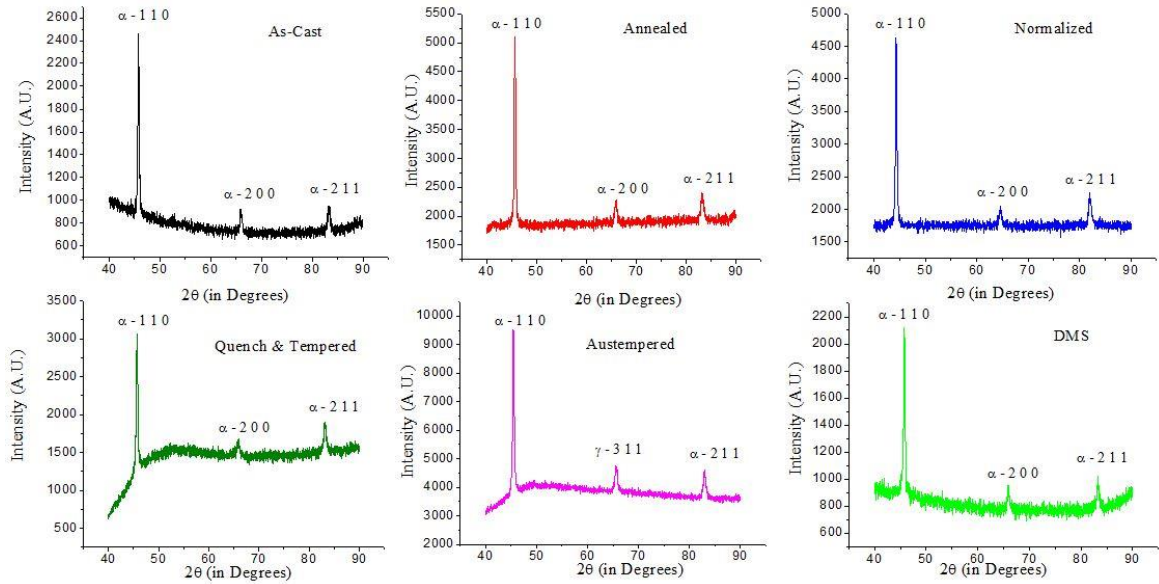


Fig. 4.3: X-ray Diffraction patterns of as-cast and heat treated specimens of individual alloys.

### 4.1.3 Effect of Alloying Elements on Microstructure

In Chapter 2 it was discussed that particular elements can promote ferrite formation whereas some promote pearlite and some nurtures the austenite transformation upon austenitizing process leading to different microstructures at room temperature upon cooling or quenching. The successful transformation of the as-cast matrix into different microstructure obtained through heat treatment processes and influence on nodularity and nodule count had been discussed in the previous section. The heat treatment parameters if varied within specified limit, can affect the phase volume fraction as well as nodularity and nodule count. However, in the present study, only a single set of process parameter was maintained for all the alloys and hence, the variation in microconstituents can only be credited to the alloying element. Chromium was present in very low quantity in each alloy i.e., 0.01 % - 0.03%, and Molybdenum in the final composition was found to be 0.001% in every alloy, hence the effect of both of these elements was insignificant. Similarly Sulphur was present in the range of 0.007 – 0.009 wt.% and that of Phosphorus in the range of 0.018 – 0.033 wt.%, and the effects were hence negligible. Sulphur and Phosphorous, generally leads to segregation in final microstructure after casting and heat treatment. But in current study no segregation was observed neither in as-cast nor in any of the heat treated specimens, that is attributed to the higher amount of Si content and high austenitizing as well as transformation temperature [116]. On the other hand, Silicon, Manganese, Nickel, Copper which was present in noticeable amount had shown their

influence on phase volume fraction and combined effect of Magnesium and Cerium was observed on nodularity and nodule count.

The influences of base elements as well as alloying elements are shown in Fig. 4.4. Silicon is inherently present in SGCI and it has the effect of modifying the Fe–C phase diagram, a three-phase region of ( $\alpha + \gamma + \text{graphite}$ ) is introduced into the Fe–C–Si phase diagram. The ferrite volume fraction of as-cast and annealing treated specimens was observed to increase with an increase in Silicon content Fig. 4.4 (a). Silicon also plays a significant role in graphite stabilization and was evident from the quantitative metallographic analysis. The graphite nodularity was observed to increase with Si content, and the growth in nodule count was credited to the combined effect of Si and C as well as Mg and Ce [117].

The normalizing treatment led to the pearlitic/ferritic matrix, although the austenitizing temperature and time were high enough to convert the parent matrix into the fully pearlitic matrix. Even though the combined effect of Mn, Cu and P content is sufficient to produce a fully pearlitic matrix [118], but was not enough to suppress the effect of Si leading to the presence of ferrite in the final structure. The pearlite fraction was observed to increase with Mn content Fig. 4.4 (b) and simultaneously there was an increase in ferrite volume fraction, Fig. 4.4 (c), with an increase in Si [117]. The amount of austenite is largely influenced by the presence of Mn, Ni, Cu and Mo and helps in dissolving carbon during austenitization process. As mentioned in the previous chapter that the Mo contributes only 0.001 wt.% of the chemical composition of every alloy, its effect on the final micro-constituents cannot be distinguished and so as the case for Chromium whose contribution to composition do not have varied significantly (or the difference is minor). The combined effect of Manganese, Nickel and Copper was observed for quench&tempered and austempered specimens. The quantitative metallographic analysis reveals that volume fraction of tempered martensite and bainite was increased with the increase of these alloying elements, Fig. 4.4 (d) and Fig. 4.4 (e) respectively [119]. A similar effect was also observed for DMS-treated specimens. The martensite volume fraction was observed to be increased by Mn content, and as Ni promotes austenite during austenitization process, the ferrite in the final matrix was observed to decrease. However, the presence Si only contributes to maintaining the graphite characteristics. The nodularity value didn't observe to change, whereas a slight increase in nodule count was noticed.

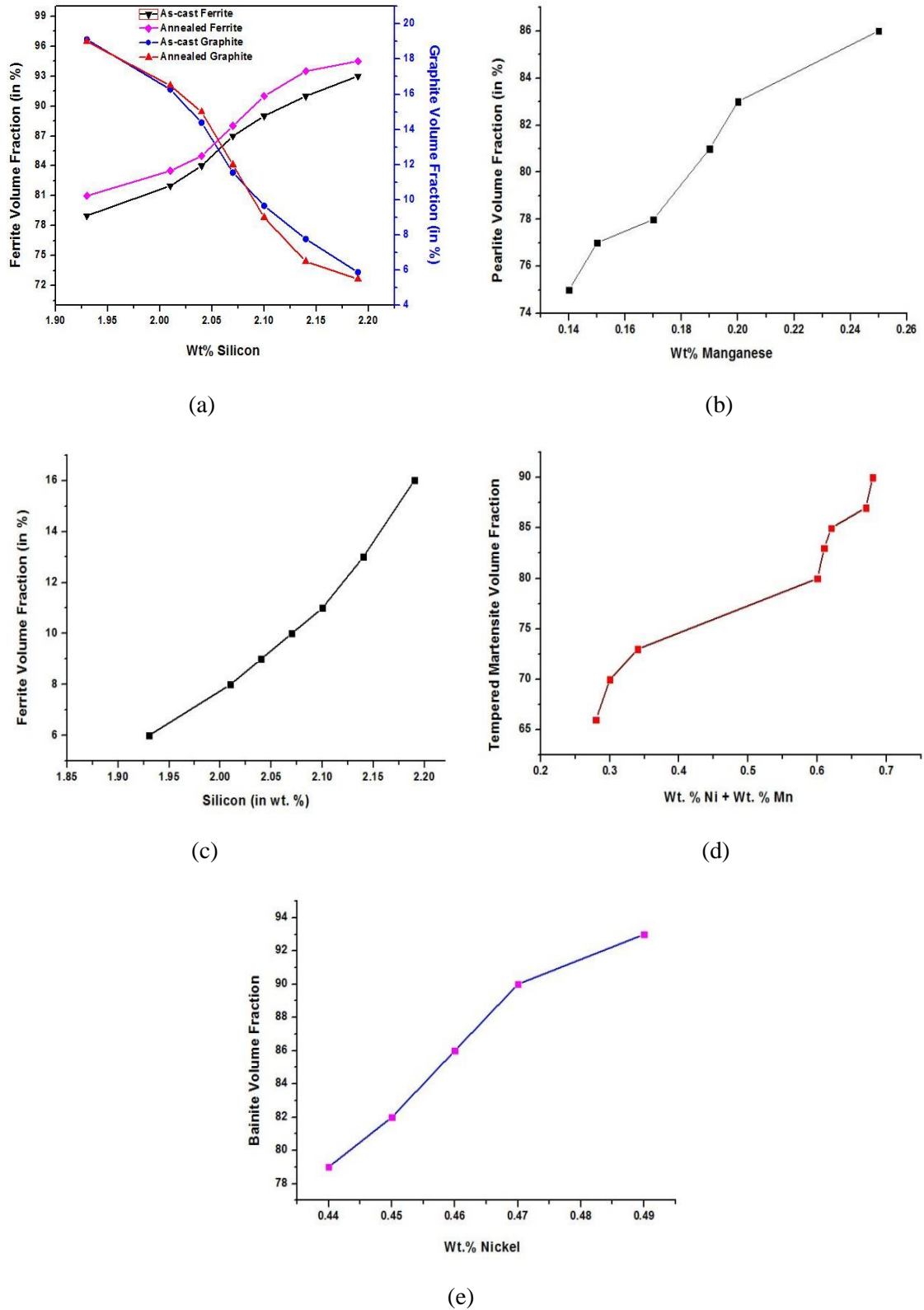


Fig. 4.4: (a) Wt. % of Silicon vs. Ferrite and Graphite volume fraction, (b) Wt. % of Manganese vs. Pearlite volume fraction, (c) Wt. % of Silicon vs. Ferrite volume fraction for normalized specimens, (d) Combined effect of Manganese and Nickel on tempered martensite volume fraction, (e) Wt. % of Nickel vs. Bainite volume fraction.

## 4.2 Mechanical Properties

### 4.2.1 Vickers Hardness

The bulk hardness was determined using Vickers hardness tester applying 20 KN load. The hardness values of as-cast and heat treated specimens of respective alloys are illustrated in Fig. 4.5. It is interesting to note that the standard deviation in hardness values is minuscule, which is an indication of uniform and homogeneous matrix, achieved by heat treatment processes. The difference in hardness of as-cast and annealed specimen was not noticeable, but slight decrement was observed in the case of the annealed sample. The highest and lowest hardness values of 301HV20 and 265HV20 respectively in the as-cast state were obtained for alloy SG-2 and SG-1 respectively, whereas the maximum and minimum hardness values in annealed condition were 292HV20 and 235HV20 for alloy SG-2 and SG-1 respectively. Annealing treatment involves a very slow cooling process; that softens the matrix by removing the internal stresses present in the as-cast samples during casting and machining process, consequentially lowering the hardness value even though the matrix was similar.

On the other hand, the normalizing treatment which might have transformed the parent matrix into pearlitic matrix had resulted in increased hardness. The highest hardness, i.e., 470HV20 was achieved for alloy SG-7 and that of lowest, i.e., 405HV20 for alloy SG-5. These values may be related to the pearlite volume fraction in respective alloys, as increased pearlite volume fraction enhances the hardness of material [106]. The hardness values of quench and tempered specimens range from a minimum of 565HV20 to maximum 609HV20 for alloys SG-2 and SG-7 respectively. On the other hand, alloy SG-7 showed lowest hardness value of 588HV20 in austempering condition and that highest value of 640HV20 was obtained for alloy SG-6. The hardness of quench & tempered and austempered specimens, were observed to be in agreement with the results reported by Dommarco et.al [104]. Bulk hardness of specimen subjected quenching and tempering heat treatment was found to be more than that of subjected to austempering treatment.

The hardness of DMS-treated specimens showed values greater than normalized and lower than quench & tempered and austempered treated samples. Alloy SG-8 was

appeared to have the lowest hardness of 497HV20 and alloy SG-6 had the maximum hardness of 522HV20 in DMS-treated condition.

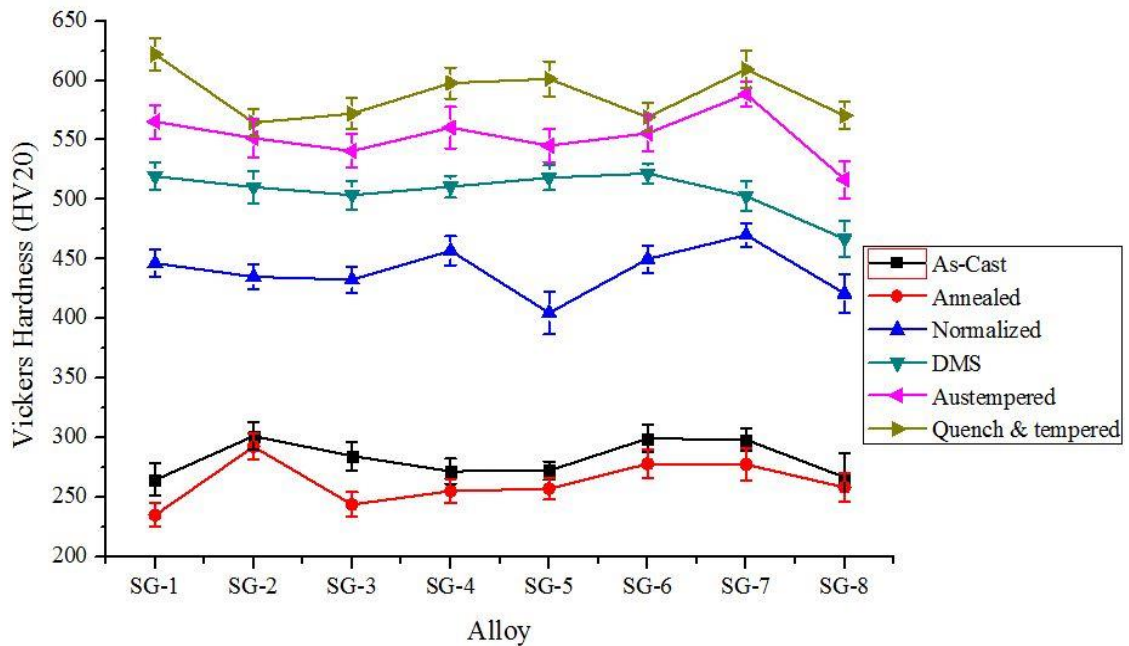


Fig. 4.5: Vickers hardness of as-cast and heat treated specimens of respective alloys.

#### 4.2.2 Tensile Strength & Ductility

The tensile strength and % elongation were obtained from the computer integrated INSTRON 1195 Universal Testing Machine, conducting the tensile test at a crosshead speed of 1mm/min, and the results were presented in Fig. 4.6. Specimens underwent full annealing treatment resulted with the lowest strength values and highest ductility, and that of greatest strength and lowest ductility was obtained for alloys in quench and tempered specimens. The strength and elongation values of the as-cast and annealed specimens were pretty close to each other without any significant difference, which may be due to the presence of similar matrix microstructure. However as mentioned in section 4.1.1; the large transformation window and the slow cooling process of annealing treatment led to lower hardness value; a similar effect was observed for decreased tensile strength and a favorable effect for improved ductility [103]. The alloy SG-7 had highest ductility (33.4%) and lowest tensile strength of 318.5 MPa, whereas that of alloy SG-6 had the lowest ductility of 26.1% and tensile strength of 364.8 MPa, in the as-cast state. Both the alloys were observed to have similar behavior for annealed specimens with 34% and 27.6% ductility and strength value of 310.6 MPa and 390.6 MPa for alloy SG-7 and SG-6 respectively. The highest ductility and lowest tensile strength of alloy SG-7 in as-cast and

annealed heat-treated condition was attributed to the higher Si content, i.e., 2.19 wt. % that would have resulted in maximum ferrite volume fraction [120].

The normalizing treatment led to the transformation of the as-cast matrix into the pearlitic-ferritic matrix, and the pearlite volume fraction has a directly proportional relationship with the amount of Mn in the chemical composition. The tensile strength value of 815.5 MPa was found to be the maximum for alloy SG-7, and that of the minimum strength was found to be 721.4 MPa for alloy SG-5, in normalized condition. Alloy SG-7 had 0.25wt.% of Mn content that could have led to highest pearlite volume fraction resulting maximum strength whereas the Mn content for Alloy SG-5 was 0.14wt.%, that end up with least strength. On the contrary, the elongation value was observed to increase with the increase in Si content as it promotes the ferrite volume fraction [118]. Even though alloy SG-7 had maximum Mn content leading to highest pearlite content, the maximum Si content also supported the retention of ferrite resulting highest ductility. Whereas alloy SG-6 had achieved the least ductility of 11.7% because of the lowest Si (1.93wt.%) amount.

In the case of quench & tempered specimens, a strength value of 1075.4 MPa was obtained to be the highest for alloy SG-6 with the least % elongation at break of 10.2% and that of alloy SG-7 had the least strength value of 853.6 MPa with maximum % elongation at break of 14.3%. On the other hand, the austempering treatment led to reduced tensile strength and improved ductility for all the alloys compared to that of in case of the quench & tempering heat treatment process. The reduced strength and improved ductility may be due to the bainitic matrix of austempered specimens. Alloy SG-6 with 0.49wt.% of Ni that fosters the formation of the bainitic matrix, had achieved maximum strength value of 1024.8 MPa and 13.8% ductility, and that of lowest strength value of 795.9 MPa and 18.5% ductility was obtained for alloy SG-7.

The properties of specimen underwent intercritical austenitizing followed by quenching treatment (DMS treatment) observed to have a good balance of tensile strength and ductility. Austenitization in intercritical region transform the parent phase into partial austenite and led to retention of parent phase in the final microstructure after quenching. The combined effect of Ni and Mn was observed for DMS-treated specimens, having a maximum strength value of 532.2 MPa for alloy SG-6 with 15.65% elongation at fracture and that of the least was 358.8 MPa tensile strength value for alloy SG-5 with 19.67%

elongation at fracture. The maximum ductility of 21.71% at fracture was obtained for alloy SG-7, which was having 2.19 wt.% of Silicon. Table 4.3 and Table 4.4 represent the tensile and 0.2% yield strength values of respective as-cast and heat treated specimens respectively, and % elongation at fracture for respective alloys in as-cast and heat treated conditions are shown in Table 4.5.

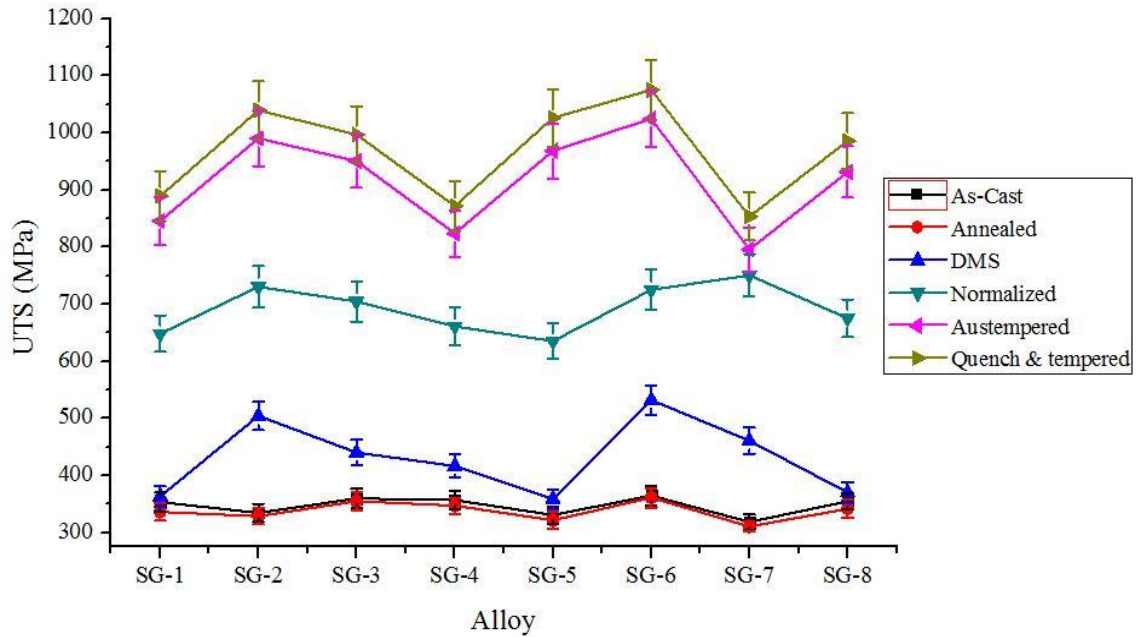


Fig. 4.6: UTS of as-cast and heat treated specimens of respective alloys.

Table 4.3: Tensile strength of respective alloys in as-cast and heat treated conditions.

Alloy	As-Cast	Annealed	DMS	Normalized	Austempered	Quench & tempered
SG-1	353.3	336.1	363.3	648.5	845.7	889.6
SG-2	334.5	328.7	504.4	730.5	990.4	1039.6
SG-3	359.9	355.1	440.1	704.8	950.7	997.1
SG-4	356.9	347.2	416.4	661.3	823.8	872.2
SG-5	330.9	321.5	358.8	635.2	968.6	1026.4
SG-6	364.8	361.2	532.2	725.4	1024.8	1075.4
SG-7	318.5	310.6	460.9	750.6	795.9	853.6
SG-8	354.7	341.8	370.3	675.2	931.5	985.7



Table 4.4: % Elongation of respective alloys in as-cast and heat treated conditions.

Alloy	As-Cast	Annealed	DMS	Austempered	Normalized	Quench & tempered
SG-1	30.2	31.3	20.53	17.7	13.8	13.2
SG-2	31.2	32.8	19.01	14.6	14.1	11.2
SG-3	26.8	28	16.43	15.6	12.2	11.8
SG-4	28.7	29.4	18.7	18.1	12.8	12.5
SG-5	32.5	33.4	16.13	15.2	14.6	11.7
SG-6	26.1	27.6	15.65	13.8	11.7	10.2
SG-7	33.4	34	21.71	18.5	15.4	14.3
SG-8	29.7	30.4	19.67	16	13.2	12.3

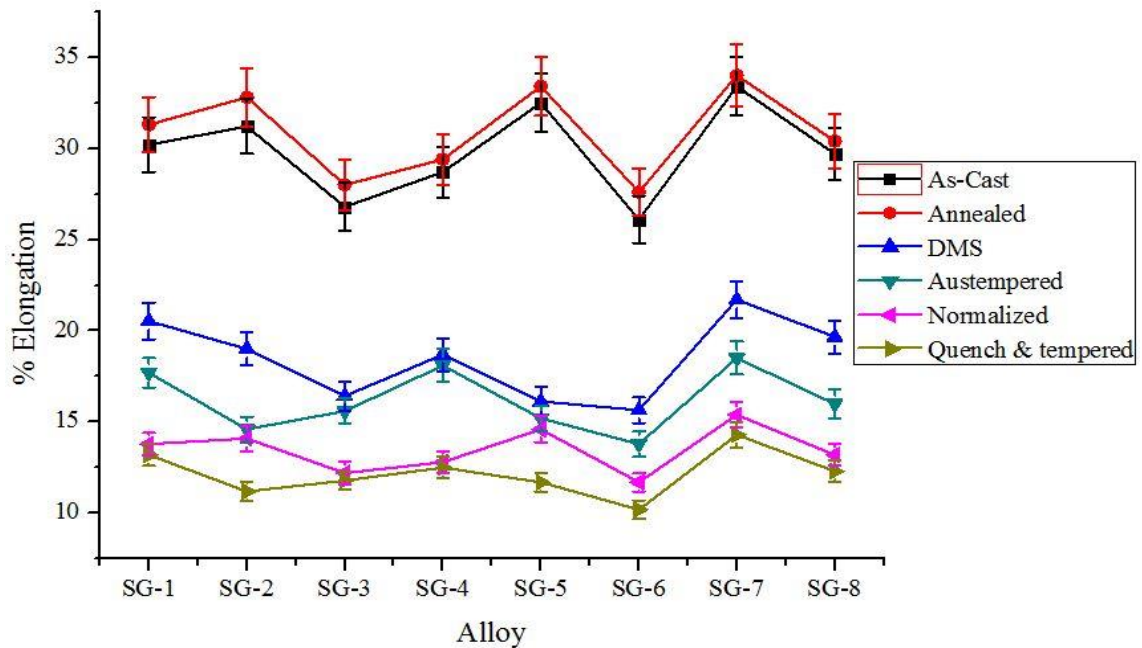


Fig. 4.7: % Elongation of as-cast and heat treated specimens of respective alloys.

### 4.2.3 Impact Energy

The as-cast and heat treated specimens of all the respective alloys were subjected to Izod impact test, to study the behavior of the materials under dynamic loading and the impact energies obtained for individual specimens are presented in Table 4.5. Each of the alloys in as-cast and heat treated condition was observed to have an impact energy of more than 10J, which is the recommended value of impact energy for the spent nuclear fuel container. Specimens subjected to annealing treatment exhibited highest impact energy value than the other conditions in the case of every alloy composition. The reason behind this was quite convincing that the longer transformation time, i.e., 330 minutes that might have resulted in the transformation of the fully ferritic matrix without any amount of

residual stresses. Alloy SG-7 had the maximum value of impact energy, i.e., 34.7 J, whereas that of alloy SG-6 had the lowest value of 24.84 J. Both of the alloys had the highest and lowest ductility value respectively, hence the impact energy values. Also for as-cast, and other heat treated conditions alloy SG-7 has the maximum impact energy value and alloy SG-6 has the least impact energy value. The highest impact energy for alloy SG-7 can be due to the highest Si content that promoted ferrite formation and retention in respective matrices as well as encouraging graphite nodularity that restricted the crack propagation leading to increased impact energy.

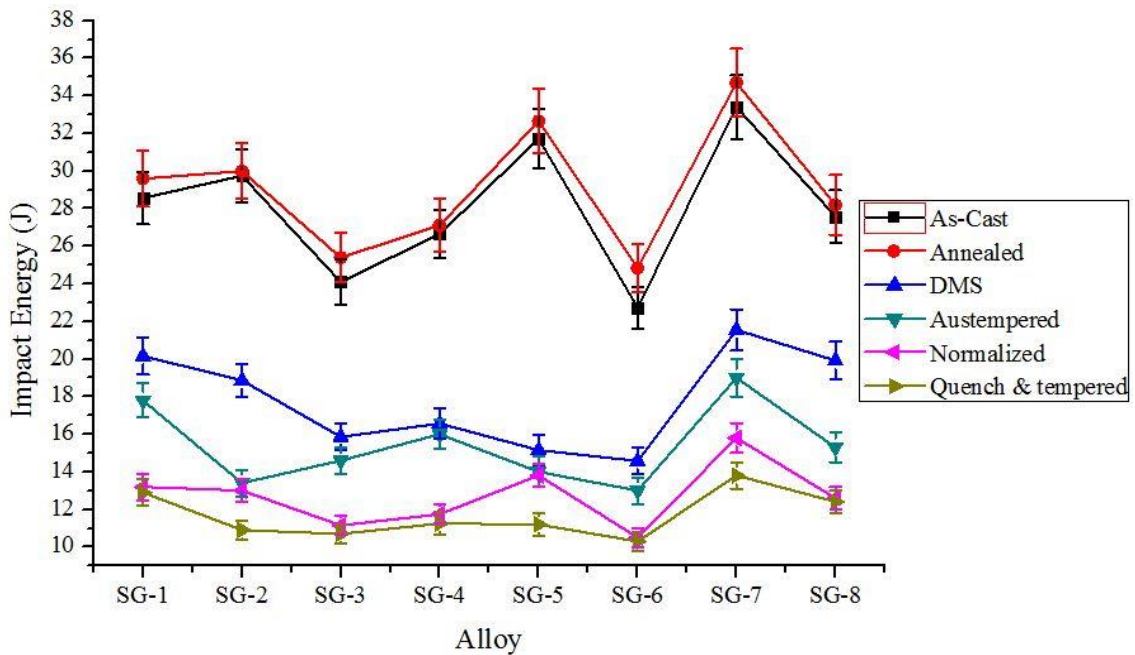


Fig. 4.8: Izod impact energies of as-cast and heat treated specimens of respective alloys.

Table 4.5: Impact energy of as-cast and heat treated specimens of respective alloys.

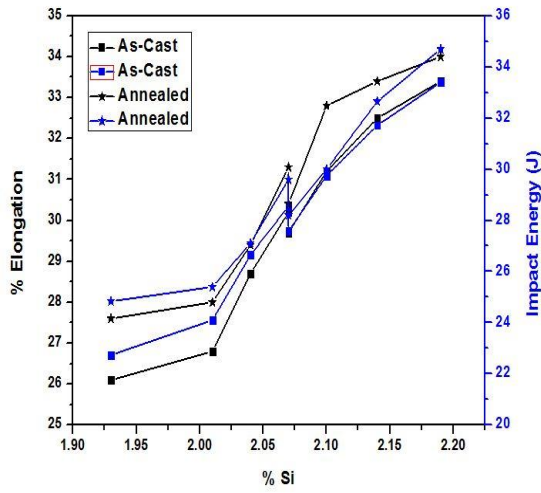
Alloy	As-Cast	Annealed	DMS	Austempered	Normalized	Quench & tempered
SG-1	28.56	29.6	20.16	17.8	13.2	12.9
SG-2	29.75	30	18.86	13.4	13	10.9
SG-3	24.1	25.4	15.86	14.6	11.15	10.7
SG-4	26.65	27.11	16.57	16	11.75	11.25
SG-5	31.72	32.65	15.15	14	13.8	11.2
SG-6	22.74	24.84	14.58	13	10.5	10.3
SG-7	33.4	34.7	21.55	19	15.8	13.8
SG-8	27.58	28.2	19.92	15.3	12.6	12.4

#### 4.2.4 Effect of Composition

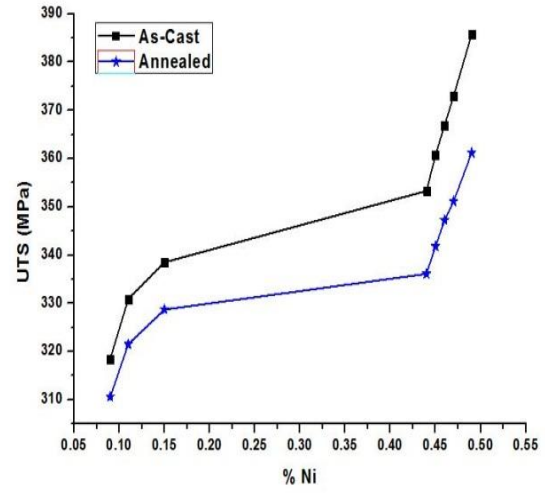
The mechanical properties viz. UTS, 0.2% YS, % elongation, Vickers hardness, and Izod impact energy, of the alloys in as-cast and heat treated condition were briefly discussed in previous sections. However, the primary aspect that influences and differentiates the alloys in terms of the mechanical properties was the chemical composition or alloying elements in individual alloys. Incorporation of alloying element into the base composition governs the phase volume fraction; consequentially increased or decreased mechanical properties. In the present study, a total of eight alloys were used with different wt.% of alloying and base elements. However, the amount of Molybdenum was same, i.e., 0.001 wt.% in every alloy and hence its effects on properties could not be justified. Similarly, the effect of Cr and Cu cannot be explained as because the amount and the difference between them are very less. Hence, the effect of these elements on the properties is insignificant. However, on the other hand, the wt.% of Carbon, Silicon, Manganese, and Nickel had noticeable variation, and their effects were observed.

The as-cast and annealed specimens found to have a marginal difference in ductility value compared to the other heat treated conditions. That points towards the presence of either austenitic or ferritic microstructure; as these are the most ductile phases in Fe-C or Fe-C-Si system. To stabilize austenite in as-cast microstructure at room temperature, the minimum amount of Ni required is 10% [107]. However, 4% of Ni can also encourage retention of austenite at room temperature if proper heat treatment parameters were maintained [111]. Since in the present case of study, Ni is present from 0.09 wt.% for alloy SG-7 to a maximum of 0.49 wt.% for alloy SG-6, the as-cast microstructure was definitely not austenitic. Hence, the only microstructure possible for such high amount of ductility was ferritic, and as because the chemical composition was maintained to obtain a ferritic matrix, it can be assumed that the as-cast microstructure was possibly ferritic. At a closer view when the ductility and impact energy values are compared among the alloys, it was observed that both ductility and impact energy were increased with increase in Si content for as-cast as well as annealed specimens. On the other hand, the UTS of samples under both conditions was increased with increase in Ni content. For normalizing treated specimens the UTS was increased with increasing Mn content whereas %elongation at fracture was increased with Si content. The quench & tempered and DMS-treated specimens were found to increased tensile strength with increase in Mn and Ni content. On the other hand, the ductility of DMS-treated specimens

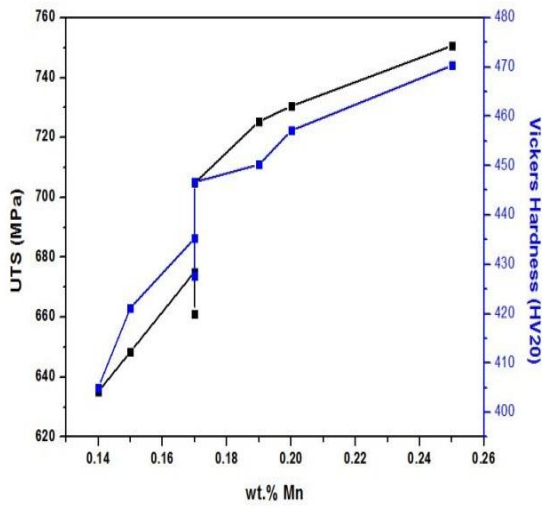
was again increased with Si content. The specimens treated with the austempering process, observed to have increased UTS with Ni content.



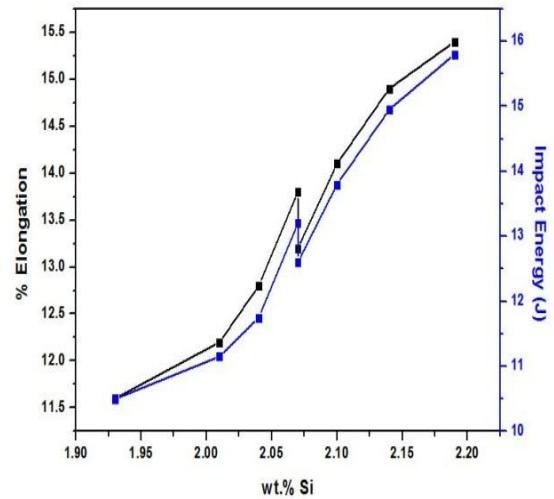
(a)



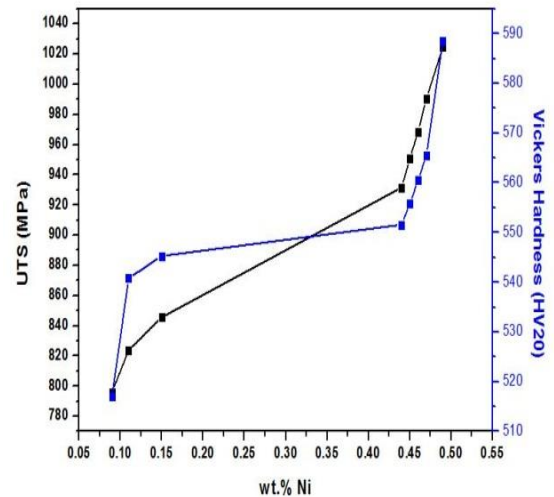
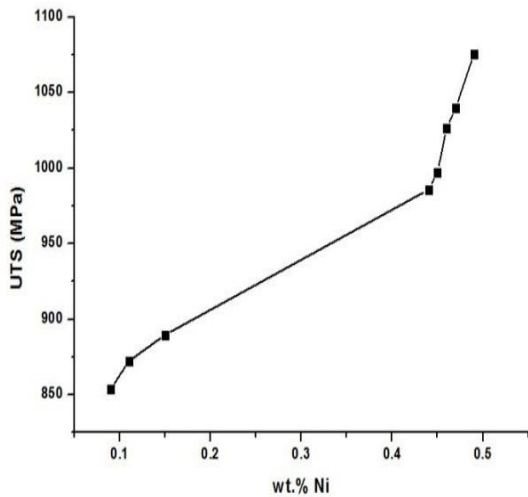
(b)



(c)



(d)



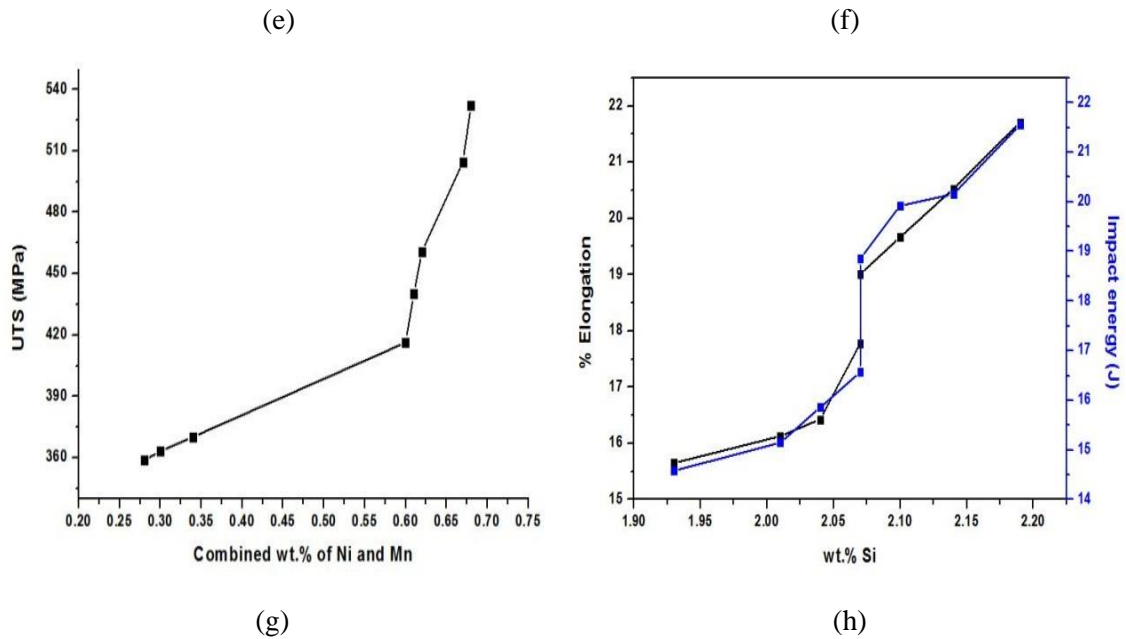


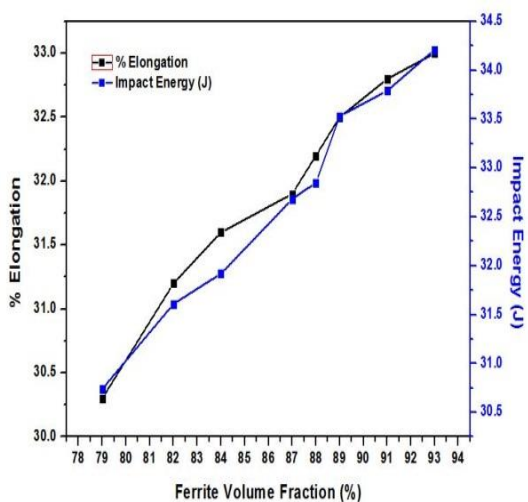
Fig. 4.9: (a) wt.% Si vs. Elongation and Impact energy of as-cast and annealed specimens, (b) wt.% Ni vs. UTS of as-cast and annealed specimens, (c) wt.% of Mn vs. UTS and Hardness of normalized specimens, (d) wt.% Si vs. Elongation and Impact energy of normalized specimens, (e) wt.% of Ni vs. UTS of quench & tempered specimens, (f) wt.% of Ni vs. UTS and hardness of austempered specimens, (g) combined effect of Ni and Mn on UTS of DMS-treated specimens, (h) wt.% Si vs. Elongation and Impact energy of DMS-treated specimens.

#### 4.2.5 Effect of Phase Volume Fraction

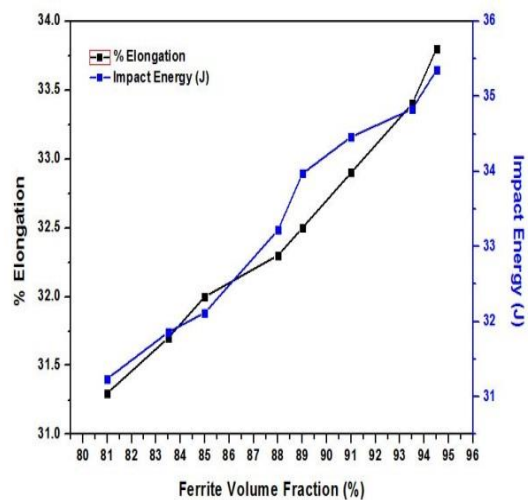
The mechanical properties viz., UTS, 0.2% YS, Vickers hardness, ductility, and Izod impact energy of as-cast as well heat treated specimens of individual alloys were elaborately discussed in Section 4.1. It was also mentioned in Section 4.1 that, how the alloying elements affect the respective properties of the alloys in every state. The alloying elements were also responsible for increasing or decreasing the phase volume fractions of respective alloys in individual states, and the properties have a direct or indirect relationship with the respective phase volume fraction.

The as-cast, normalized, quench and tempered and DMS-treated specimens observed to have strength and hardness values intermediated to that of processed with annealing and austempering. The annealing treatment led to highest elongation and impact energy, respectively, whereas, quench & tempered specimens had the lowest ductility and impact toughness. On the other hand, the as-cast, normalized, austempered and DMS-treated specimen had ductility and impact energy values intermediate to that of annealed and quench & tempered condition. The relationship between different phase volume

fractions with corresponding mechanical properties of respective alloys has been illustrated in Fig. 4.10. The behaviour of soft ferritic as-cast and annealed specimen has demonstrated in Fig. 4.10 (a) and (b) respectively. The % elongation at break and impact energy observed to behave directly proportional manner with ferrite volume fraction, whereas the ultimate tensile strength (UTS) and Vickers hardness was found to behaved a little peculiar with ferrite volume fraction, Fig. 4.10 (c). The increasing value of UTS and hardness with increased ferrite volume fraction can be attributed to the effect of increasing Ni and Mn content that provides strength to the matrix through solid solution strengthening for respective alloys [121]. The normalized specimen showed increased UTS and hardness and decreased ductility and impact energy with increasing pearlite content, Fig. 4.10 (d) & (e) respectively. The results obtained were well in agreement with that of results reported by [117]. Similar results were obtained for quench and tempered (Fig. 4.10 (f)) as well as austempered (Fig. 4.10 (g)) specimens, i.e., the UTS and hardness were directly proportional to the corresponding phase volume fraction, and ductility and impact energy had inversely proportional relation. The DMS-treated specimens exhibited an increase in strength with increasing martensite volume fraction whereas ductility and impact energy are proportional to ferrite volume fraction. The hardness value didn't show any particular behaviour with either martensite or ferrite volume fraction. The hardness value for all alloys in as-cast and heat treated state is presented in Fig. 4.5, showed a considerable difference in the standard deviation in hardness of DMS-treated specimens compared to other conditions.



(a)



(b)

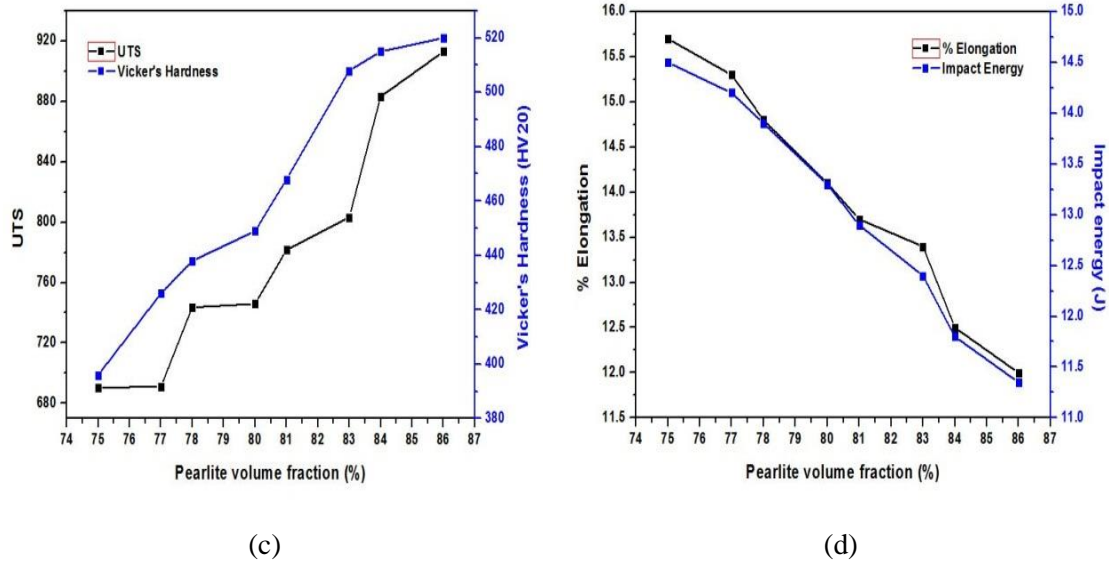


Fig. 4.10: Relationship between different phase volume fractions with corresponding mechanical properties. (a) Ferrite volume fraction vs. ductility and impact energy of as-cast specimen, (b) Ferrite volume fraction vs. ductility and impact energy of annealed specimen, (c) Pearlite volume fraction vs. UTS and Hardness, (d) Pearlite volume fraction vs. % elongation and impact energy.

#### 4.2.6 Fractographic Investigation

The Fractographic images of as-cast and heat treated specimens after tensile, and impact fracture is shown in Fig. 4.11 and Fig. 4.12 respectively. The as-cast and annealed specimens with ferritic matrix observed to have dimples around the graphite nodule and on the matrix as well, Fig. 4.11 (a) & (b) respectively. Due to decohesion at the ferrite graphite interface the microvoids nucleates at the naked region and grows at the grain boundary; suggesting that extensive deformation has occurred for ferrite prior to the fracture and the material is highly ductile. The deformation of ferrite matrix during the end period of straining before the fracture was evident from the dimples around graphite nodule [122]. Dimples are formed because of the microvoid coalescence phenomenon that arises under uniaxial tensile loading state leading to formation and growth of microvoids, signifying the ductile behaviour of the material [123]. On the other hand, the pearlitic, tempered martensitic and bainitic specimens had river markings and cleavage facets over the matrix justifying the brittle nature of the fracture. Martensite characterizes lower strain leading to a low rate of deformation mechanism culminating brittle fracture. The quenching process results in segregation of sulphur and phosphorus impurities before the austenite grain boundaries that result in the favorable growth of transgranular paths, thereby reducing the cohesive strength [122]. The transgranular cracks were initiated at graphite/matrix interface and start to propagate where there is an atomic mismatch

between the phases such as ferrite/austenite interface in case of austempered specimens. The austenite being soft tends to deform whereas ferrite starts cracking and the crack propagates along the length of ferrite sheaves [122], [124]. The cleavage facets appeared due to the plastic deformation of the matrix, and the growth of deformation was because of the presence of secondary phase particles [115]. The transgranular, low energy stress paths (river markings) that signify cleavage fracture are derived from the separation of atomic bonding and change direction when passes through the sub-grain boundaries graphite nodules [125], [126]. The DMS-treated specimen had both dimples around the graphite nodules and river markings which are an indication of the mixed mode of fracture that justifies the semi-ductile nature of the specimen. The voids nucleate at the ferrite-martensite interface associated with decohesion from the adjacent martensite [115]. The continuous martensite along the intercellular boundaries is a vital factor that determines the deformation extent of ferrite around graphite nodules. Alloys with higher martensite fraction were observed to have zero deformation of ferrite under tensile loading, suggesting decreased ductility with martensite continuity in the matrix. All the specimens showed similar kind of behaviour under impact loading condition that observed under monotonic uniaxial tensile loading and is shown in Fig. 4.12.

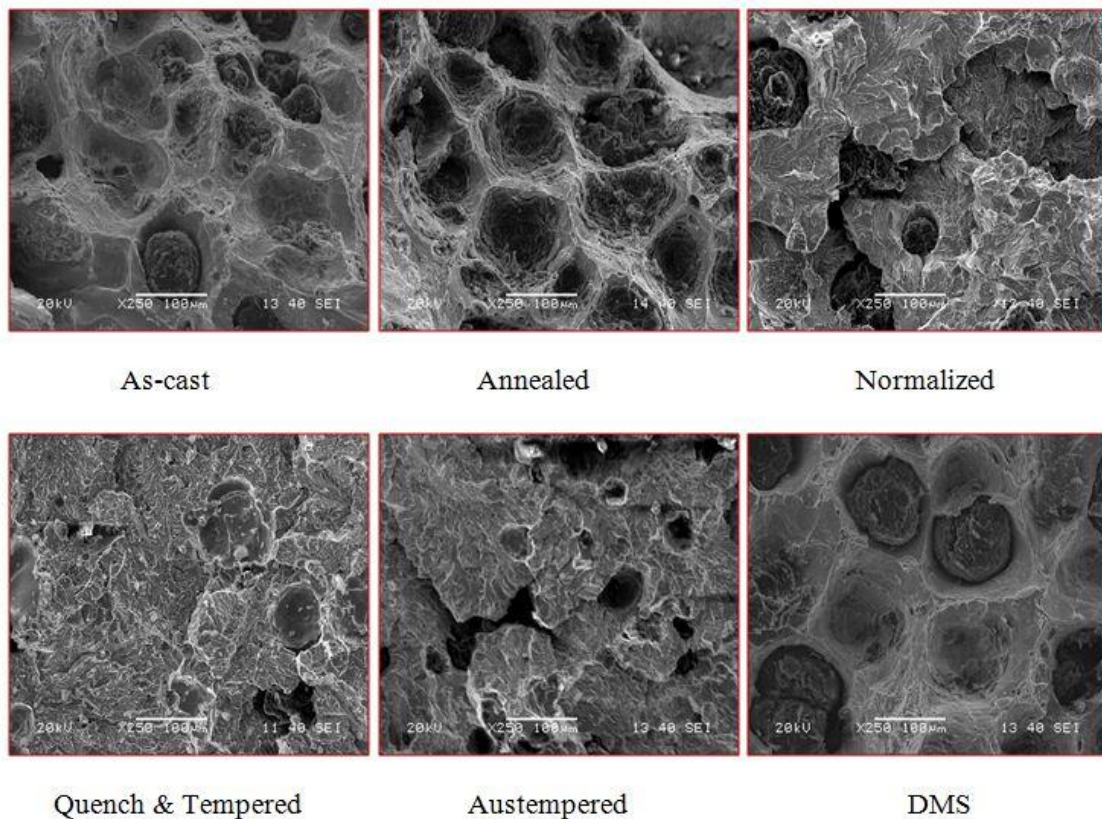


Fig. 4.11: Fracture surfaces of as-cast and heat treated specimens after tensile failure.



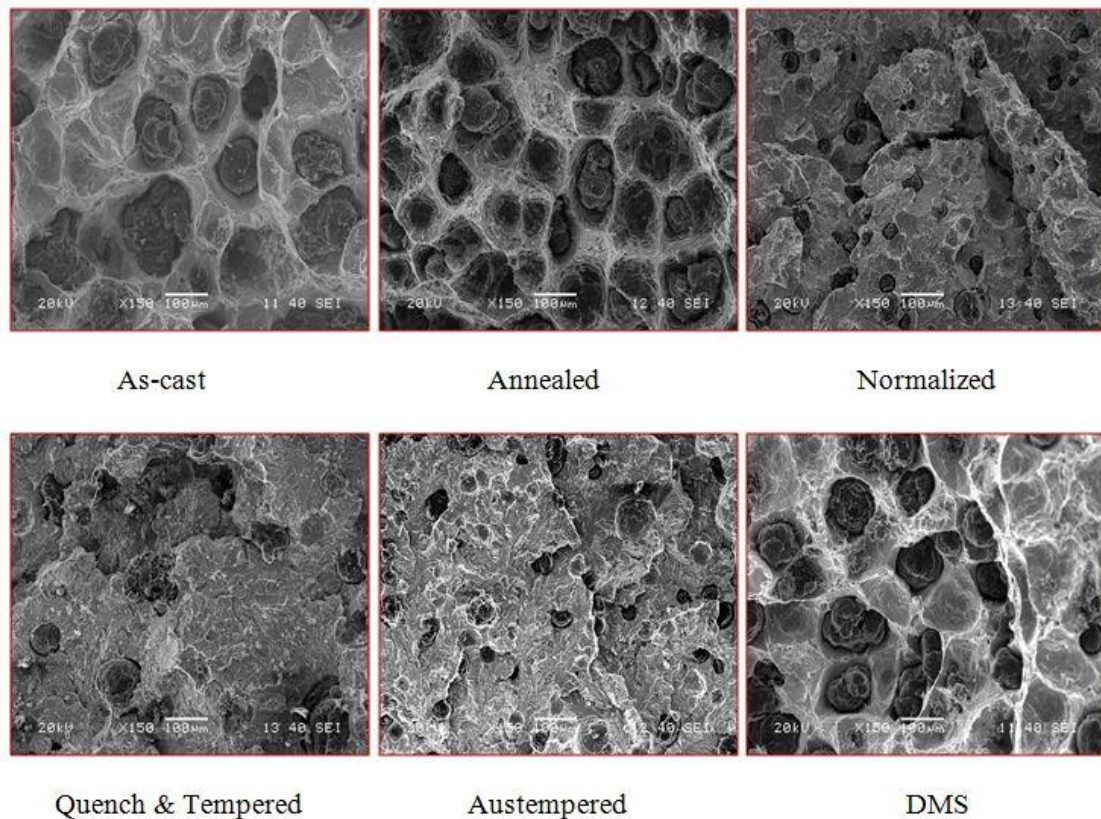


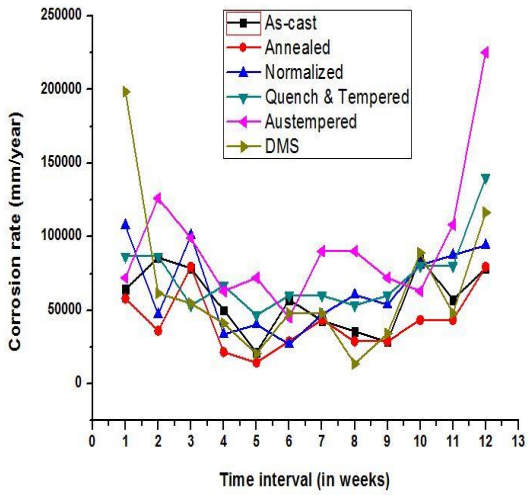
Fig. 4.12: Fracture surfaces of as-cast and heat treated specimens after Impact failure.

## 4.3 Corrosion Studies

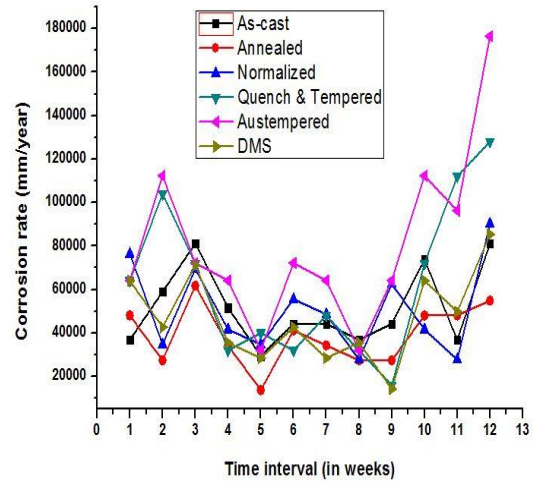
### 4.3.1 Corrosion Rate Of Alloys

The nuclear spent fuel casks often disposed under the sea at distance of 30m deep from the sea level. The purpose is twofold; first, if in any case the containment fails to serve its purpose, nuclear radiations won't scatter into the environment and consequentially do not pose a threat neither to the environment nor to the living being. And the second is to cool the container, from the liberating heat of spent nuclear fuel. Cast iron is the least corrosion resistive material among the other ferrous materials in the Fe-C-Si system. The free form of graphite or carbon in the matrix acts as cathode and accelerates anodic dissolution of nearby iron. A continuous graphite network leads to higher corrosion tendency which can be seen for gray cast iron. Whereas, in the case of SG cast iron the graphite is present distinctively rather than as chain and hence corrosion takes place uniformly. The formation of graphite nodules and its uniform distribution results in the evolution of regular barrier film that protects the iron from corrosion [127].

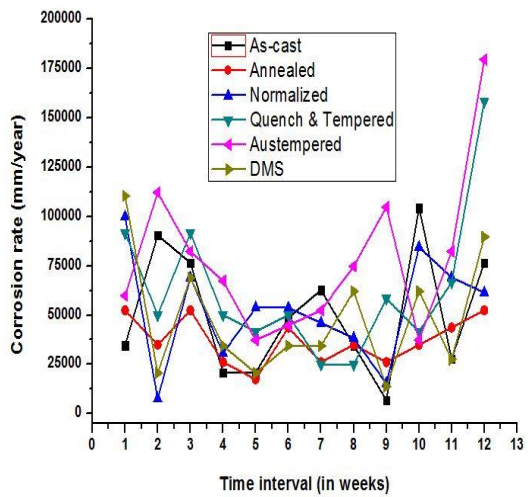
The as-cast and heat treated specimens of respective alloys were immersed in sea water under room temperature and atmospheric pressure for 12 weeks. The difference in weight of the specimens was noted after a regular time interval of 173 hours and contaminated water was replaced with fresh sea water. The response of SGCI samples of each alloy in as-cast and heat treated conditions, with sea water environment are illustrated in Fig. 4.13 in terms of corrosion rate vs. time plot. It can be noted that there was no significant pattern obtained for any of the as-cast or heat treated specimens over the time. This unusual corrosion behaviour in as-cast and heat treated conditions can only be attributed to the fact that after every regular time interval the specimens had been subjected to fresh sea water, resulting variation in the reactivity level of sea water that was exposed to the specimens. The reactivity level of sea water was evident from the pH value noted at the end of every 173 hours. The highest rate of corrosion was obtained for austempered specimens with coarse upper bainitic matrix and that of lowest for the DMS treated specimens having ferrite and martensite in matrix microstructure. The corrosion rate follows DMS-treated < annealed < as-cast < normalized < quench & tempered < austempered, pattern for all the alloys. The rate of corrosion was lowest for the DMS specimens ranging from 8 $\mu\text{m}/\text{year}$  to 200 $\mu\text{m}/\text{year}$  for alloys SG-4 and SG-1 respectively. On the other hand, the highest rate of corrosion was found to be in the range of 20 $\mu\text{m}/\text{year}$  to 225 $\mu\text{m}/\text{year}$  for alloys SG-5 and SG-1 respectively in austempered condition. The tempered martensitic and pearlitic/ferritic grade SG cast iron observed to have 2<sup>nd</sup> and 3<sup>rd</sup> order of corrosion resistance. The large corrosion exhibition of normalizing, austempered and Quench & tempered specimens can be attributed to the fact that, increased rate of cooling resulted in increased nodule count leading to increased potential sites for graphitic corrosion. Although in many observations some values are higher than 50 $\mu\text{m}/\text{year}$ , but some values below 50 $\mu\text{m}/\text{year}$  is also observed in some cases. Moreover, these data are acceptable and also not yet objected after the sample tests conducted by Bhaba Atomic Research Centre (The purpose of the BRNS sponsored project).



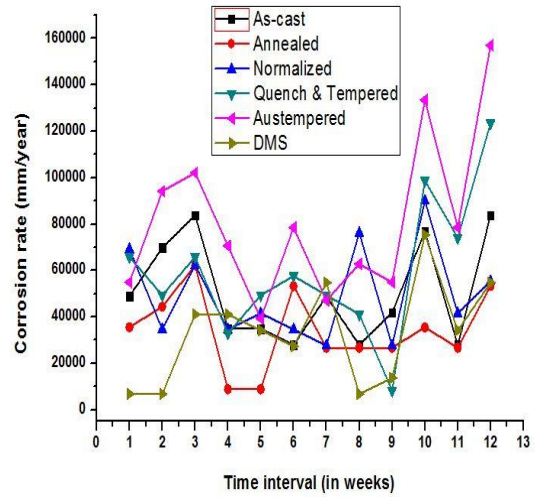
(a) SG-1



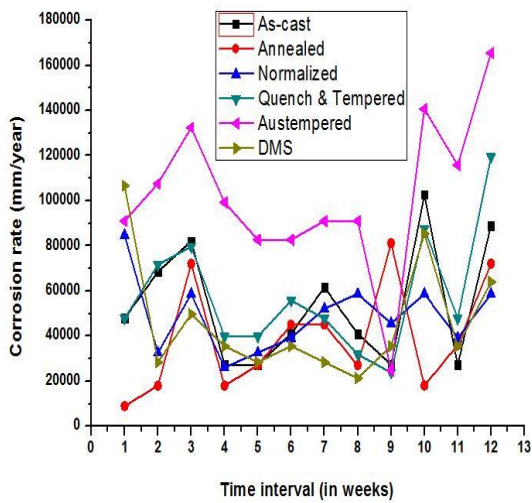
(b) SG-2



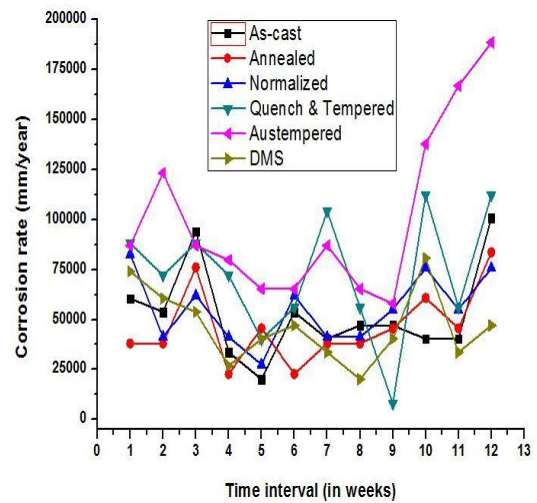
(c) SG-3



(d) SG-4



(e) SG-5



(f) SG-6

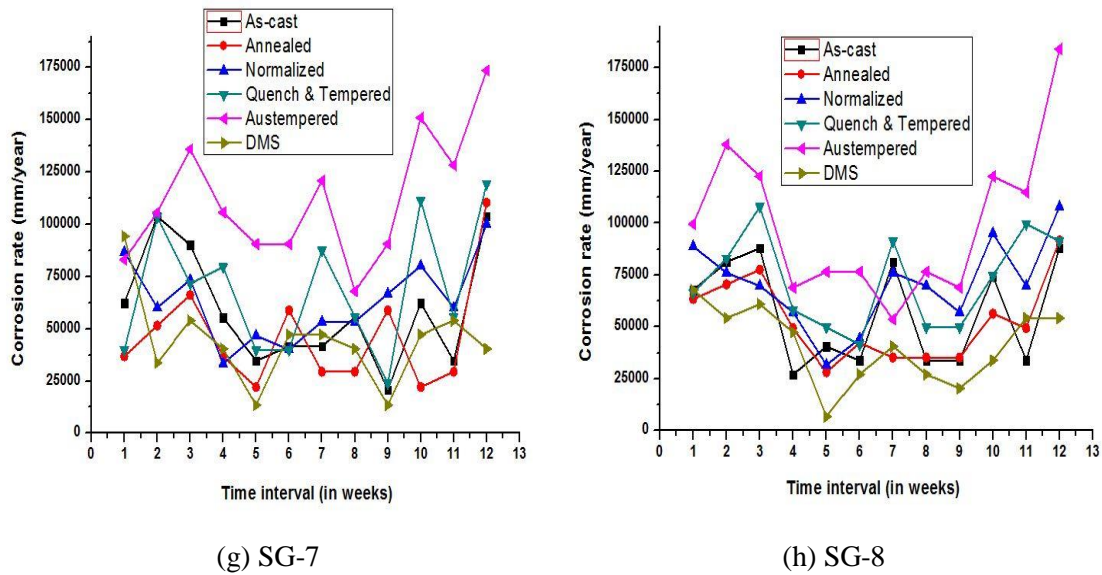


Fig. 4.13: Corrosion rate vs. time interval plot for as-cast and heat treated condition for individual alloys.

### 4.3.2 Effect of Alloying Elements on Rate of Corrosion

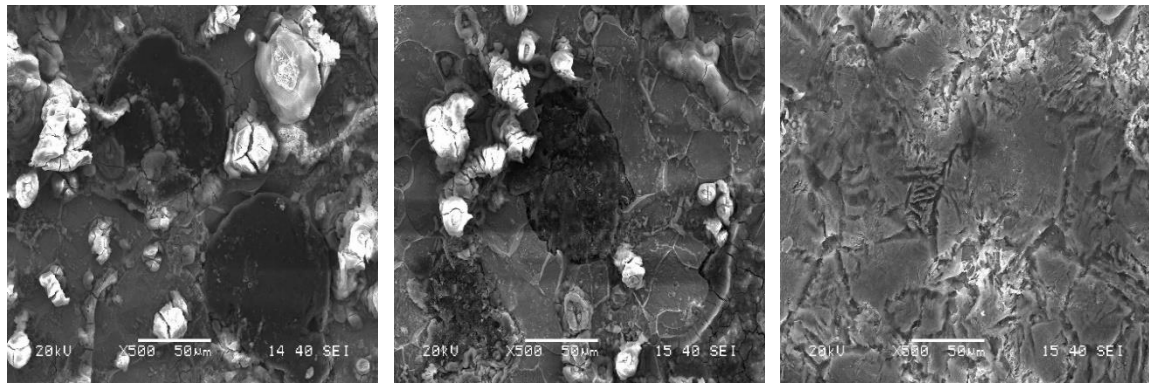
The corrosion characteristic of SG cast iron not only depends on microconstituents but also on the chemical composition. The resistance to corrosion can be improved by the addition of Ni, Cu, and Cr. It was clear that the austempering treatment exhibited highest corrosion rate and that of annealed, and DMS are the lowest for every alloy composition. In this case, the difference of Cr content in respective alloys is very minor and hence its effect was not significant or negligible. On the other hand, the corrosion resistance was observed to decrease with increase in Ni and Cu content. Copper addition reduces the nodule count and additionally forms a compact  $\text{Cu}_2\text{O}$  passive oxide film over the alloy surface in chloride solution which is mainly responsible for better corrosion resistance [128]. Additionally, Nickel and Copper shifts the open circuit potential to more positive values resulting the alloy to enter into the passive region under natural immersion in solutions with high pH like seawater [128]. Furthermore, the addition of Nickel results in reduced nodule count and consequentially reduces the graphitic corrosion potential of the concerned alloy [98]. The formation of  $\text{Cu}_2\text{O}$  has not been observed on the corroded surface but found in the porous product. It was quite possible that during the cleaning with alcohol the scales were peeled off from the surface and hence found in the porous product that was evident from the XRD and EDAX analysis. Also, the sea water contains ions of other than  $\text{Na}^+$  &  $\text{Cl}^-$ , so it was quite possible that during the reaction other ions might have led to the formation similar potential that was repellent to each other and leading to

removal of scale from the surface. Hence the  $\text{Cu}_2\text{O}$  compound was only observed in the porous product, and not on the corroded surface.

### 4.3.3 Morphology of Corroded Surfaces

The corrosion products were investigated under SEM/EDAX, to understand the role of chemical composition in preventing corrosion. Two different type of products were analysed i.e., the corroded surfaces of specimens and the porous product collected after 1<sup>st</sup> and 12<sup>th</sup> week of immersion. The surface micrographs of as-cast and heat treated specimens as well as porous product, after 1<sup>st</sup> week of immersion are presented in Fig. 4.14. It was observed that, the specimens were experienced with localized attack at the boundaries of the spherical nodules and at the grain boundaries. The localized attack resulted in fine network of cracks near the grain boundaries covered with non-homogeneous loose scale like layer. The results observed were quite in agreement with the observation made by Zeng et.al [95], who studied the corrosion response of SGCI and laser surface alloyed SGCI in HCl solution. Similar results were also observed by Venkatesan et.al [129] for austempered specimens treated in still deep sea water. Pitting corrosion was observed over the specimen surfaces, with porous layers allowing to the water to impinge through the scale and react with base material resulting increased rate of corrosion, which may be the reason of highest rate of corrosion in present case. The pitting corrosion mechanism was attributed to the reaction of SGCI samples with sea water under physico-chemical condition. The EDAX spectra of as-cast and heat treated specimens revealed that after 1 week (173 hours) of immersion the corrosion was still not fully grown. At some places the sea water has not affected the surface, which can be accredited to the growth of corrosion at the graphite nodules. The results obtained from elemental mapping showed presence of Fe, O, Cr, Ni, and Mn in major percentage whereas, Si and Mg was found in traces. The mapping led to the conclusion that Fe, Cr, Ni and Mn oxide layers had formed over the corroded surface. Ogundare et.al [130] in their work reported that alloying with Chromium enhances the resistance to corrosion through a passivation process by forming a complex spinel-type  $\{(\text{FeNi})\text{O}(\text{FeCr})_2\text{O}_3\}$  passive film. This complex produces a coherent, adherent insulating and regenerating chromium oxide protective film on the metal surface leading to resistance to further increase in weight loss. On the other hand the porous product was found to have Na, Cl, and Cu in addition to the elements found on the corroded surface.

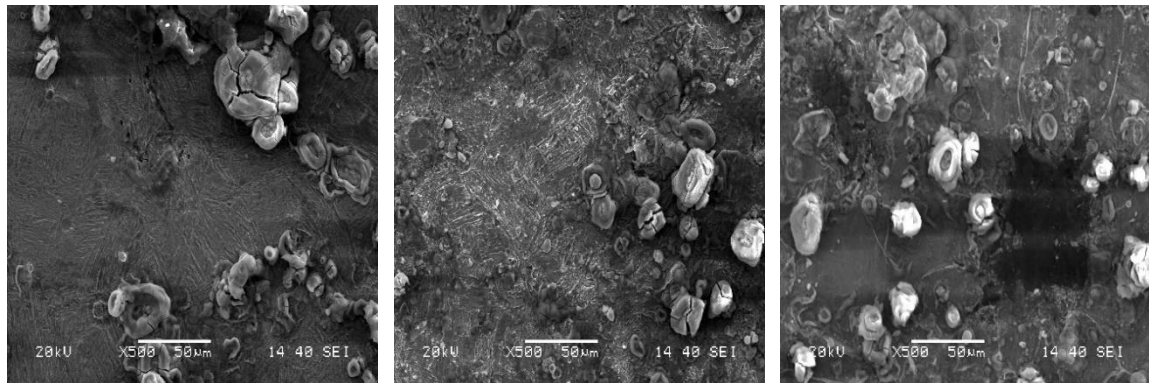
The surface micrographs of as-cast and heat treated specimens as well as porous product, after 12th week of immersion are presented in Fig. 4.15. The surfaces after 12th week of immersion were observed to be covered fully with corroded layer and no graphite particle was found. The EDAX spectra reveals the presence of Fe, O, and C in major quantity whereas other alloying elements were found in traces. The absence of Ni, Cr, Mn was the evidence of iron oxide layers over the surface which can due to the reaction between sea water and the base material. As compared to the 1st week fewer cracks were found on the corroded layer suggesting precipitation of corrosion products when subjected to longer time period. The porous products were also found to have Fe and O in major quantity.



(a) As-cast

(b) Annealed

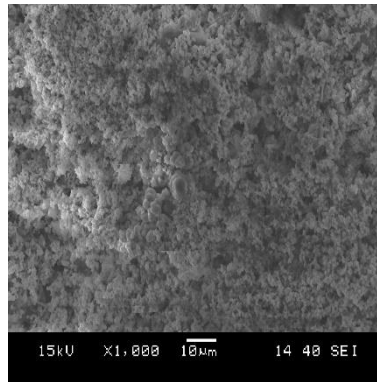
(c) Normalized



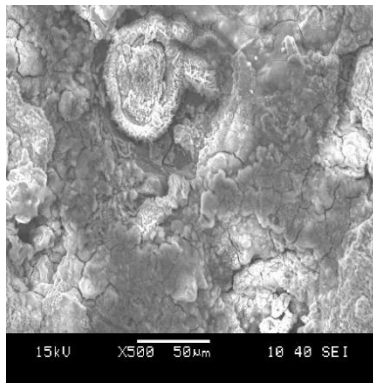
(d) Quench &amp; tempered

(e) Austempered

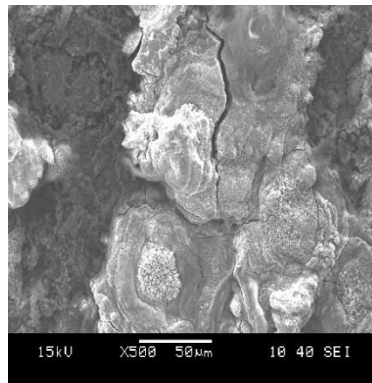
(f) DMS



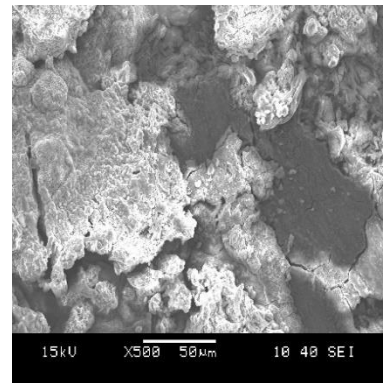
(g) Porous product

Fig. 4.14: surface morphology of corroded surfaces and the porous product after 1<sup>st</sup> week of immersion.

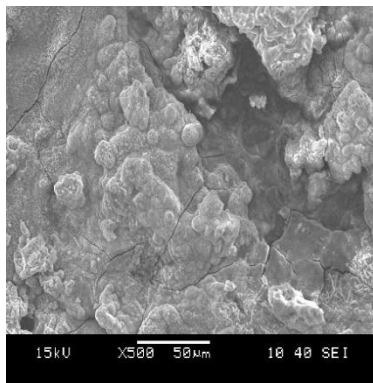
(a) As-cast



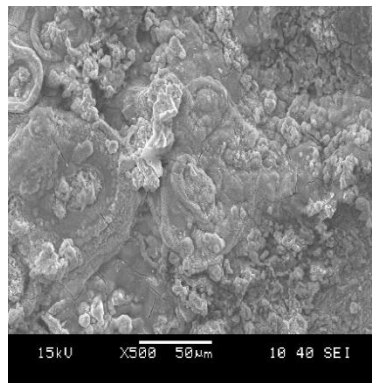
(b) Annealed



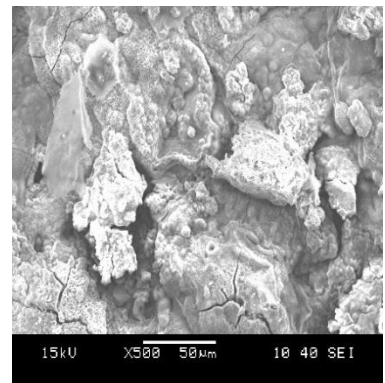
(c) Normalized



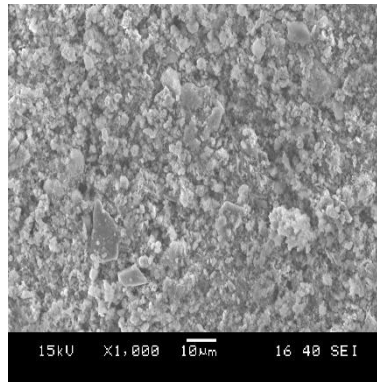
(d) Quench &amp; tempered



(e) Austempered



(f) DMS



(g) Porous product

Fig. 4.15: Surface morphology of corroded surfaces and the porous product after 12<sup>th</sup> week of immersion.

#### 4.3.4 X-Ray Diffraction Study of Corrosion Product

To understand the role of alloying elements in the process of corrosion, specimens after 1<sup>st</sup> week of exposure and 12<sup>th</sup> week of exposure, were subjected to XRD investigation. Two different corrosion products were analysed. One was the precipitated layer over the specimen surface and another was the porous settled product in the reactor that was taken carefully and dried. The XRD patterns were shown in Fig. 4.16. It was observed from the XRD analysis that Chromium, Iron and Oxygen have played a major role. Besides these elements Copper and Nickel also had significant role in the process. The major compounds found from the specimen surface are FeOOH, Cr<sub>2</sub>O<sub>3</sub> and Fe-Cr-Ni. The result was quite obvious and convincing as it was well known that when iron comes in contact with water it forms iron hydroxide. The results are also in agreement with that obtained from the EDAX analysis. It was observed that after the end of 1<sup>st</sup> week oxides of Chromium, Magnesium, Chlorine, and Iron were found. The as-cast specimen was observed to have FeOOH, and Cr<sub>3</sub>O were found after 1<sup>st</sup> week of immersion, which was absent after 12<sup>th</sup> week. At the end of 12<sup>th</sup> week FeOOH compound was found in as-cast and heat treated specimens, justifying the observation of EDAX analysis. Copper and Molybdenum was found to have significant role in case of normalized and quench & tempered specimen after 12<sup>th</sup> week of exposure, whereas in case of austempered and DMS specimens, MgO was found to be replaced by FeOOH.



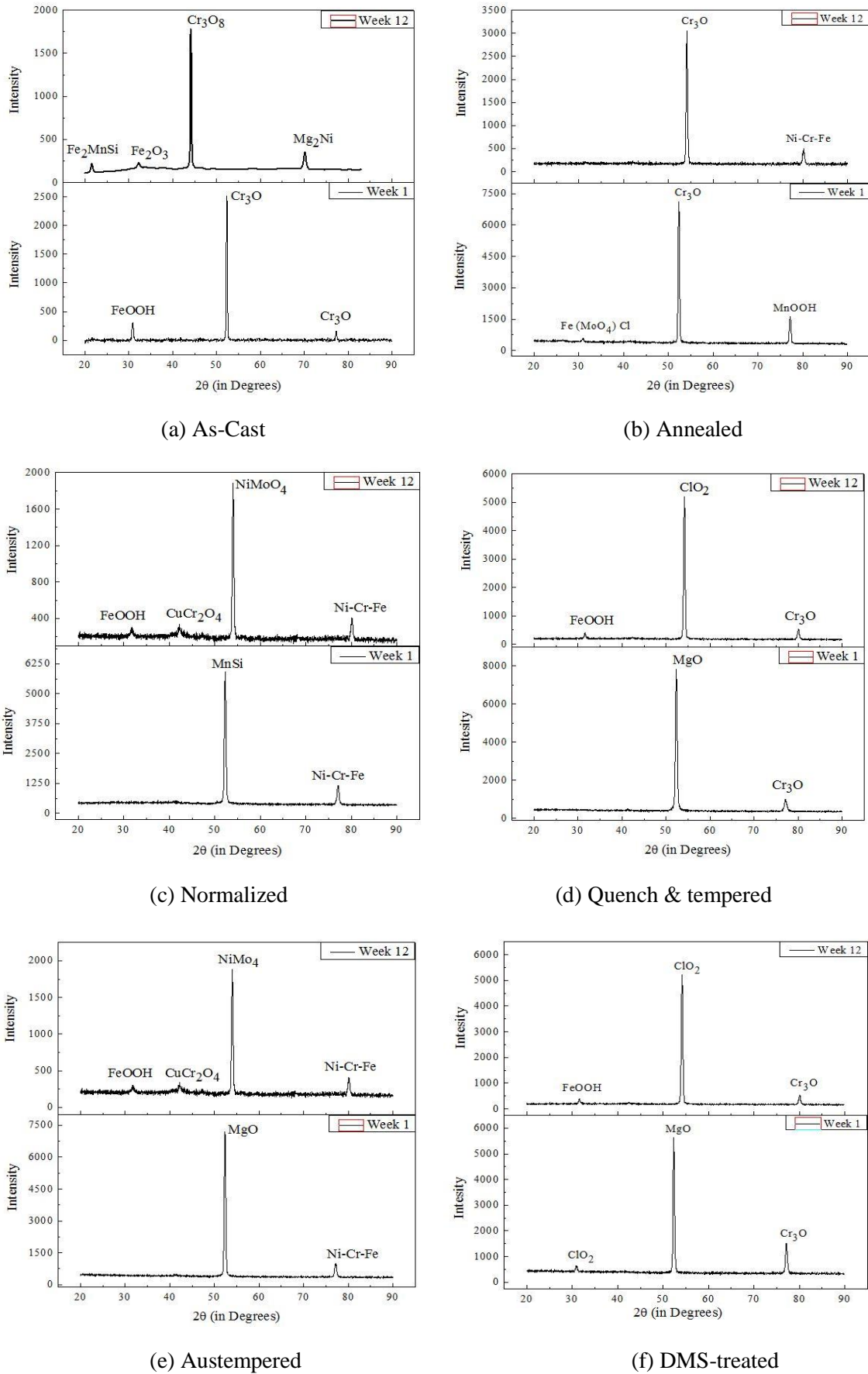


Fig. 4.16: XRD pattern for corroded surfaces after 1<sup>st</sup> and 12<sup>th</sup> week of exposure.

## 5. CONCLUSIONS

The power generations by nuclear power plants are growing day by day all over the world. Although the electricity production by an NPP is pollution free and considered as a green source of energy, the post-processing of nuclear fuel is a critical task failing of which cause a significant loss to the living being and environment. It is, therefore, necessary to dispose of the spent fuels away from the civilization and utmost care need to be taken so that the radiation leakage can be prevented. Hence, a small step was taken towards this issue and properties of spheroidal graphite cast iron (SGCI) are developed by alloying addition and heat treatment processes.

SGCI cast blocks were fabricated by conventional sand casting technique, from which tensile and Izod impact specimens were machined. The specimens were then subjected to annealing, normalizing, quench & tempering, austempering and intercritically austenitizing followed by quenching, heat treatment processes. The as-cast and heat treated specimens were characterized by optical microscope as well as X-ray diffraction technique. The mechanical properties and corrosion studies were carried out on the as-cast and heat treated specimens and the results were correlated to the morphological characteristics as well as effect of alloying was studied. The concluding remarks of the whole research work is stated as follows.

1. Every alloy possesses ferritic matrix and graphite spheroids embedded within in as-received state. The graphite spheroids belong to Type I (fully spherical) nodule with nodularity value more than 90% and the nodule count ranges from 28 - 40 nodules per unit area.
2. Ferrite volume fraction was observed to increase with increased Si content whereas the nodularity and nodule count was attributed to the increased amount of Mg as well as presence Ce, Cu and Si.
3. Annealing of SGCI did not observed to have any significant effect on the matrix as it remained ferritic, but slight increase in nodularity was observed due to a large transformation window provided during the operation.

4. Normalizing, quench & tempering, austempering treatment resulted in pearlitic/ferritic, tempered martensitic and coarse upper bainitic matrix respectively with graphite nodule lodged into the respective matrix. On the other hand, the intercritically austenitized followed by quenching in mineral oil led to transformation of as-cast ferritic matrix into ferritic + martensitic matrix.
5. The heat treatments except annealing resulted in increased nodule count due to increased rate of cooling during subsequent cooling and quenching process that restricted the carbon movement from the austenite to neighbouring graphite nodules resulting increased nucleation of graphite nodules in the matrix.
6. The pearlite volume fraction of normalized specimens was increased with increased Mn content, consequentially improving strength and hardness with considerable amount of ductility and impact toughness. On the other hand in case of the quench & tempered specimens, increased tempered martensite volume fraction was credited to the combined effect of Mn and Ni.
7. The bainitic volume fraction in austempered specimens observed to increase with increased Ni content resulting increased tensile strength and decreased ductility and impact toughness. On the other hand the DMS specimen showed a quite balance of ferrite and martensite with Si and Mn content respectively.
8. The objective of achieving greater amount of austenite after austempering treatment is almost achieved because of the longer holding time at higher austempering temperatures, leading to improved impact toughness as well as maximum strength.
9. The maximum UTS of 1200 MPa was obtained for austempered specimen for alloy SG-6 and that of the lowest was 295 MPa in case of annealed specimens for alloy SG-3. The corresponding ductility and impact energy was obtained lowest for quench and tempered specimens and that of highest was for annealed specimens.
10. The soft ferritic matrix of as-cast and annealed specimens resulted in microvoid coalescence leading to formation of dimples around the graphite globules and on the matrix suggesting ductile nature failure. Whereas the normalized, quench

&tempered and austempered specimens showed the brittle nature of material characterized by the presence of low energy stress paths (river markings) and cleavage facets. The DMS treated specimens have illustrated both dimples around the nodules as well as river marking on the matrix elucidating mixed mode of fracture. There was no significant difference observed in the fracture phenomena of tensile and impact fracture.

11. The corrosion behaviour of as-cast and heat treated specimens of respective alloys didn't show any significant pattern over the time. This unusual corrosion behaviour in as-cast and heat treated condition can only be attributed to two reasons. The first one is that after every regular time interval the specimens had been subjected to fresh sea water, resulting variation in the reactivity level of sea water with the exposed surfaces of specimens. And secondly, the area of specimen exposed to the corrosion environment.
12. The austempered specimens observed to corrode more rapidly than the other heat treated and as-cast specimens, whereas the DMS treated specimen had the least rate of corrosion. The rate of corrosion was also decreased with increased amount of Nickel.
13. The mechanical properties obtained for respective alloys in as-cast and heat treated condition are well above the desired properties of SGCI nuclear fuel cask specification.

## 6. REFERENCES

- [1] <http://foundrymag.com/feature/metalcasting-business-outlook-2015-present-results-future-prospects>.
- [2] <http://flexicast-euproject.com/expect-and-impact/>.
- [3] [http://www.globalcastingmagazine.com/wp-content/uploads/2013/08/IFF\\_2014\\_Europe.pdf](http://www.globalcastingmagazine.com/wp-content/uploads/2013/08/IFF_2014_Europe.pdf).
- [4] <http://www.afsinc.net/pdfs/TOC/MT1400.pdf>.
- [5] <http://trade.dts.dp.ua/en/news/show/6>.
- [6] Konečná R, Nicoletto G, Bubenko L, Fintová S. A comparative study of the fatigue behavior of two heat-treated nodular cast irons. *Eng Fract Mech* 2013;108:251-62
- [7] Dommarco R, Sousa M, Sikora J. Abrasion resistance of high nodule count ductile iron with different matrix microstructures. *Wear* 2004;257:1185-92.
- [8] Rashidi A, Moshrefi-Torbati M. Dual Matrix Structure (DMS) Ductile Cast Iron: The effect of heat treating variables on the mechanical properties. 2001.
- [9] Zhou R, Jiang Y, Lu D, Zhou R, Li Z. Development and characterization of a wear resistant bainite/martensite ductile iron by combination of alloying and a controlled cooling heat-treatment. *Wear* 2001;250:529-34.
- [10] Martins R, Seabra J, Magalhaes L. Austempered ductile iron (ADI) gears: Power loss, pitting and micropitting. *Wear* 2008;264:838-49.
- [11] Erić O, Jovanović M, Šid L, Rajnović D, Zec S. The austempering study of alloyed ductile iron. *Mater Des* 2006;27:617-22.
- [12] Putatunda SK, Kesani S, Tackett R, Lawes G. Development of austenite free ADI (austempered ductile cast iron). *Materials Science and Engineering: A* 2006;435:112-22.
- [13] Murthy KN, Sampathkumaran P, Seetharamu S. Abrasion and erosion behaviour of manganese alloyed permanent moulded austempered ductile iron. *Wear* 2009;267:1393-8.
- [14] El-Baradie Z, Ibrahim M, El-Sisy I, El-Hakeem AA. Austempering of spheroidal graphite cast iron. *Materials Science* 2004;40:523-8.
- [15] Murat B, Akray SI. Successive boronizing and austempering for GGG-40 grade ductile iron. *Journal of Iron and Steel Research, International* 2009;16:50-4.
- [16] Ghaderi A, Ahmadabadi MN, Ghasemi H. Effect of graphite morphologies on the tribological behavior of austempered cast iron. *Wear* 2003;255:410-6.
- [17] Peng Y, Jin H, Liu J, Li G. Influence of cooling rate on the microstructure and properties of a new wear resistant carbidic austempered ductile iron (CADI). *Mater Charact* 2012;72:53-8.
- [18] [http://www.afsinc.org/files/images/jan\\_15\\_forecast.pdf](http://www.afsinc.org/files/images/jan_15_forecast.pdf).
- [19] [http://www.ductile.org/didata/Section3/Figures/pfig3\\_26.htm](http://www.ductile.org/didata/Section3/Figures/pfig3_26.htm).
- [20] <https://www.euronuclear.org/info/encyclopedia/n/nuclear-power-plant-world-wide.htm>.
- [21] [https://en.wikipedia.org/wiki/Nuclear\\_power\\_by\\_country](https://en.wikipedia.org/wiki/Nuclear_power_by_country).

- [22] <http://www.npcil.nic.in/main/AllProjectOperationDisplay.aspx>.
- [23] <http://www.world-nuclear.org/info/current-and-future-generation/nuclear-power-in-the-world-today/>.
- [24] [https://en.wikipedia.org/wiki/Nuclear\\_power\\_in\\_India](https://en.wikipedia.org/wiki/Nuclear_power_in_India).
- [25] <http://newenergyandfuel.com/wp-content/uploads/2013/01/Nuclear-Plant-Block-Diagram.gif>.
- [26] Forsberg CW, Swaney PM, Tiegs TN. Characteristics and Fabrication of Cermet SNF Casks (Ceramic Particulates Embedded In Steel).
- [27] Haire MJ, Forsberg CW, Matveev V, Shapovalov V. Characteristics of Next-Generation Spent Nuclear Fuel (SNF) Transport and Storage Casks. 2004.
- [28] Brynda J, Hosnedl P, Jilek M, Picek M. Material issues in manufacturing and operation of transport and storage spent fuel casks. 1999;15.
- [29] Huang F. Container materials in environments of corroded spent nuclear fuel. J Nucl Mater 1996;231:74-82.
- [30] Saegusa T, Shirai K, Arai T, Tani J, Takeda H, Wataru M et al. Review and future issues on spent nuclear fuel storage. Nuclear Engineering and Technology 2010;42:237-48.
- [31] T. Shin, K. Kim, J. S. Kim, and K. S. Choi, "Drop Impact Analysis for Basket Design Selection in Spent Fuel Shipping Cask for Korean Standard Nuclear Power Plant," pp. 1–6, 2007.
- [32] <http://www.nrc.gov/waste/spent-fuel-storage/diagram-typical-trans-cask-system.doc>.
- [33] Blatz H. REGULATIONS FOR THE SAFE TRANSPORT OF RADIOACTIVE MATERIALS. American Journal of Public Health and the Nations Health 1968;58:989-90.
- [34] <http://www.ductile.org/didata/Section2/2intro.htm#Types of Cast Irons>.
- [35] [http://www.ductile.org/didata/Section2/figures/pfig2\\_4.htm](http://www.ductile.org/didata/Section2/figures/pfig2_4.htm).
- [36] [http://www.ductile.org/didata/Section2/figures/pfig2\\_5.htm](http://www.ductile.org/didata/Section2/figures/pfig2_5.htm).
- [37] [http://www.ductile.org/didata/Section2/figures/pfig2\\_7.htm](http://www.ductile.org/didata/Section2/figures/pfig2_7.htm).
- [38] [http://www.ductile.org/didata/Section2/figures/pfig2\\_8.htm](http://www.ductile.org/didata/Section2/figures/pfig2_8.htm).
- [39] <http://www.ductile.org/didata/Section12/12intro.htm>.
- [40] D. This, U. S. Government, U. S. Government, U. S. Government, and U. S. Government, "Mase ,6."
- [41] L. Livermore and N. R. Commission, "Recommendations for Ductile and Brittle Failure Design Criteria for Ductile Cast Iron Spent-Fuel Shipping Containers."
- [42] Mochizuki S, Matsushita H. Physical properties of nodular cast iron for shipping containers and safety analysis by fracture mechanics. Nucl Eng Des 1986;94:309-16.
- [43] Völzke H, Rödel R, Droste B. A fracture mechanics safety concept to assess the impact behavior of ductile cast iron containers for shipping and storage of radioactive materials. Nucl Eng Des 1994;150:357-66.

- [44] Sorenson KB, Salzbrenner R. Quality assurance aspects in using ductile cast iron for transportation casks 1988.
- [45] T. H. E. Existing, "Extended Drop Tests of Dci Casks With Artificial Flaws Demonstrating the Existing Safety Margins," vol. 5, pp. 177–182, 1995.
- [46] Teng T, Chu Y, Chang F, Chin H, Lee M. The dynamic analysis of nuclear waste cask under impact loading. *Ann Nucl Energy* 2003;30:1473-85.
- [47] Jakšić N, Nilsson K. Finite element modelling of the one meter drop test on a steel bar for the CASTOR cask. *Nucl Eng Des* 2009;239:201-13.
- [48] Nilsson K, Vokál V. Analysis of ductile cast iron tensile tests to relate ductility variation to casting defects and material microstructure. *Materials Science and Engineering: A* 2009;502:54-63.
- [49] Baer W, Bösel D, Eberle A, Klingbeil D. Determination of dynamic crack resistance of ductile cast iron using the compliance ratio key curve method. *Eng Fract Mech* 2010;77:374-84.
- [50] Baer W, Wossidlo P, Abbasi B, Cassau M, Haecker R, Kossert R. Large scale testing and statistical analysis of dynamic fracture toughness of ductile cast iron. *Eng Fract Mech* 2009;76:1024-36.
- [51] Zencker U, Zeisler P, Droste B. Dynamic fracture mechanics assessments for cubic ductile cast iron containers. *Int J Radioact Mater Transp* 2000;11:113-8.
- [52] Nilsson K, Blagoeva D, Moretto P. An experimental and numerical analysis to correlate variation in ductility to defects and microstructure in ductile cast iron components. *Eng Fract Mech* 2006;73:1133-57.
- [53] Zencker U, Qiao L, Weber M, Kovacs O, Droste B. Application limits of low-ductile cast iron for radioactive waste containers. 2007:21-6.
- [54] Fatahalla N, AbuElEzz A, Semeida M. C, Si and Ni as alloying elements to vary carbon equivalent of austenitic ductile cast iron: microstructure and mechanical properties. *Materials Science and Engineering: A* 2009;504:81-9.
- [55] Jafar K, Behnam A. Influence of mold preheating and silicon content on microstructure and casting properties of ductile iron in permanent mold. *Journal of Iron and Steel Research, International* 2011;18:34-9.
- [56] [http://www.foundrysolution.com/pemsil/intfondus.nsf/Vs\\_WebDL/30EEB29999E7962BC1256AAF0052A36B?OpenDocument&](http://www.foundrysolution.com/pemsil/intfondus.nsf/Vs_WebDL/30EEB29999E7962BC1256AAF0052A36B?OpenDocument&).
- [57] Bai Y, Luan Y, Song N, Kang X, Li D, Li Y. Chemical Compositions, Microstructure and Mechanical Properties of Roll Core used Ductile Iron in Centrifugal Casting Composite Rolls. *Journal of Materials Science & Technology* 2012;28:853-8.
- [58] [http://www.ductile.org/didata/Section3/Figures/pfig3\\_43.htm](http://www.ductile.org/didata/Section3/Figures/pfig3_43.htm).
- [59] Ingole P, Awate A, Saharkar S. Effect Of Basic Chemical Element In Sgi (Ductile Iron). 2012;1.
- [60] Neri M, Carreño C. Effect of copper content on the microstructure and mechanical properties of a modified nodular iron. *Mater Charact* 2003;51:219-24.
- [61] <http://www.ductile.org/didata/Section3/3part2.htm#ManganeseCopperNickelPhosphorus>.

- [62] Briki J, Ben Slima S. Influence of Manganese Content on the Dissolution of the Fe<sub>3</sub>C Iron Carbide Phase (Cementite) during a Graphitization Anneal of Spheroidal Graphite Cast Iron. *Journal of Metallurgy* 2012;2012.
- [63] Rao L, TAO W, WANG S, GENG M, Cheng G. Influence of the composition ratio of manganese and copper on the mechanical properties and the machining performance of ductile iron. *Indian Journal Of Engineering And Materials Sciences* 2014;573-9.
- [64] Rashidi MM, Idris MH. Microstructure and mechanical properties of modified ductile Ni-resist with higher manganese content. *Materials Science and Engineering: A* 2013;574:226-34.
- [65] LIU S, Yang C, Xin C, MIAO H. Microstructures and Mechanical Properties of Helical Bevel Gears Made by Mn-Cu Alloyed Austempered Ductile Iron. *Journal of Iron and Steel Research, International* 2012;19:36-42.
- [66] Rashidi MM, Idris MH. Effect of inoculation on microstructure, mechanical and corrosion properties of high manganese ductile Ni-resist alloy. *Mater Des* 2013;51:861-9.
- [67] Rashidi MM, Idris MH. The effects of solidification on the microstructure and mechanical properties of modified ductile Ni-resist iron with a high manganese content. *Materials Science and Engineering: A* 2014;597:395-407.
- [68] Källbom R, Hamberg K, Wessén M, Björkegren L. On the solidification sequence of ductile iron castings containing chunky graphite. *Materials Science and Engineering: A* 2005;413:346-51.
- [69] Uma T, Simha J, Murthy KN. Influence of nickel on mechanical and slurry erosive wear behaviour of permanent moulded toughened austempered ductile iron. *Wear* 2011;271:1378-84.
- [70] Erić O, Rajnović D, Zec S, Sidjanin L, Jovanović MT. Microstructure and fracture of alloyed austempered ductile iron. *Mater Charact* 2006;57:211-7.
- [71] Hsu C, Chen M, Hu C. Microstructure and mechanical properties of 4% cobalt and nickel alloyed ductile irons. *Materials Science and Engineering: A* 2007;444:339-46.
- [72] Zammit A, Mhaede M, Grech M, Abela S, Wagner L. Influence of shot peening on the fatigue life of Cu-Ni austempered ductile iron. *Materials Science and Engineering: A* 2012;545:78-85.
- [73] Shelton P, Bonner A. The effect of copper additions to the mechanical properties of austempered ductile iron (ADI). *J Mater Process Technol* 2006;173:269-74.
- [74] Ji C, Zhu S. Study of a new type ductile iron for rolling: composition design (1). *Materials Science and Engineering: A* 2006;419:318-25.
- [75] Lin B, Chen E, Lei T. The effect of alloy elements on the microstructure and properties of austempered ductile irons. *Scripta metallurgica et materialia* 1995;32:1363-7.
- [76] Ferro P, Fabrizi A, Cervo R, Carollo C. Effect of inoculant containing rare earth metals and bismuth on microstructure and mechanical properties of heavy-section near-eutectic ductile iron castings. *J Mater Process Technol* 2013;213:1601-8.
- [77] Choi J, Kim J, Choi C, Kim J, Rohatgi P. Effect of rare earth element on microstructure formation and mechanical properties of thin wall ductile iron castings. *Materials Science and Engineering: A* 2004;383:323-33.



- [78] Sheikh MA, Iqbal J. Effect of lanthanum on nodule count and nodularity of ductile iron. *Journal of Rare Earths* 2007;25:533-6.
- [79] Behera R, Mahto B, Dubey J, Mishra S, Sen S. Property enhancement of cast iron used for nuclear casks. *International Journal of Minerals, Metallurgy, and Materials* 2016;23:40-8.
- [80] El-Banna E. A study of ferritic centrifugally cast ductile cast iron. *Mater Lett* 1994;20:99-106.
- [81] Toktaş G, Tayanç M, Toktaş A. Effect of matrix structure on the impact properties of an alloyed ductile iron. *Mater Charact* 2006;57:290-9.
- [82] Shaker M. A note on the effect of nodularization characteristics on the workability of quench-hardened and tempered cast irons. *J Mater Process Technol* 1992;32:545-52.
- [84] Ghaderi A, Ahmadabadi MN, Ghasemi H. Effect of graphite morphologies on the tribological behavior of austempered cast iron. *Wear* 2003;255:410-6.
- [85] Putatunda SK. Comparison of the mechanical properties of austempered ductile cast iron (ADI) processed by conventional and step-down austempering process. *Mater Manuf Process* 2010;25:749-57.
- [86] Peng Y, Jin H, Liu J, Li G. Effect of boron on the microstructure and mechanical properties of carbide austempered ductile iron. *Materials Science and Engineering: A* 2011;529:321-5.
- [87] Sidjanin L, Smallman R, Young J. Electron microstructure and mechanical properties of silicon and aluminium ductile irons. *Acta metallurgica et materialia* 1994;42:3149-56.
- [88] Elsayed AH, Megahed M, Sadek A, Abouelela K. Fracture toughness characterization of austempered ductile iron produced using both conventional and two-step austempering processes. *Mater Des* 2009;30:1866-77.
- [89] Bosnjak B, Radulovic B. Effect of austenitising temperature on austempering kinetics of Ni-Mo alloyed ductile iron. *Materials and Technology* 2004;38:307-12.
- [90] [http://www.ductile.org/didata/Section3/Figures/pfig3\\_44.htm](http://www.ductile.org/didata/Section3/Figures/pfig3_44.htm).
- [91] Krawiec H, Stypuła B, Stoch J, Mikołajczyk M. Corrosion behaviour and structure of the surface layer formed on austempered ductile iron in concentrated sulphuric acid. *Corros Sci* 2006;48:595-607.
- [92] Mohammadi F, Alfantazi A. Corrosion of ductile iron exhaust brake housing in heavy diesel engines. *Eng Failure Anal* 2013;31:248-54.
- [93] Ukoba O, Oke P, Ibegbulam M. Corrosion Behaviour of Ductile Iron in Different Environment. *International Journal of Science and Technology* 2012;2.
- [94] Sosa A, Echeverría M, Moncada O, Simison S. Surface reactivity of thin wall ferritic ductile iron. The effect of nodule count and grinding variables. *Mater Lett* 2008;62:100-2.
- [95] Zeng D, Yung K, Xie C. Investigation of corrosion behavior of high nickel ductile iron by laser surface alloying with copper. *Scr Mater* 2001;44:2747-52.
- [96] Sun Y, Hu S, Xiao Z, You S, Zhao J, Lv Y. Effects of nickel on low-temperature impact toughness and corrosion resistance of high-ductility ductile iron. *Mater Des* 2012;41:37-42.
- [97] Hsu C, Lin K. Effects of Copper and Austempering on Corrosion Behavior of Ductile Iron

- in 3.5 Pct Sodium Chloride. *Metallurgical and Materials Transactions A* 2014;45:1517-23.
- [98] Hsu C, Chen M. Corrosion behavior of nickel alloyed and austempered ductile irons in 3.5% sodium chloride. *Corros Sci* 2010;52:2945-9.
- [99] Han CF, Wang Q, Sun Y, Li J. Effects of Molybdenum on the Wear Resistance and Corrosion Resistance of Carbide Austempered Ductile Iron. *Metallography, Microstructure, and Analysis* 2015;4:298-304.
- [100] Hsu C, Chen K, Lee C, Lu K. Effects of low-temperature duplex coatings on corrosion behavior of austempered ductile iron. *Surface and Coatings Technology* 2009;204:997-1001.
- [101] Hemanth J. The solidification and corrosion behaviour of austempered chilled ductile iron. *J Mater Process Technol* 2000;101:159-66.
- [102] Abedi H, Fareghi A, Saghafian H, Kheirandish S. Sliding wear behavior of a ferritic–pearlitic ductile cast iron with different nodule count. *Wear* 2010;268:622-8.
- [103] R.K.BEHERA, S.C.MISHRA, S.SEN, J. S. Dubey. Suitability of SG Iron to Be Used as Nuclear Fuel Transport Cask, 3<sup>rd</sup> Annual International Conference on Computational Materials Science, Metal and Manufacturing, 2016, pp. 54–60.
- [104] Dommarco R, Jaureguiberry A, Sikora J. Rolling contact fatigue resistance of ductile iron with different nodule counts and matrix microstructures. *Wear* 2006;261:172-9.
- [105] Górný M, Tyrała E. Effect of cooling rate on microstructure and mechanical properties of thin-walled ductile iron castings. *Journal of Materials Engineering and Performance* 2013;22:300-5.
- [106] Bockus S, Zaldarys G. Production of Ductile Iron Castings with Different Matrix Structure. *Material Science (Medziagotyra)* 2010;16:p307-3010.
- [107] Balachandran G, Vadiraj A, Kamaraj M, Kazuya E. Mechanical and wear behavior of alloyed gray cast iron in the quenched and tempered and austempered conditions. *Mater Des* 2011;32:4042-9.
- [108] Putatunda SK, Gadicherla PK. Influence of austenitizing temperature on fracture toughness of a low manganese austempered ductile iron (ADI) with ferritic as cast structure. *Materials Science and Engineering: A* 1999;268:15-31.
- [109] Fordyce E, Allen C. The dry sliding wear behaviour of an austempered spheroidal cast iron. *Wear* 1990;135:265-78.
- [110] Achary J. Tensile properties of austempered ductile iron under thermomechanical treatment. *Journal of materials Engineering and Performance* 2000;9:56-61.
- [111] Delia M, Alaalam M, Grech M. Effect of austenitizing conditions on the impact properties of an alloyed austempered ductile iron of initially ferritic matrix structure. *Journal of materials engineering and performance* 1998;7:265-72.
- [112] Erfanian-Naziftoosi H, Haghdadi N, Kiani-Rashid A. The effect of isothermal heat treatment time on the microstructure and properties of 2.11% Al austempered ductile iron. *Journal of materials engineering and performance* 2012;21:1785-92.
- [113] Sohi MH, Ahmadabadi MN, Vahdat AB. The role of austempering parameters on the structure and mechanical properties of heavy section ADI. *J Mater Process Technol* 2004;153:203-8.

- [114] Aristizabal R, Foley R, Druschitz A. Intercritically austenitized quenched and tempered ductile iron. *International Journal of Metalcasting* 2012;6:7-14.
- [115] Kocatepe K, Cerah M, Erdogan M. Effect of martensite volume fraction and its morphology on the tensile properties of ferritic ductile iron with dual matrix structures. *J Mater Process Technol* 2006;178:44-51.
- [116] Batra U, Ray S, Prabhakar S. The influence of Nickel and Copper on the Austempering of Ductile iron. *Journal of materials Engineering and Performance* 2004;13:64-8.
- [117] Gonzaga RA, Carrasquilla JF. Influence of an appropriate balance of the alloying elements on microstructure and on mechanical properties of nodular cast iron. *J Mater Process Technol* 2005;162:293-7.
- [118] Gonzaga R. Influence of ferrite and pearlite content on mechanical properties of ductile cast irons. *Materials Science and Engineering: A* 2013;567:1-8.
- [119] Eric O, Sidjanin L, Miskovic Z, Zec S, Jovanovic M. Microstructure and toughness of CuNiMo austempered ductile iron. *Mater Lett* 2004;58:2707-11.
- [120] Al-Ghonamy A, Ramadan M, Fathy N, Hafez K, El-Wakil A. Effect of graphite nodularity on mechanical properties of ductile iron for waterworks fittings and accessories. *Int J Civil Environ Eng* 2010;10:1-5.
- [121] Aristizabal R, Foley R, Druschitz A. Intercritically austenitized quenched and tempered ductile iron. *International Journal of Metalcasting* 2012;6:7-14.
- [122] Kilicli V, Erdogan M. The nature of the tensile fracture in austempered ductile iron with dual matrix microstructure. *Journal of materials engineering and performance* 2010;19:142-9.
- [123] Gonzaga R. Influence of ferrite and pearlite content on mechanical properties of ductile cast irons. *Materials Science and Engineering: A* 2013;567:1-8.
- [124] Martínez RA. Fracture surfaces and the associated failure mechanisms in ductile iron with different matrices and load bearing. *Eng Fract Mech* 2010;77:2749-62.
- [125] Dhanasekaran S, Vadiraj A, Balachandran G, Kamaraj M. Mechanical behaviour of an austempered ductile iron. *Transactions of the Indian Institute of Metals* 2010;63:779-85.
- [126] Zandira M, Boutorabi SMA. Fracture characteristics of austempered spheroidal graphite aluminum cast irons. *Journal of Iron and Steel Research, International* 2010;17:31-5.
- [127] Liang J, Deng A, Xie R, Gomez M, Hu J, Zhang J et al. Impact of seawater reverse osmosis (SWRO) product remineralization on the corrosion rate of water distribution pipeline materials. *Desalination* 2013;311:54-61
- [128] Surendranathan A, Prabhu KN, Nayak HS. Assessment of Corrosion Behavior of Ductile Irons by Factorial Experiments. *Journal of materials engineering and performance* 2009;18:1241-7.
- [129] Venkatesan R, Venkatasamy M, Bhaskaran T, Dwarakadasa E, Ravindran M. Corrosion of ferrous alloys in deep sea environments. *Br Corros J* 2013.
- [130] Ogundare O, Babatope B, Adetunji AR, Olusunle SOO. Atmospheric corrosion studies of ductile iron and austenitic stainless steel in an extreme marine environment. *Journal of Minerals and Materials Characterization and Engineering* 2012;11:914.

## APPENDIX - I

### ADVANTAGES OF SG IRON NUCLEAR FUEL CASK OVER OTHER CASK MATERIALS & DESIGN

Sl. No.	CASKS MADE OF OTHER MATERIALS	SG IRON CASK
1.	Casks manufactured by materials like combination of steel & lead or cermet required various post-processing before the final assembly of different components.	SG cast iron casks are monolithic and can directly be cast into the desired shape.
2.	These casks are quite like composite structures, so there is no homogeneity in the final product, a consequence of which chances of failure increased during severe accidental conditions.	Due to monolithic and direct casting technology, SG cast iron becomes homogeneous and isotropic in nature resulting better strength and toughness combination. It also offers better corrosion resistance to various environments employed.
3.	There is the probability of radiation leakage during accidental conditions and lead or depleted uranium is used as radiation absorbing agent, which may escape if the containment material fails.	There is no need to use lead or depleted uranium as SG cast iron itself is good enough to absorb gamma radiations and also possess sufficient mechanical properties as required for nuclear fuel cask.

## **APPENDIX - II**

### **HIGHLIGHTS OF THE CURRENT RESEARCH**

1. The previous works carried out regarding nuclear fuel cask was mainly focused on the fracture toughness investigation of spheroidal graphite cast iron. However, it is well established that in the case of high strength and toughness, the fracture toughness study can be ignored. Hence, in this current work priority is given towards the investigation of mechanical properties of SG cast iron to be used for nuclear fuel cask production.
2. The investigation of mechanical properties of SG cast iron by previous researchers was mainly carried out on the austempering behaviour of SG cast iron and the effect of austempering temperature and time were discussed. The conduct of annealed, normalized, quench& tempered SG cast iron is not reported frequently. Hence, the present investigation is centred towards the effect of annealing, normalizing, quench & tempering and intercritically austenitizing followed by quenching (DMS) heat treatment processes on morphological and mechanical properties of SGCI.
3. So far the austenitizing temperature was kept in the range of 900-950°C, and very few have reported beyond this range. In this research, an austenitizing temperature of 1000°C was chosen in order to achieve a complete transformation of final microstructure after every heat treatment process and also tempering at 500°C was opted to avoid the precipitation of unnecessary carbides and martensite.
4. The effect of chemical composition on morphological parameters viz. nodularity, nodule count and their influence on mechanical properties were less discussed. A thorough study is carried out in this research to have a better visualization of the role of morphological parameters on the mechanical properties and corrosion response to sea water environment.

## **APPENDIX - III**

### **FUTURE SCOPE OF WORK**

1. The fracture mechanics approach has to be employed for all the alloys in as-cast and heat treated conditions to get optimum composition and heat treatment condition of SG cast iron material for nuclear and hazardous waste container fabrication.
2. To minimize the prototype manufacturing & testing cost as well as time-saving a relation in mathematical form may be developed, between chemical composition, heat treatment parameters, and mechanical properties.
3. Finite element analysis approach will be employed to understand the behavior of SGCI cask with different designs and composite structures, in actual accidental condition.

# Dissemination

## **Internationally indexed journals** (*Web of Science, SCI, Scopus, etc.*)<sup>1</sup>

1. R.K.BEHERA, B.P.MAHTO, J.S.DUBEY, S.C.MISHRA, S.SEN. Property Enhancement of Cast Iron To Be Used For Nuclear Cask, International Journal Of Minerals, Metallurgy And Materials, VOL. 23 NO. 1 (2016), PP. 40-48. (DOI: 10.1007/s12613-016-1209-0)

## **Conferences** <sup>1</sup>

1. R.K.BEHERA, S.C.MISHRA, S.SEN, Characterization Of Heat Treated Ductile Iron Through Fractographic Analysis, International Conference On Emerging Materials And Processes – 2014(ISBN: 978-81-9285252-1-9), Organized By CSIR-IMMT Bhubaneswar.
2. R.K.Behera, S.C.Mishra, S.Sen, J.S.Dubey, “Suitability of SG Iron to Be Used As Nuclear Fuel Transport Cask”, 3rd Annual International Conference on Materials Science, Metal & Manufacturing (M3 2016), and Date: 18 – 19 January 2016, Singapore. [DOI: 10.5176/2251-1857-M316.19]

## **Article under preparation** <sup>2</sup>

1. R.K.BEHERA, J.S.DUBEY, S.C.MISHRA, S.SEN. Influence of Micro-Constituents on Ductile Iron Behaviour under Static and Dynamic Loading. (Communicated to Materials and Design, Elsevier).
2. R.K.BEHERA, S.C.MISHRA, S.SEN. Effect of Cooling Rate and Cooling Media on Mechanical Properties of Ni-Alloyed SG Cast Iron. (Communicated to Journal of Alloys and Compounds, Elsevier).
3. R.K.BEHERA, S.C.MISHRA, S.SEN. Behaviour of SG Cast Iron Under Static and Dynamic Loading Condition, Subjected to Various Heat Treatment Processes, for Use as Nuclear Fuel Cask. (Communicated to Nuclear Engineering Design, Elsevier).
4. R.K.BEHERA, S.C.MISHRA, S.SEN. Response to Sea Water Corrosive Environment of SGCI with Different Chemical Composition and Heat Treated Conditions. (Communicated to Corrosion, Elsevier).

<sup>1</sup>Articles already published, in press, or formally accepted for publication.

<sup>2</sup>Articles under review, communicated, or to be communicated.

## Response to examiner comments

### Reviewer 1:

1. In the corrosion tests, there were weight gain owing to the formation of scale on the surface; and weight loss as the ferrous ions dissolved in the seawater. How do you determine the W (mass loss) in equation 3.2?

**Response:** The gain and loss in weight during the corrosion test were observed and attributed to the same reasons as mentioned by the examiner. The abrupt pattern in the corrosion rate was due to the replacement of contaminated sea water with the fresh sea water, which results in increased reactivity level of the fresh sea water. However, the mass loss W, was determined by weighing the specimens with the help of a micro balance. Prior to measuring the weight, the specimens were gently cleaned by alcohol. The mass loss was noted by the difference in weight as that of measured in the previous week. This might also be a case, that during cleaning with alcohol some scales have been peeled off from the surface even.

2. State in details how you assess the nodularity and nodule count. As they are main parts of your work it is just not sufficient to cite the ASTM standard E2567-13a only.

**Response:** The as-cast and heat treated specimens without etching were observed under optical microscope, to determine the nodularity and nodule count. The optical microscope was incorporated with computer interface and “Metal Power” image analyser tool. The magnification was set to 10X for each and every specimen, before taking the image. A set of 10 clean and appropriate frame was captured for each and every specimen. Once the frames were captured, post processing was carried out with the image analyser tool. The graphite particles and the respective phases were differentiated by Yellow and Blue colour code. The minimum diameter of the nodule was measured by “Linear Measurement” option, which was found to be 8  $\mu\text{m}$ , and in the analyser tab the minimum nodule area was set to 50  $\mu\text{m}^2$ , and all the frames were put for Nodularity and Nodule count analysis. Based on the colour code and area of the nodule a computer generated report was obtained for each specimen, mentioning nodularity and nodule count for each frame and average value as well, which has been reported in the dissertation.

3. The different heat-treatment processes as given in Fig. 3.2 suggest that the samples were put at different temperatures for different periods of time. Some examples; the annealed samples were initially heated at 1000°C for 90 minutes and then maintained at 700°C for 5.5 hours; while DMS-treated samples were only exposed to 800°C for only 2 minutes. Thus the amount of grain growth would be much different, as illustrated in Fig. 4.2. Has the candidate considered the difference in grain size of the samples treated under different conditions? Would that have an effect on the mechanical properties and corrosion resistance?



**Response:** The careful observation made by the examiner regarding the grain growth in respective heat treated specimens, as each heat treatment process is different than the other. It is quite possible that the grain growth owing to the heat treatment process can change and may have affected the mechanical and corrosion properties as well. However, in the current study the kinetics of phase transformation has not been considered (as of the major importance). I am thankful to the examiner for noticing this point; which can be considered as a future aspect for the investigation.

4. The XRD patterns of different samples should be put into the same graph for comparisons.

**Response:** The XRD patterns of different samples has been put into a single graph for better comparison as suggested by the examiner and incorporated in the appropriate place in the dissertation.

5. How can you differentiate the (311) peak and (200) peak, if they are both located at  $65^\circ 2\theta$ ?

**Response:** It was clearly observed from the microstructure that, the specimens treated with austempering treatment had Coarse Upper Bainitic matrix (sometimes also referred as Ausferrite) indicating presence of austenite and ferrite in the microstructure. This is an evidence of presence of both BCC and FCC crystal structure in the (grains of) samples. Whereas, in the as-cast and other heat treated specimens the crystal structure was BCC only as no retained austenite was observed in their microstructure. Hence in the XRD study, the (3 1 1) FCC peak was observed at  $65^\circ 2\theta$  for austempered specimens, whereas other specimens have (2 0 0) BCC peak. The similar type of results was also observed by Putatunda et.al [12].

6. Where are equations 4.1 and 4.2?

**Response:** The equations 4.1 and 4.2 were mentioned in the dissertation (page no. 49) as pointed out by the examiner.

7. What evidence do you have to show “no segregation of sulphur and phosphorus” in the SGCI?

**Response:** The composition of Sulphur and Phosphorus was well maintained within the limit as desired to avoid any segregation. Also neither in the microstructure nor in XRD analysis any kind of segregation or precipitation of any Sulphur or Phosphorus compound was observed. It can be attributed to the fact that the austenitizing temperature (i.e.  $1000^\circ\text{C}$ ) is quite well above the upper critical temperature and the austenitizing time (90 minutes) is long enough to avoid any kind of segregation in the final microstructure.

8. The corrosion rate of  $>50\mu\text{m}/\text{year}$  is considered as high for SNF cask?

**Response:** Although in many observations some values are higher than  $50\mu\text{m}/\text{year}$ , but some values below  $50\mu\text{m}/\text{year}$  is also observed in some cases. Moreover, these

data are acceptable and also not yet objected after the sample tests conducted by Bhaba Atomic Research Centre (The purpose of the BRNS sponsored project).

9. Would the candidate comment on the degree of pitting of different samples? This is an important factor as leaking of the SNF cask usually initiates from the pits. How can the candidate relate section 4.3.3 to 4.3.1?

**Response:** The section 4.3.1 explains the rate of corrosion for as-cast and heat treated specimens for respective alloys studied. Whereas the section 4.3.3 has reported the mechanism of corrosion that was involved in the process. The two major mechanism has been observed in the study i.e., pitting corrosion and graphitic corrosion. However, the degree of pitting has not been a major investigation point in this study, because assessing the degree of pitting is difficult while conducting corrosion test in sea water environment. Also as far as the SNF cask is considered the degree of pitting is of not as important as that of corrosion rate. Hence in this study the degree of pitting has not been considered as part of major investigation. However, to understand this phenomena necessary investigations can be considered as a future study.

10. Section 4.3.2 seems to be a compilation of previous works, without confirmation from the present research. For example, did the candidate observed the formation of  $\text{Cu}_2\text{O}$  on the surface? From the EDAX study in section 4.3.3 only Fe, Cr, Ni, Mn are present, but not Cu. Cu was only found in the porous product (i.e. not protective) Similar results were obtained in the XRD study.

**Response:** The findings reported in sections 4.3.2 and 4.3.3 are inter related. The effect of alloying elements on the corrosion behaviour was reported in section 4.3.2 and validated in section 4.3.3. However, the facts observed by the examiner was also reported in the dissertation. The formation of  $\text{Cu}_2\text{O}$  has not been observed on the corroded surface but found in the porous product. It was quite possible that during the cleaning with alcohol the scales were peeled off from the surface and hence found in the porous product that was evident from the XRD and EDAX analysis. Also, the sea water contains ions of other than  $\text{Na}^+$  &  $\text{Cl}^-$ , so it was quite possible that during the reaction other ions might have led to the formation similar potential that was repellent to each other and leading to removal of scale from the surface. Hence the  $\text{Cu}_2\text{O}$  compound was only observed in the porous product, and not on the corroded surface.

#### **Reviewer 2:**

1. Austempered components are corroding rapidly than the as-cast and heat-treated specimens. Why austempered specimens are indicating more rapid corrosion and what is the mechanism of corrosion?

**Response:** The austempered specimens were observed to have higher no. of graphite nodules as compared to the other as-cast and heat treated specimens. The micrographs of corroded surface after 1<sup>st</sup> week of immersion was observed to have corrosion layers surrounding the graphite nodules indicating graphitic corrosion mechanism. The SEM investigation also revealed that the corroded surface had significant amount of cracks,

which led to penetration of sea water into the scale and react with the specimen surface, leading to higher rate of corrosion. Similar case was also observed for the quench & tempered specimens.

2. Increase in Nickel content clearly indicated increase in Tensile Strength with decreased Ductility and Impact properties. Do you find any co-relationship of Nickel content with the carbon equivalent vis-à-vis mechanical properties?

**Response:** The addition of Nickel content results in strengthening the as-cast matrix via solid solution strengthening. And as the annealing process undergoes a slow transformation process and does not alter the as-cast matrix, as observed in this case; hence effect of Ni will remain unaltered. Hence the UTS was observed to be increasing for the as-cast and annealed specimens with decreasing ductility and impact energy. On the other hand, for the specimens undergone different heat treatment processes the amount of phase volume fraction was proportional to Ni wt.%. This can be attributed to the fact that with increase in Ni content there was an increase in austenite content at austenitizing state resulting higher volume fraction of bainite, martensite in respective specimen, consequentially increasing strength and decreasing ductility as well as impact energy.

3. Can we cryogenically treat this Cast Iron for the given set of applications? Offer your comment.

**Response:** The desired property for SNF cask fabrication requires high strength as well as considerable amount of ductility and impact strength, to prevent the failure from severe accidental conditions. The cryogenic treatment of SGCI leads to increase in hardness and lowers the ductility and impact toughness. Hence, it may not be suitable to treat this cast iron cryogenically for present application. However, for future study can be considered to obtain a suitable cryogenic treatment condition, so that the cast iron can be used for SNF cask fabrication.